Energy Reports 8 (2022) 15249–15285

Contents lists available at ScienceDirect

Energy Reports

journal homepage: www.elsevier.com/locate/egyr

Research paper

An enhanced Gradient-based Optimizer for parameter estimation of various solar photovoltaic models

M. Premkumar [a,*], Pradeep Jangir [b], C. Ramakrishnan [c], C. Kumar [d], R. Sowmya [e], Sanchari Deb [f,*], Nallapaneni Manoj Kumar [g,h,i,**]

[a] Department of Electrical and Electronics Engineering, Dayananda Sagar College of Engineering, Bengaluru, Karnataka 560078, India
[b] Rajasthan Rajya Vidyut Prasaran Nigam, Sikar 332025, Rajasthan, India
[c] Department of Electrical and Electronics Engineering, SNS College of Technology, Coimbatore 641035, Tamil Nadu, India
[d] Department of Electrical and Electronics Engineering, M.Kumarasamy College of Engineering, Karur 639113, Tamil Nadu, India
[e] Department of Electrical and Electronics Engineering, National Institute of Technology, Tiruchirappalli 620015, Tamil Nadu, India
[f] School of Engineering, University of Warwick, Coventry CV4 7AL, UK
[g] School of Energy and Environment, City University of Hong Kong, Kowloon, Hong Kong
[h] Department of Electrical Engineering, Graphic Era (Deemed to be University), Dehradun 248002, Uttarakhand, India
[i] Center for Research and Innovation in Science, Technology, Engineering, Arts, and Mathematics (STEAM) Education, HICCER – Hariterde International Council of Circular Economy Research, Palakkad 678631, Kerala, India

ARTICLE INFO

Article history:
Received 22 July 2022
Received in revised form 2 November 2022
Accepted 7 November 2022
Available online xxxx

Keywords:
Criss-cross algorithm
Gradient-Based Optimizer
Nelder–Mead simplex
Parameter estimation
Solar photovoltaic models

ABSTRACT

The performance of a PhotoVoltaic (PV) system could be inferred from the features of its current–voltage relationships, but the PV model parameters are uncertain. Because of its multimodal, multivariable, and nonlinear properties, the PV model requires that its parameters be extracted with high accuracy and efficiency. Therefore, this paper proposes an enhanced version of the Gradient-Based Optimizer (GBO) to estimate the uncertain parameters of various PV models. The Criss-Cross (CC) algorithm and Nelder–Mead simplex (NMs) strategy are hybridized with the GBO to improve its performance. The CC algorithm maximizes the effectiveness of the population and avoids local optima trapping. The NMs strategy enhances the individual search capabilities during the local search and produces optimum convergence speed; therefore, the proposed algorithm is called a Criss-Cross-based Nelder–Mead simplex Gradient-Based Optimizer (CCNMGBO). The primary objective of this study is to propose a simple and reliable optimization algorithm called CCNMGBO for the parameter estimation of PV models with five, seven, and nine unknown parameters. Firstly, the performance of CCNMGBO is validated on 10 benchmark numerical optimization problems, and secondly, applied to the parameter estimation of various PV models. The performance of the CCNMGBO is compared to several other state-of-the-art optimization algorithms. The results proved that the proposed algorithm is superior in handling the numerical optimization problem and obtaining the uncertain parameters of various PV models and performs better during different operating conditions. The convergence speed of the proposed CCNMGBO is also better than selected optimization algorithms with highly reliable output solutions. The average objective function value for case 1 is 9.83E−04, case 2 is 2.43E−04, and the average integral absolute error and relative error values are 1.05E−02 and 3.51E−03, respectively, for all case studies. With Friedman's rank test values of 2.21 for numerical optimization and 1.66 for parameter estimation optimization, the CCNMGBO stood first among all selected algorithms.

1. Introduction

The massive expansion of the world economies has contributed to an ongoing increase in electricity consumption. The enormous usage of coal and oil has led to immediate electricity crises and growing atmospheric emissions. The challenging growth stage in the country's economy becomes the electricity issue. Solar photovoltaic (PV) systems have recently gained attention to overcome these crises. The PV cell converts solar energy

* Corresponding authors.
** Corresponding author at: School of Energy and Environment, City University of Hong Kong, Kowloon, Hong Kong.
E-mail addresses: mprem.me@gmail.com (M. Premkumar), pkjmtech@gmail.com (P. Jangir), ramramki.krishnan@gmail.com (C. Ramakrishnan), ckumarme81@gmail.com (C. Kumar), sowmyanitt@gmail.com (R. Sowmya), sanchari.deb@warwick.ac.uk (S. Deb), mnallapan2-c@my.cityu.edu.hk (N.M. Kumar).

https://doi.org/10.1016/j.egyr.2022.11.092

into electrical energy, and now the technique is progressively being developed (Premkumar et al., 2018, 2020a; Manoharan et al., 2020). The equivalent circuit of such PV cells is necessary to analyze the cell characteristics during various operating conditions. In particular, the single-diode model (SDM) and the double-diode model (DDM) are developed and reported in various literature for parameter estimation problems, and the SDM and DDM are highly preferred and commonly utilized models (Ćalasan et al., 2019a; Moshksar and Ghanbari, 2017). Since solar PV cells are exposed to the outside environment, the performance of the cells and the overall system are reduced. The overall performance of the PV system is heavily dependent on uncertain parameters, such as photocurrent (I_p), reverse saturation current of the diode (I_{sd}), diode ideality factor (a), shunt resistance (R_{sh}), and series resistance (R_{se}) for SDM and photocurrent (I_p), the reverse saturation current of the two diodes (I_{sd1} and I_{sd2}), ideality factor of two diodes (a_1, a_2), shunt resistance (R_{sh}), and series resistance (R_{se}) for DDM that makes it essential to estimate the uncertain variables of different PV models. Nevertheless, the current equations of both SDM and DDM PV models are transcendental, it is hard to estimate cell variables, as mentioned earlier, and it is difficult to analyze the performance of the cell or module. Hence it is crucial to introduce a technique that can quickly and successfully estimate the parameters of the cell/module (Long et al., 2020; Premkumar et al., 2020c; Li et al., 2019).

The researchers have reported several approaches, including numerical, cognitive, statistical, and other conventional optimization techniques, to ensure accurate assessment parameters of solar cell models (Jordehi, 2016; Fathabadi, 2013). However, the extent of using similar computational methods is explicitly prohibited by several constraints on the optimization process (Chen et al., 2018). Thus, the swarm intelligence (SI) optimizers have accepted a position in order to ensure a positive value since such an algorithm can identify the approximated solutions over a specified period of time (Chin et al., 2015; Oliva et al., 2017). Therefore, SI optimizers have drawn the attention of researchers, and these methods have been successfully implemented for energy conservation problems. The differential evolution (DE) optimizer was used to evaluate a seven-parameter solar cell equivalent circuit and proved its reliability in handling the parameter estimation problem (Sheraz and Abido, 2014). The authors of Ma et al. (2016) implemented a particle swarm optimizer (PSO) to extract the parameters of the RTC France Si solar cell and proved its reliability. However, the PSO is stuck at local optima due to the multimodal optimization function. The authors of Shayeghi et al. (2010) implemented an enhanced version of PSO with stable convergence features and reasonable computation time with good efficacy for tuning PID controllers' gains of the heat exchanger to determine the appropriate dimensions of wind-powered energy storage to achieve the energy demands. The authors of Laghari et al. (2013) also applied the PSO algorithm to optimize power station size and reduce the overall cost. The SDM and DDM of the solar cell and panel recently attracted researchers to analyze the cell or module conveniently. The authors of Oliva et al. (2014) and Askarzadeh and Rezazadeh (2013) presented an artificial bee colony (ABC) algorithm for PV parameter estimation of different models. The authors of Chen et al. (2019b) applied a whale optimization algorithm (WOA) to extract the PV module variables and proved its proficiency in terms of the accuracy and reliability of the solutions for the PV module. For the same optimization problem, the flower pollination optimizer was applied, and even the efficacy of an approach was recorded by the experimental results (Alam et al., 2015). The authors of Benayad and Berrah (2019) directly applied hybrid PSO algorithms to evaluate the parameters of the PV module by utilizing the Integral Absolute Error (IAE) as the objective function. The authors of Messaoud (2020a) reported the salp swarm optimizer (SSO) to effectively balance the PV module with a diode as a core framework to obtain the variables of the DDM based on PV cells and demonstrated that SSO is a successful technique in handling this optimization problem. The authors of Zhang et al. (2020) combined the techniques, such as NMs and orthogonal learning, to develop a new orthogonal-based moth flame optimizer (MFO) and obtained excellent outcomes for all PV models. The authors of Qais et al. (2020) merged the basic version of the Harris Hawk's optimizer (HHO) with the computation approach to obtain unknown variables of all PV models, including SDM, DDM, and photovoltaic modules. The authors also proved the reliability of the algorithm under various solar irradiance and temperature conditions. The authors of Liu et al. (2020) applied an improved version of HHO using vertical and horizontal crossover with Nelder–Mead simplex to the solar parameter estimation problem. Moreover, the three-diode model (TDM) is also a hot subject compared to the SDM and the DDM because these models are inadequate in describing the various current of the PV cell and module. The authors of Ramadan et al. (2020), Liao et al. (2020) and Yu et al. (2017a) proposed a teacher-learning-based optimization algorithm (TLBO) and different variants for solar parameter estimation problems. A modified version of HHO called Whippy HHO was proposed in Naeijian et al. (2021) to estimate the parameters of the different PV models. The parameter of the SDM and DDM of the PV cell and module was extracted using a chemistry-inspired algorithm called Equilibrium Optimizer (EO), and the authors have presented that EO can extract the parameters in less time (Ndi et al., 2021). A new optimization algorithm called tree–seed optimization was presented in Beşkirli and Dağ (2022), and the authors have claimed that the algorithm can extract the parameters accurately.

Therefore, many algorithms were applied to TDM to explain the analytical results further, and it was used as a useful method for the parameter extraction of TDM of the cell and module (Md Sabudin and Jamil, 2019; Khanna et al., 2015; Elazab et al., 2020). For the first time, the authors of Montano et al. (2020) suggested a grasshopper optimizer algorithm (GOA) to test the I–V curve of the TDM of the PV module. The authors of Qais et al. (2019b) and Yuan et al. (2020) suggested the Coyote optimizer algorithm (COA) and the Sunflower optimizer algorithm (SOA) to estimate the unknown parameters of the TDM, and the authors proved that both SOA and COA gives reliable solutions even during different operating conditions of the PV cell or module. The authors of Premkumar et al. (2020e) reported various techniques called the Rao algorithm (RAO), slime mould algorithm (SMA) (Kumar et al., 2020), political optimizer algorithm (POA) (Premkumar et al., 2020b), and a hybrid version of PSO and gray wolf optimizer (GWO) (Premkumar et al., 2020c) to handle this optimization problem for various PV models and the authors proved the superiority of all techniques in handling the parameter identification optimization task. The authors of Nayak et al. (2019) and Abdel-basset et al. (2020) introduced EO and gray wolf optimizer (GWO) for parameter estimation problems, however, the solution accuracy is less, and the computational time is high. The authors of Louzazni et al. (2017) and Beigi and Maroosi (2018) presented a firefly optimization (FFO) algorithm for various real-world optimization problems, including the PV parameter estimation problem. The authors of Soliman and Hasanien (2020), Naraharisetti et al. (2020), Ridha (2020), Sankaranarayanan (2022) and Rezk and Abdelkareem (2022) recently presented a marine-predator algorithm (MPA) for different PV models' PV parameter estimation problems. A modified and improved variant of the DE algorithm was reported in Wang et al. (2022) to estimate the parameters of various PV models, and the authors compared the performance with 14 well-known algorithms.

Presently, researchers have reported several improved optimization techniques to increase the solution accuracy of the basic versions of many algorithms. The authors of Oliva et al. (2017) chaotic version of WOA modified a few important parameters of the WOA and applied them to the solar PV parameter estimation problem. The authors of Wu et al. (2017) reported an improved version of the ant lion optimizer to improve the exploration and exploitation ability of the basic version of the ant lion algorithm. Various chaotic maps are integrated with the basic PSO version to improve the precision of the solar PV parameter estimation (Kiani et al., 2020). The authors of Kang et al. (2018) reported an enhanced cuckoo search (CS) technique by merging the quasi-opposition-based learning (OBL) framework, Levy flight, and the self-adapting phase. The authors of Abd Elaziz and Oliva (2018) suggested including the OBL scheme with WOA to improve the solution accuracy while handling the parameter estimation problem. The authors of Javier Toledo et al. (2018) reported a least-square method to determine three unknown variables, such as R_{sh}, I_{sd}, and I_p. However, a slight error occurs between the estimated values and the experimental values. The authors of Premkumar et al. (2021e) suggested an enhanced version of the JAYA algorithm called IJAYA, developed using self-adaptive weight and chaotic strategy to improve the solution accuracy. However, the computation time is higher than other state-of-the-art algorithms. The basic version of PSO is improved with the adaptive mutation approach to increase the accuracy while evaluating the variables of various PV models under diverse operating environments, and the same has been reported in Nunes et al. (2018). The authors of Xiong et al. (2018b) introduced a hybrid version by combining WOA and sine–cosine algorithm (SCA) to compute the uncertain variables of various PV models. The authors of Yousri et al. (2020) utilized a chaotic fractional scheme with the particle swarm optimizer to find the unknown variables of SDM, DDM, and TDM under various environmental conditions. The authors of Kumari and Geethanjali (2017) introduced a multiobjective version of a genetic algorithm to find the unknown variable of various PV models. The authors of Chen et al. (2019a) reported an improved version of SCA by employing NMs and OBL and applied it to solve the design optimization of the solar PV systems. The authors of Bendaoud et al. (2019) suggested a hybrid version of GA by combining the simulated annealing to extract the unknown variables of SDM of the PV cell or module. The authors of Chen and Yu (2019) reported a hybrid version of CS with the biogeography-based optimizer to estimate the PV array variables closer to the experimental values. A summary of the literature survey is presented in Table 1.

The gradient-based optimizer (GBO) is a new population-based algorithm suggested by Ahmadianfar et al. and the algorithm was originally inspired by Newton's method (Ahmadianfar et al., 2020). The GBO algorithm simulates dimension maintenance (DM) and several strategies for the local escaping operator (LEO). The GBO algorithm gives a very efficient performance than several other optimizers, including the PSO (Bana and Saini, 2017), WOA (Rana et al., 2020), GWO (Mirjalili et al., 2014), SMA (Li et al., 2020), SCA (Mirjalili, 2016), RAO (Rao, 2020), EO (Faramarzi et al., 2020), and POA (Askari et al., 2020), and it can also be extended to other areas in future. To improve the accuracy of the basic version of GBO, different variants of the GBO algorithm are proposed for various real-world optimization problems. The performance of GBO is improved by a hybrid version of GBO-MFO is presented to optimal power flow problems (Mohamed et al., 2022). The authors of Yu et al. (2022) have proposed a new variant of GBO called Orthogonal Learning GBO (OLGBO), in which the boosting mechanism called orthogonal learning is combined with GBO to improve the solution accuracy and applied the same to the parameter estimation of PV models. Similarly, the authors of Ma et al. (2013) have proposed another new variant of GBO called Ranking-Based GBO (RBGBO), in which a ranking mechanism is hybridized with GBO to improve the estimation accuracy of the PV models. The authors of Yu et al. (2021), Abd Elminaam et al. (2022) and Premkumar et al. (2021b) have introduced Chaotic GBO (CGBO) to improve the performance of the GBO and applied them to various real-world engineering optimization problems. Multi-objective and many-objective variants of the GBO algorithm are developed and applied to various multi-objective optimization problems and optimal power flow problems (Premkumar et al., 2021c,d). The opposition-based learning (OBL) strategy is combined with GBO to improve the accuracy of the PV model parameter estimation problem. Even though different variants are introduced for various optimization problems, each algorithm and variant has its own merits and demerits. This statement was proved by the no-free-lunch (NFL) theory (Wolpert and Macready, 1997). As per the statement provided by the NFL theory, no single algorithm is effective for all types of optimization problems. This statement motivated us to propose a new variant of the GBO algorithm.

A new enhanced GBO called CCNMGBO is proposed in this paper, which incorporates the key strategies that occurred in the criss-cross (CC) algorithm (Meng et al., 2014) and NMs method (Gao and Han, 2012) to enhance the ability of the population location during the local search and strengthen the convergence speed that can be applied to solar photovoltaic parameter estimation problem. This paper outlines for the very first time the key mechanisms that emerged at CC in GBO, which encourage not just the exchange rate of information among various individuals. Also, it emphasizes a convergence of multiple dimensions for a single entity, ensuring population diversity and avoiding the local optimization problem. Further to the CC optimizer, the NMs are configured to conduct an intensive search process in the current population to find an effective solution that boosts the enhancement patterns of the algorithm and dramatically improves the solution accuracy. The performance of the proposed CCNMGBO is compared with the other competitive algorithms on SDM, DDM, and PV models to illustrate the capability of the CCNMGBO algorithm. In addition, the parameters of various PV models at various temperatures and solar irradiance conditions. Few observations justify the reasonable results of the CCNMGBO comparison to another competitive algorithm. The main contributions of this paper are summarized as follows.

- Development of a new GBO variant called CCNMGBO by merging the logic of CC and NMs methods to estimate the PV parameters of various PV models. The CC optimizer helps to develop agent diversity and convergence rate, while NMs are introduced in every iteration to improve the solution quality.
- The proposed algorithm is tested on 10 benchmark problems and compared with the basic version of the GBO and other well-known algorithms
- The performance of the proposed CCNMGBO algorithm is also verified on parameter estimation of SDM, DDM, TDM, and PV module models.
- The proposed CCNMGBO algorithm was validated using three commercial PV models under different irradiance levels and temperatures and demonstrated significant accuracy in the experimental and estimated values.
- In addition, statistical tests, such as Wilcoxon's rank-sum test and Friedman rank test, are carried out to evaluate the performance of all selected algorithms.

The remainder of the paper is structured as follows. Section 2 discusses various PV models and introduces the objective function of each PV model. Section 3 presents the basic version of GBO

Table 1
Summary of applications of different algorithms on solar PV parameter estimation.

Algorithm	SDM	DDM	PV type	Merits	Demerits
DE (Abido and Khalid, 2018)	✓	–	SM55 Module	(i) Good accuracy under different operating conditions (ii) Good exploration capability	(i) Parameter tuning required (ii) Poor exploitation capability
GA (Jervase et al., 2001)	✓	–	RTC France Si cell	(i) Fair accuracy (ii) Find solutions in promising search space	(i) Trapped by local minima (ii) Poor local searching
JAYA (Jian and Weng, 2020)	✓	✓	RTC France Si cell	(i) Less complicated and less computation time (ii) High rate of convergence and robustness	(i) Trapped by local minima (ii) Poor solution accuracy
IJAYA (Yu et al., 2017b)	✓	✓	RTC France Si cell and PhotoWatt-PWP201	(i) Chaotic scheme increases the solution accuracy (ii) Good exploration and exploitation ability	(i) High computation time (ii) Not tested for commercial modules
Rao (Premkumar et al., 2020e)	✓	✓	RTC France Si cell and PhotoWatt-PWP201	(i) Easy to implement (ii) Good exploration ability	(i) Trapped by local minima (ii) Not tested for commercial modules
TLBO (Ramadan et al., 2020)	✓	✓	RTC France Si cell	(i) Easy to implement (ii) Fewer control parameters (iii) High speed of convergence	(i) High computation cost (ii) Poor solution accuracy
PSO (Ye et al., 2009)	✓	✓	Not specified	(i) High solution accuracy (ii) Easy to implement (iii) Robust	(i) Trapped by local minima (ii) Early convergence
ABC (Oliva et al., 2014)	✓	✓	RTC France Si cell	(i) Robust and high accuracy (ii) Noise insensitive	(i) High computation time (ii) Frequent parameter tuning is required (iii) Early convergence
MFO (Zhang et al., 2020)	✓	✓	Q6-1380 solar cell and CS6P-240P module	(i) High speed of convergence (ii) Less complex	(i) High computation time (ii) Not tested for commercial modules
CS (Ma et al., 2013)	✓	–	RTC France Si cell	(i) High solution accuracy (ii) High exploration capability	(i) Poor convergence speed
FFO (Louzazni et al., 2017)	✓	–	PhotoWatt-PWP201	(i) Simple to implement	(i) Solution is better only when compared to very old techniques
GWO (Saxena et al., 2020)	✓	–	KC200GT	(i) Robust (ii) Less chance for local optima trap (iii) High solution accuracy	(i) Very less convergence speed
WOA (Xiong et al., 2018a)	✓	✓	KC200GT	(i) Easy to implement (ii) Less computational cost (iii) Fair exploitation ability	(i) Poor exploration ability (ii) Trapped by local minima (iii) Early convergence
SCA (Montoya et al., 2020)	✓	–	KC200GT	(i) Simple and easy to implement (ii) Fair accuracy	(i) Tested only for the KC200GT module (ii) Trapped by local minima
SSO (Messaoud, 2020b)	–	✓	TITAN-12–50	(i) Speed of convergence is high (ii) High exploitation and exploration balance (iii) Avoid local optima	Not specified
COA (Diab et al., 2020)	✓	✓	RTC France Si cell, PhotoWatt-PWP201, KC200GT, ST40, and SM55	(i) High-solution quality (ii) High speed of convergence	(i) Poor exploitation ability (ii) Early convergence
HHO (Qais et al., 2020)	✓	✓	RTC France Si cell, PhotoWatt-PWP201, PVM 752 GaAs, ST40, and SM55	(i) High speed of convergence (ii) Avoid local optima (iii) High-solution quality	Not specified
MPA (Ridha, 2020)	–	✓	KC200GT and MSX-60	(i) High solution accuracy (ii) Good exploration ability	(i) Early convergence (ii) Trapped by local minima
SMA (Kumar et al., 2020)	✓	✓	RTC France Si cell and PhotoWatt-PWP201	(i) High accurate (ii) Good exploration and exploitation ability	(i) High computation time
EO (Menesy et al., 2020)	✓	✓	RTC France Si cell, PhotoWatt-PWP201, ST40, and SM55	(i) High accurate (ii) Good exploration and exploitation ability	(i) High computation time

and introduces the improved version of GBO called CCNMGBO. The implementation procedure is also discussed in Section 3. Section 4 presents the comprehensive results of the CCNMGBO under various temperature and irradiance levels using three different PV models, such as SDM, DDM, TDM, and PV models. In addition, benchmark problem results are also presented. The statistical

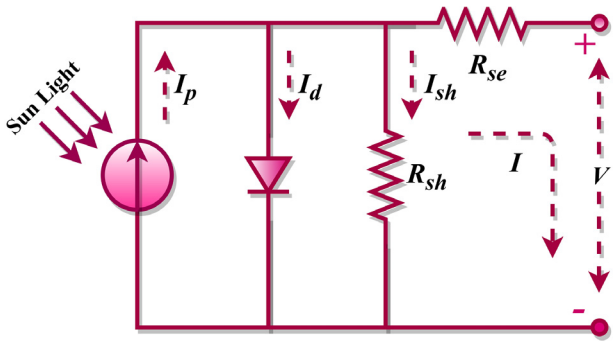

Fig. 1. Electrical equivalent schematic of SDM (Mohamed et al., 2013).

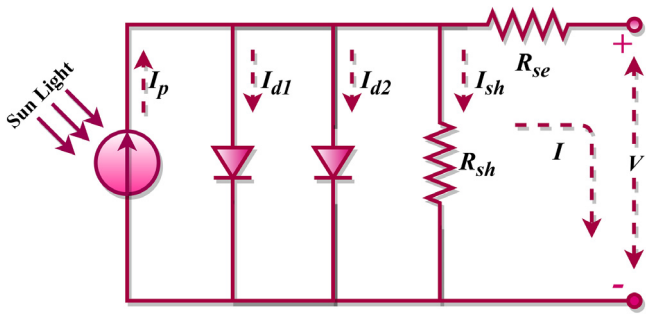

Fig. 2. Electrical equivalent schematic of DDM (Mohamed et al., 2013).

result analysis of all selected algorithms is also discussed in Section 4. Finally, Section 5 concludes the paper.

2. Photovoltaic models and problem formulation

In PV energy generation, the features of PV cells have become a vital component influencing solar power systems. The developers significantly improve technologies to build PV models with better accuracy, allowing them to develop mathematical modeling of solar cells (Premkuma et al., 2019; Premkumar et al., 2020d). Several studies have discovered appropriate circuit models by examining the critical characteristics of creating quite feasible and effective technology. Among these, SDM and DDM are the most widespread since they are simple to implement (Premkumar et al., 2020a; Ćalasan et al., 2019a; Premkumar et al., 2020e). The core idea of the two models will be briefly outlined in the following sub-section.

2.1. Photovoltaic models

2.1.1. Single-diode model

Fig. 1 illustrates the analogous electrical circuit for the SDM, developed by a single current source describing the photoelectric current I_p produced by the PV cell when subjected to the incident light. A single diode is connected in parallel with the current source to represent the PN junction effects. To acknowledge current and voltage losses and acquire a model capable of precisely representing the I–V characteristics, R_{se} and R_{sh} are also included. The resistance R_{se} denotes the resistivity of the metal contacts, accounting for ohmic losses, while the resistance R_{sh} accounts for leakage currents in cells.

Apply Kirchhoff's current law (KCL) and derive the expression for the cell output current I as follow.

$$I = I_p - I_d - I_{sh} \tag{1}$$

where I_d denotes the current through the diode and I_{sh} denotes the current through the shunt resistance. As per the Shockley equation, the equation for I_d can be represented as follows.

$$I_d = I_{sd}\left[\exp\left(\frac{V + R_{se}I}{aV_t}\right) - 1\right] \tag{2}$$

where V denotes the output voltage of the cell and V_t represents the thermal voltage. The expression for the thermal voltage is given in Eq. (3).

$$V_t = \frac{N_{se}kT}{q} \tag{3}$$

where q denotes the electronic charge and is equal to $1.60217646 * 10^{-19}$ C, k denotes the Boltzmann constant and is equal to $1.3806503 * 10^{-23}$ J/K, and T denotes the junction temperature in K. By applying Ohms' law, the current through the shunt resistance is written as follows.

$$I_{sh} = \frac{V + IR_{se}}{R_{sh}} \tag{4}$$

Therefore, the output current of the SDM of the PV cell is rewritten as follows (Ayang et al., 2019; Batzelis and Papathanassiou, 2016).

$$I = I_p - I_{sd}\left[\exp\left(\frac{V + R_{se}I}{aV_t}\right) - 1\right] - \frac{V + IR_{se}}{R_{sh}} \tag{5}$$

From the above discussions, for the SDM, there are five unknown parameters, such as I_p, I_{sd}, R_{se}, R_{sh}, and a.

2.1.2. Double-diode model

Fig. 2 illustrates the analogous electrical circuit for the DDM. In this configuration, two diodes are placed parallel with the current source to fully illustrate the effects at the PN junction. The diode (D_1) describes the junction diffusion current, i.e., replicates the diffusion phase of the minority carriers into the depletion layer, whereas the diode (D_2) represents the recombination impact, i.e., describes the charge carrier recombination in the space-charge region. Apply KCL and derive the expression for the cell output current as follow.

$$I = I_p - I_{d1} - I_{d2} - I_{sh} \tag{6}$$

where I_{d1} denotes the current of diode 1 and I_{d2} denotes the current of diode 2. The expressions for both currents are written as per the Shockley equation as follows.

$$I_{d1} = I_{sd1}\left[\exp\left(\frac{V + R_{se}I}{a_1V_t}\right) - 1\right] \tag{7}$$

$$I_{d2} = I_{sd2}\left[\exp\left(\frac{V + R_{se}I}{a_2V_t}\right) - 1\right] \tag{8}$$

Therefore, the output current of the SDM of the PV cell is rewritten as follows (Sandrolini et al., 2010; Lun et al., 2015).

$$I = I_p - I_{sd1}\left[\exp\left(\frac{V + R_{se}I}{a_1V_t}\right) - 1\right] - I_{sd2}\left[\exp\left(\frac{V + R_{se}I}{a_2V_t}\right) - 1\right] - \frac{V + IR_{se}}{R_{sh}} \tag{9}$$

From the above discussions, for the DDM, there are seven unknown parameters, such as I_p, I_{sd1}, I_{sd2}, R_{se}, R_{sh}, a_1, and a_2.

2.1.3. Three-diode model

Fig. 3 illustrates the analogous electrical circuit for the TDM. In this configuration, three diodes are placed parallel to the current source to fully illustrate the effects at the PN junction. The diode (D_1) describes the junction diffusion current, i.e., replicates the diffusion phase of the minority carriers into the depletion layer.

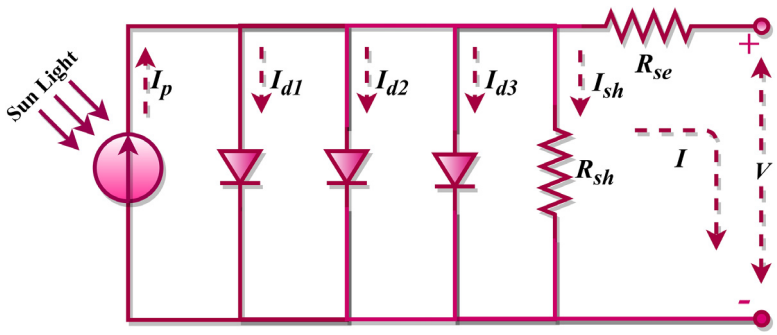

Fig. 3. Electrical equivalent schematic of TDM (Kumar and Mary, 2021; Wei et al., 2019).

The diode (D_2) represents the recombination impact, i.e., describes the charge carrier recombination in the space-charge region, and the diode (D_3) reports the properties of leakage current and grain boundaries. Apply KCL and derive the expression for the cell output current as follow.

$$I = I_p - I_{d1} - I_{d2} - I_{d3} - I_{sh} \tag{10}$$

where I_{d1} denotes the current of diode 1, I_{d2} denotes the current of diode 2, and I_{d3} denotes the current of diode 3. The expressions for both currents are written as per the Shockley equation as follows.

$$I_{d1} = I_{sd1}\left[\exp\left(\frac{V + R_{se}I}{a_1 V_t}\right) - 1\right] \tag{11}$$

$$I_{d2} = I_{sd2}\left[\exp\left(\frac{V + R_{se}I}{a_2 V_t}\right) - 1\right] \tag{12}$$

$$I_{d3} = I_{sd3}\left[\exp\left(\frac{V + R_{se}I}{a_3 V_t}\right) - 1\right] \tag{13}$$

Therefore, the output current of the TDM of the PV cell is rewritten as follows (Qais et al., 2020, 2019a; Premkumar et al., 2022).

$$I = I_p - I_{sd1}\left[\exp\left(\frac{V + R_{se}I}{a_1 V_t}\right) - 1\right] - I_{sd2}\left[\exp\left(\frac{V + R_{se}I}{a_2 V_t}\right) - 1\right] - I_{sd3}\left[\exp\left(\frac{V + R_{se}I}{a_3 V_t}\right) - 1\right] - \frac{V + IR_{se}}{R_{sh}} \tag{14}$$

From the above discussions, for the TDM, there are nine unknown parameters, such as I_p, I_{sd1}, I_{sd2}, I_{sd3}, R_{se}, R_{sh}, a_1, a_2, and a_3.

2.1.4. Photovoltaic module model

The PV panel is the device that transforms light into electric energy and comprises several PV cells in parallel or series. Furthermore, the analogous circuit of the SDM is illustrated in Fig. 4. By considering the SDM and DDM, the output current equation of the PV panel can be expressed in Eqs. (10) and (11), respectively (Ćalasan et al., 2019b; Jamadi et al., 2016).

$$I = N_{sh}\left(I_p - I_{sd}\left[\exp\left(\frac{V/N_{se} + R_{se}\,(I/N_{sh})}{aV_t}\right) - 1\right] - \frac{V/N_{se} + R_{se}\,(I/N_{sh})}{R_{sh}}\right) \tag{15}$$

$$I = N_{sh}\left(I_p - I_{sd1}\left[\exp\left(\frac{V/N_{se} + R_{se}\,(I/N_{sh})}{a_1 V_t}\right) - 1\right] - I_{sd2}\left[\exp\left(\frac{V/N_{se} + R_{se}\,(I/N_{sh})}{a_2 V_t}\right) - 1\right] - \frac{V/N_{se} + R_{se}\,(I/N_{sh})}{R_{sh}}\right) \tag{16}$$

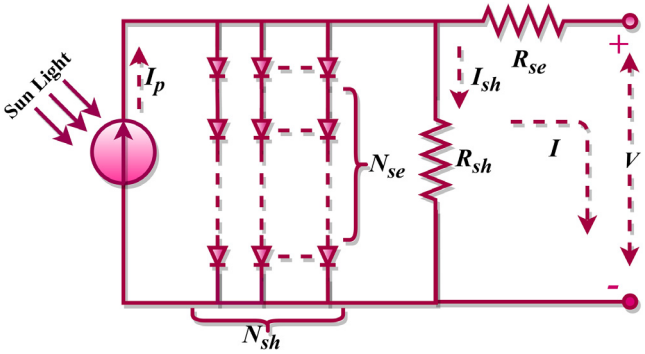

Fig. 4. Electrical equivalent schematic of the PV module model (Muhsen et al., 2016).

where N_{sh} denotes the number of parallel-connected cells, and N_{se} represents the number of series-connected cells.

2.2. Problem formulation/objective function formulation

The critical concern in many optimization problems is achieving the minimal value of the target system computed from practice, so a precise and simple objective function must be simulated. It is necessary to obtain the optimal parameters of the PV model to allow the error at each pair of the estimated and experimental current values to be as low as possible. There are various evaluation metrics, such as Mean Squared Error (MSE), Mean Absolute Error (MAE), Root Mean Square Error (RMSE), and Root Mean Square Log Error, are available to identify the parameters of the solar photovoltaic models. RMSE is the most preferred objective function, error metric, or evaluation metric, as mentioned in various literature. The advantage of RMSE over other metrics are (i) RMSE accounts for positive or negative values, (ii) RMSE is useful when lower residual values are chosen, and (iii) RMSE is better in terms of reflecting performance when dealing with large error values. Due to the above-said advantages, RMSE is considered to be an objective function to estimate the unknown parameters of various photovoltaic models. Consequently, the fitness function of all models can be seen in Eqs. (17)–(22). The RMSE is expressed in Eq. (23) as the objective function that would be a nonlinear transcendental one and is difficult to solve (Ćalasan et al., 2020). Subsequently, the primary aim of this paper is to minimize the objective function value by optimizing the vector x.

$$f_{\mathrm{SDM}}(\mathrm{V}, \mathrm{I}, x) = I_p - I - I_{sd}\left[\exp\left(\frac{V + R_{se}I}{aV_t}\right) - 1\right] - \frac{V + IR_{se}}{R_{sh}} \tag{17}$$

$$f_{\mathrm{DDM}}(\mathrm{V}, \mathrm{I}, x) = I_p - I - I_{sd1}\left[\exp\left(\frac{V + R_{se}I}{a_1 V_t}\right) - 1\right]$$

$$- I_{sd2}\left[\exp\left(\frac{V+R_{se}I}{a_2V_t}\right)-1\right]-\left(\frac{V+IR_{se}}{R_{sh}}\right) \tag{18}$$

$$\begin{aligned} f_{\mathrm{TDM}}(\mathrm{V},\mathrm{I},x) &= I_p - I - I_{sd1}\left[\exp\left(\frac{V+R_{se}I}{a_1V_t}\right)-1\right] \\ &\quad - I_{sd2}\left[\exp\left(\frac{V+R_{se}I}{a_2V_t}\right)-1\right] \\ &\quad - I_{sd3}\left[\exp\left(\frac{V+R_{se}I}{a_3V_t}\right)-1\right]-\left(\frac{V+IR_{se}}{R_{sh}}\right) \end{aligned} \tag{19}$$

$$\begin{aligned} f_{\mathrm{PV-SDM}}(\mathrm{V},\mathrm{I},x) &= N_{sh}\left(I_p - I_{sd}\left[\exp\left(\frac{V/N_{se}+R_{se}(I/N_{sh})}{aV_t}\right)-1\right]\right. \\ &\quad \left. -I-\left(\frac{V/N_{se}+R_{se}(I/N_{sh})}{R_{sh}}\right)\right) \end{aligned} \tag{20}$$

$$\begin{aligned} f_{\mathrm{PV-DDM}}(\mathrm{V},\mathrm{I},x) &= N_{sh}\left(I_p - I_{sd1}\left[\exp\left(\frac{V/N_{se}+R_{se}(I/N_{sh})}{a_1V_t}\right)-1\right]\right. \\ &\quad -I_{sd2}\left[\exp\left(\frac{V/N_{se}+R_{se}(I/N_{sh})}{a_2V_t}\right)-1\right] \\ &\quad \left. -I-\frac{V/N_{se}+R_{se}(I/N_{sh})}{R_{sh}}\right) \end{aligned} \tag{21}$$

$$\begin{aligned} f_{\mathrm{PV-TDM}}(\mathrm{V},\mathrm{I},x) &= N_{sh}\left(I_p - I_{sd1}\left[\exp\left(\frac{V/N_{se}+R_{se}(I/N_{sh})}{a_1V_t}\right)-1\right]\right. \\ &\quad -I_{sd2}\left[\exp\left(\frac{V/N_{se}+R_{se}(I/N_{sh})}{a_2V_t}\right)-1\right] \\ &\quad -I_{sd3}\left[\exp\left(\frac{V/N_{se}+R_{se}(I/N_{sh})}{a_3V_t}\right)-1\right] \\ &\quad \left. -I-\frac{V/N_{se}+R_{se}(I/N_{sh})}{R_{sh}}\right) \end{aligned} \tag{22}$$

The objective function can be written as follows.

$$F_{\mathrm{RMSE}}(x) = \sqrt{\frac{1}{m}\sum_{k=1}^{m} f^k\left(I^k, V^k, x\right)^2} \tag{23}$$

where f denotes the error function of the respective PV models and m denotes the number of current samples. The vector x denotes the unknown variable of the respective PV model. For instance, the length of vector x for SDM is five, such as $\{I_{\mathrm{p}}, I_{\mathrm{sd}}, R_{\mathrm{se}}, R_{\mathrm{sh}}, a\}$, the length of vector x for DDM is seven, such as $\{I_{\mathrm{p}}, I_{\mathrm{sd1}}, I_{\mathrm{sd2}}, R_{\mathrm{se}}, R_{\mathrm{sh}}, a_1, a_2\}$, and the length of vector x for TDM is nine, such as $\{I_{\mathrm{p}}, I_{\mathrm{sd1}}, I_{\mathrm{sd2}}, I_{\mathrm{sd3}}, R_{\mathrm{se}}, R_{\mathrm{sh}}, a_1, a_2, a_3\}$. The bounds of all these unknown variables are discussed in the result section. The problem of defining variables for solar cells and PV modules is to explore how well the experimental voltage and current values can be used to calculate the values of other unknown parameters. Therefore, by changing the values of vector x, the value of RMSE is optimized in this paper. Also, to test the accuracy of the proposed algorithm, the RMSE is also an excellent determinant. Alternatively, the lower the RMSE value, the nearer the results extracted to the experimental value. It is also important to note that the measured dataset is obtained from a commercial module in the manufacturer's specification sheet.

3. Methodology — Criss-cross nelder mead simplex gradient-based optimizer

In this section, concepts of the basic version of GBO (Ahmadianfar et al., 2020), the CC algorithm (Meng et al., 2014), and the NMs method (Gao and Han, 2012) are introduced briefly, and the process of combining the GBO, CC, and NMs to extract the parameters of the PV model is introduced.

3.1. Gradient-based optimizer (GBO)

The basic GBO integrates the population-based and gradient-based methods, and it uses Newton's equations for search space exploration using two operators called local escaping operators (LEO) and gradient search rule (GSR) and a few sets of control parameters.

3.1.1. Initialization phase

In any optimization problem, objective function, design variables, and constraints, including equality and inequality constraints, are very important. The exploration and exploitation ability of the GBO is controlled through the variable called probability rate, which is denoted as α. The number of populations (N) and the maximum number of iterations (l_{max}) are chosen based on the optimization problem complexity. Each population is denoted as a vector in a search space with the dimension *dim*. Therefore, the population vector is expressed as follows.

$$X_{d,N} = \left[X_{1,N}, X_{2,N}, \ldots, X_{dim,N}\right] \tag{24}$$

where N is the population size and d denotes the problem dimension and is equal to 1, 2, …, *dim*. The individual vectors are generated randomly, similar to all metaheuristic algorithms, and expressed as follows.

$$X_N = X_l + rand\,(0,1) \times (X_u - X_l) \tag{25}$$

where X_u and X_l are the upper and lower bounds of the decision variables X, and *rand* is a random number between [0,1].

3.1.2. Gradient search rule (GSR)

The variable's movement is monitored in order to enhance the search in the probable region and attain good positions in the GSR. The exploration process is increased by increasing the convergence speed of the basic GBO. The basic principle of the gradient search rule is gradients. The recommended GSR helps the GBO adapt to random movements throughout optimization, encouraging exploration and preventing early convergence (Saxena et al., 2020). The convergence speed accelerates the direction of movement (DM) to create an appropriate local search behavior. Consequently, the present vector location is modified using the following equation based on GSR and DM (Ahmadianfar et al., 2020; Premkumar et al., 2021a).

$$X1_N^l = x_N^l - GSR + DM \tag{26}$$

$$DM = rand \times \rho_2 \times \left(x_b - x_N^l\right) \tag{27}$$

$$GSR = randn \times \rho_1 \times \frac{2\Delta x \times x_N^l}{(x_w - x_b + \varepsilon)} \tag{28}$$

The vector x_N^l is updated using Eq. (19), and the new vector $X1_N^l$ is updated. The parameter ρ_1 is used to balance the exploitation and exploration phases. The worst and best solutions during the optimization are denoted as x_w and x_b, respectively. Also, the value of ε is restricted in the range of (0, 0.1) (Ahmadianfar et al., 2020).

$$\rho_1 = 2 \times rand \times \alpha - \alpha \tag{29}$$

$$\beta = \beta_{min} + (\beta_{max} - \beta_{min}) \times \left(1 - \left(\frac{l}{l_{max}}\right)^3\right)^2 \tag{30}$$

$$\alpha = \left| \beta \times \sin\left(\frac{3\pi}{2} + \sin\left(\beta \times \frac{3\pi}{2} \right) \right) \right| \tag{31}$$

where l denotes the current iteration, *randn* is a uniformly distributed random number, and the values of β_{min} and β_{max} are selected as 0.2 and 1.2, respectively. The term Δx denotes the difference between the current best solution and random positions. The variable δ verifies the value of $\Delta\ x$ during each iteration (Ahmadianfar et al., 2020).

$$\Delta x = rand\,(1:N) \times |step| \tag{32}$$

$$\delta = 2 \times rand \times \left| \frac{x_{r_1}^l + x_{r_2}^l + x_{r_3}^l + x_{r_4}^l}{4} - x_N^l \right| \tag{33}$$

$$step = \frac{\left(x_b - x_{r1}^l\right) + \delta}{2} \tag{34}$$

The various integers, such as r_1, r_2, r_3, and $r_4 (r_1 \neq r_2 \neq r_3 \neq r_4 \neq n)$ are chosen randomly between [1, D]. The step size is represented by *step*, and it can be calculated by x_{r1}^m and x_{best}. In addition, ρ_2 is another random variable that helps the GBO to increase its exploration phase, and it aids each population vector with variable step sizes. The equation for ρ_2 as expressed as follows.

$$\rho_2 = 2 \times rand \times \alpha - \alpha \tag{35}$$

Newton's method increases the diversity of the solution and exploration phase of GBO. The population-based search is generated using Eq. (26) (Ahmadianfar et al., 2020).

$$X1_N^l = x_N^l - randn \times \rho_1 \times \frac{2\Delta x \times x_N^l}{\left(yp_N^l - yq_N^l + \varepsilon\right)} + rand \times \rho_2 \times \left(x_b - x_N^l\right) \tag{36}$$

In Eq. (36), the position of the current vector is replaced by the position of the best vector. Thus, the position of the new vector is expressed as follows (Ahmadianfar et al., 2020).

$$X2_N^l = x_b - randn \times \rho_1 \times \frac{2\Delta x \times x_N^l}{\left(yp_N^l - yq_N^l + \varepsilon\right)} + rand \times \rho_2 \times \left(x_{r1}^l - x_{r2}^l\right) \tag{37}$$

$$yp_N = rand \times \left(\frac{[z_{N+1} + x_N]}{2} + rand \times \Delta x \right) \tag{38}$$

$$yq_N = rand \times \left(\frac{[z_{N+1} + x_N]}{2} - rand \times \Delta x \right) \tag{39}$$

The exploitation phase of the GBO is increased by the search direction method as represented in Eq. (37), and it is valid only for the local search; however, the global search is increased by Eq. (36). Thus, the exploitation and exploration phases are increased by Eqs. (36) and (37). The solutions are updated during the next iteration using Eqs. (40)–(41) (Ahmadianfar et al., 2020).

$$x_N^{tl+1} = r_a \times \left(r_b \times X1_N^l + (1 - r_b) \times X2_N^l\right) + (1 - r_a) \times X3_N^l \tag{40}$$

$$X3_N^l = X_N^l - \rho_1 \times \left(X2_N^l - X1_N^l\right) \tag{41}$$

3.1.3. Local escaping operator (LEO)

The validity of the basic GBO in handling real-time problems, the operator called LEO, is applied. The LEO gives the best solution, which includes the random solutions, such as x_{r1}^l and x_{r2}^l, x_b, updated random solution x_k^l, $X1_N^l$ and $X2_N^l$. The solution X_{LEO}^t is generated using the following framework (Ahmadianfar et al., 2020).

if $rand < P_r$

  if $rand < 0.5$

$$X_{LEO}^l = X_N^{l+1} + a \times \left(u_1 \times x_b - u_2 \times x_k^l\right) + b \times \rho_1 \times (u_3 \times (X2_N^l - X1_N^l) + u_2 \times (x_{r1}^l - x_{r2}^l))/2$$

$$X_N^{l+1} = X_{LEO}^l$$

Else (42)

$$X_{LEO}^l = x_b + a \times \left(u_1 \times x_b - u_2 \times x_k^l\right) + b \times \rho_1 \times (u_3 \times (X2_N^l - X1_N^l) + u_2 \times (x_{r1}^l - x_{r2}^l))/2$$

$$X_n^{l+1} = X_{LEO}^l$$

End

End

where a denotes a uniform random number between [−1,1], b denotes a normally distributed random number with a mean of 0 and standard deviation (STD) of 1, P_r denotes the probability rate, and u_1, u_2, and u_3 denotes the random numbers, and it is expressed as follows (Ahmadianfar et al., 2020).

$$u_1 = \begin{cases} 2 \times rand, & if\ P < 0.5 \\ 1, & otherwise \end{cases} \tag{43}$$

$$u_2 = \begin{cases} rand, & if\ P < 0.5 \\ 1, & otherwise \end{cases} \tag{44}$$

$$u_3 = \begin{cases} rand, & if\ P < 0.5 \\ 1, & otherwise \end{cases} \tag{45}$$

where the value of P varies between [0,1] and *rand* denotes a random number between [0,1]. Eqs. (43)–(45) are revised and expressed as follows (Ahmadianfar et al., 2020).

$$u_1 = Z_1 \times 2 \times rand + (1 - Z_1) \tag{46}$$

$$u_2 = Z_1 \times rand + (1 - Z_1) \tag{47}$$

$$u_3 = Z_1 \times rand + (1 - Z_1) \tag{48}$$

The Z_1 value is 0 when P is greater than or equal to 0.5; otherwise, the value is 1. Eq. (49) is an update scheme and applied to Eq. (42) to get the x_k^l solution.

$$x_k^l = \begin{cases} x_{rand}, & if\ Q < 0.5 \\ x_p^l, & otherwise \end{cases} \tag{49}$$

$$x_{rand} = X_l + rand \times (X_u - X_l) \tag{50}$$

where Q denotes a random number between [0,1], x_p^l denotes a random population solution, and x_{rand} denotes the new solution. Thus, Eq. (49) is revised and expressed as follows.

$$x_k^l = Z_2 \times x_p^l + (1 - Z_2) \times x_{rand} \tag{51}$$

where Z_2 denote a binary parameter equal to 0 when the Q is greater than or equal to 0.5; otherwise, Z_2 is equal to 1. The pseudocode of the basic version of the GOA is shown in *Algorithm 1*.

3.2. Criss-Cross (CC) optimization algorithm

The CC optimization algorithm is a robust technique that takes advantage of the crossover in genetic algorithm and is profoundly inspired by the Confucian gold process, which contains the vertical crossover operator and the horizontal crossover

Algorithm 1: Gradient-Based Optimizer (GBO) Algorithm

Step-1 Initialization
Assign the parameters, such as pr, ε, and l_{max}
Initial population, $X_0 = [x_{0,1}, x_{0,2}, \ldots, x_{0,dim}]$
Evaluate the objective function value, $f(X_0)$, n=1,2,...,N
Specify the worst and best solutions x_w^l and x_b^l
Step-2 Main loop
While ($l<l_{max}$)
for n = 1:N
for i = 1:dim
Choose randomly $r1 \neq r2 \neq r3 \neq r4 \neq n$ in range of [1, N]
Find the position $x_{n,i}^{l+1}$ using Eq. 29
end for
------ Local escaping operator ------
if $rand < pr$
Find the position x_{LEO}^l, $X_n^{l+1} = x_{LEO}^l$
End if
Position update (x_b^l and x_w^l)
end for
l=l+1
end
Step-3 Return x_b^l

operator (Meng et al., 2014). The convergence speed is very fast when these two operators are used simultaneously, in addition to reducing the average error (Meng et al., 2016). The two operators execute the crossover procedures to produce new candidate solutions during each iteration. The greedy selection process has been implemented to choose the best individuals, and it can still retain them.

3.2.1. Vertical crossover

The primary aim is that the technique trapped into an optimal local solution is the inactivity of certain parameters of the individual in other traditional algorithms. The primary objective of the vertical crossover is to function among randomly designated variables of each individual. The candidate solution through the vertical crossover is generated by Eq. (52) (Meng et al., 2014, 2021).

$$S_{id1}^{VC} = rX_{id1} + (1-r)\,X_{id2} \tag{52}$$

where S_{id1}^{VC} denotes the generation of the dimension d_1 of the individual i in dimensions d_1 and d_2, respectively, over vertical cross-generation ($d_2 \neq d_1$), r denotes a random number between [0,1], X_{id1} and X_{id2} denote ith individual value in dimensions, d_1 and d_2, respectively.

3.2.2. Horizontal crossover

The horizontal crossover (HC) focuses primarily on two individuals and facilitates sharing of information between the different individuals. Considering that X_i and X_j are the parent individuals, then the horizontal crossover is performed out towards the d^{th} dimension, and based on Eq. (53), the moderate candidate solution is produced (Meng et al., 2014).

$$\left.\begin{aligned} S_{id}^{HC} &= r_1 \times X_{id} + (1-r_2)\,X_{id} + a_1\left(X_{id} - X_{jd}\right) \\ S_{jd}^{HC} &= r_1 \times X_{jd} + (1-r_2)\,X_{jd} + a_2\left(X_{jd} - X_{id}\right) \end{aligned}\right\} \tag{53}$$

where S_{jd}^{HC} and S_{id}^{HC} denote two new moderate candidate solutions, X_{id} and X_{jd} denote ith and jth individual ($j \neq i$) values in dimension d. r_1 and r_2 denote uniform random numbers between [0,1], and a_1 and a_2 are the uniform random numbers between $[-1,1]$. After crossover, the competitive procedure between the S_{id}^{HC} and X_i required to be carried out, and individuals with lower fitness are removed. This activity would guarantee that the best performers stay in each iteration, thus improving the population's efficiency. Also, the global ability for exploration and the convergence speed can be increased.

3.3. Nelder–Mead simplex (NMs) method

The Nelder–Mead simplex method was commonly used as a derivative-free optimization approach due to its ease of implementation and robust local search capability (Gao and Han, 2012). The simplex phase guarantees that the output during every iteration is not inferior to the past instance. Next, find the initial viable solution and check whether the solution is the best or not. If the solution is not good, then turn to the next enhanced and good viable solution via a pre-set rule and then recognize it. Still, if the solution is not optimal, then turn back and repeat the procedure. Meanwhile, the feasible area solutions are small; the best solution is found after many transformations. The basic principle of the simplex process is to frame a polyhedron through a $d+1$ vertex in d-dimensional space, determine the capability of the polyhedron, and compare the objective value to classify the worst, best, and suboptimal individuals. In many studies, NMs, along with different metaheuristic algorithm, is utilized to extract the parameters of the PV cell and module (Zhang et al., 2020; Liu et al., 2020; Weng et al., 2021).

The worst individual is transformed into the best individual by performing reflection, expansion, and contraction, and finally, it is transformed into the best individual by performing reflection, expansion, and contraction/compression, and finally, it forms the new polyhedron. Thus, this method is based on a search that enhances the solution of the worst individual by comparing the fitness of simple polyhedron vertex and steadily reaching the best value. The readers are highly encouraged to read Ref. Gao and Han (2012) for the detailed implementation of NMs. The *fminsearchbnd* command in MATLAB is formulated as similar to NMs. Therefore, the *fminsearchbnd* command is used in this paper to find the unknown parameters of the solar PV cell parameters.

Algorithm 2: Pseudocode of the CCNMGBO Algorithm

Step 1: **Initialization -** Assign values for parameters (pr, ε, and M).
Generate an initial population $X_0 = [x_{0,1}, x_{0,2}, \ldots, x_{0,D}]$
Evaluate the objective function value, $f(X_0)$, n=1,...,N
Specify the best and worst solutions x_b^l and x_w^l
Step 2: **While** (l<l_{max})
For n=1:N
For i=1:dim
Select randomly $r1 \neq r2 \neq r3 \neq r4 \neq n$ in the range of [1, N]
Find the position $x_{n,i}^{l+1}$ using Eq. 29
end for
------ Local escaping operator ------
if $rand < pr$
Find the position x_{LEO}^l, $X_n^{l+1} = x_{LEO}^l$
End if
Position update (x_b^l and x_w^l)
The current position of the individual and the location are used as parents to accomplish HC to produce a new position based on Eq. 53.
end for
l=l+1
The values of individual fitness are calculated and stored;
Choose the first best N individuals as a new population;
On new population, execute vertical crossover based on Eq. 52;
The fitness of all individuals is found and stored;
Choose the first best N individuals as a new population;
Perform NMs MATLAB command (*fminsearchbnd*) and it updates the current best position as the initial value;
end While
Step 3: Return x_b^l

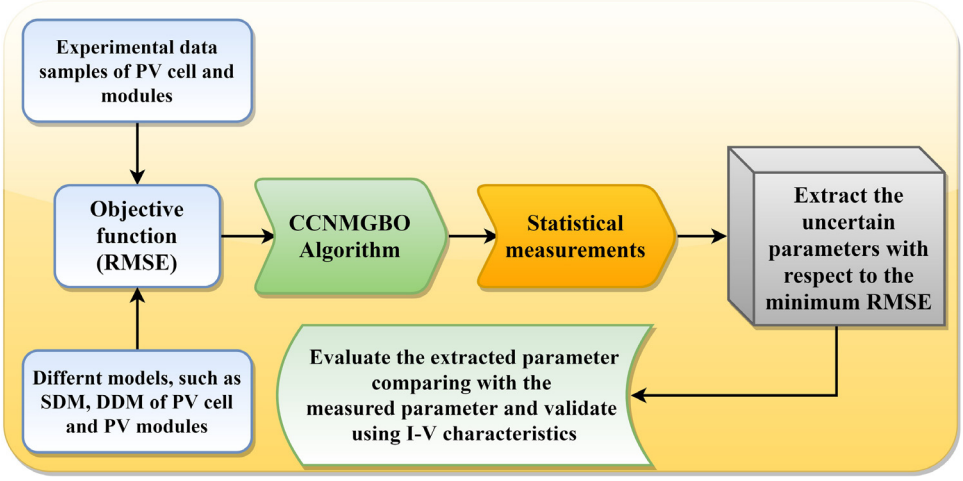

Fig. 5. Application of CCNMGBO algorithm for PV parameter estimation problem (Methodology) (Premkumar et al., 2021b).

Because all the unknown variables are defined as vectors, and the variables are bounded. The Pseudocode (in *Algorithm 2*) explains the overall implementation procedure of the proposed algorithm.

The proposed CCNMGBO algorithm is applied to the parameter estimation problem of different PV models. Finally, the workflow of the proposed CCNMGBO algorithm to estimate the unknown parameters of PV models is demonstrated in Fig. 5.

4. Simulation results and discussions

This section presents the experimental results to illustrate the efficacy of the enhanced algorithm proposed in this paper. Firstly, the proposed algorithm's performance is validated using 10 numerical optimization problems with unimodal and multimodal features. Secondly, CCNMGBO is directly applied to parameter estimation (multimodal problem) of SDM, DDM, and TDM under different operating conditions to check its reliability in handling the real-world multi-modal problem. The performance of CCNMGBO is compared with seven state-of-the-art algorithms, such as CCNMGBO, OBLWOA, GWO, HHO, SCA, WOA, GBO, and EO.

All algorithms are developed using the MATLAB software tool, and the simulation is carried out using MATLAB installed on a laptop with 2.40 GHz bandwidth, 8 GB RAM, and a Windows 8.1 operating system. The common parameters of all algorithms are selected as follows: population size = 30 (for benchmark problems) and 40 (for parameter estimation problems), the maximum number of iterations = 500 (for benchmark problems) and 1000 (for parameter estimation problems), and the number of runs = 30. In order to rank the selected algorithms, two different statistical tests were also carried out, such as Wilcoxon signed-rank test (WSRT) and Friedman's Ranking Test (FRT). The novelty of this study is properly justified using the obtained results for numerical optimization and parameter estimation problems.

Table 2
Classical benchmark test functions and their ranges (Premkumar, 2021).

Function	Dim	Range	f_{min}
$f_1(x) = \sum_{i=1}^{n} x_i^2$	30	[−100, 100]	0
$f_2(x) = \sum_{i=1}^{n} \lvert x_i \rvert + \prod_{i=1}^{n} \lvert x_i \rvert$	30	[−10, 10]	0
$f_3(x) = \sum_{i=1}^{n} \left(\sum_{j-1}^{i} x_j \right)^2$	30	[−100, 100]	0
$f_4(x) = \max_i \{ \lvert x_i \rvert , 1 \leqslant i \leqslant n \}$	30	[−100, 100]	0
$f_5(x) = \sum_{i=1}^{n} [x_i^2 - 10\cos(2\pi x_i) + 10]$	30	[−5.12, 5.12]	0
$f_6(x) = -20\exp\left(-0.2\sqrt{\frac{1}{n}\sum_{i=1}^{n} x_i^2}\right) - \exp\left(\frac{1}{n}\sum_{i=1}^{n}\cos(2\pi x_i)\right) + 20 + e$	30	[−32, 32]	0
$f_7(x) = \frac{1}{4000}\sum_{i=1}^{n} x_i^2 - \prod_{i=1}^{n}\cos\left(\frac{x_i}{\sqrt{i}}\right) + 1$	30	[−600, 600]	0
$f_8(x) = -\sum_{i=1}^{5} [(X - a_i)(X - a_i)^T + c_i]^{-1}$	4	[0, 10]	−10.1532
$f_9(x) = -\sum_{i=1}^{7} [(X - a_i)(X - a_i)^T + c_i]^{-1}$	4	[0, 10]	−10.4028
$f_{10}(x) = -\sum_{i=1}^{10} [(X - a_i)(X - a_i)^T + c_i]^{-1}$	4	[0, 10]	−10.5363

4.1. Results on benchmark problems

As discussed earlier, 10 benchmark numerical optimization problems are selected to validate the proposed algorithm. Table 2 comprehensively explains all 10 standard benchmark functions and other useful information. The benchmark functions are unimodal (F1–F4), multimodal functions (F5–F7), and fixed-dimension multimodal functions (F8–F10). The exploitation capability of the CCNMGBO is evaluated through the use of unimodal function analysis. The exploratory potential of the CCNMGBO is evaluated using multimodal functions. Multimodal functions with fixed dimensions evaluate the CCNMGBO's low-dimensional exploration.

Fig. 6 depicts the outcomes of CCNMGBO's qualitative studies in handling unimodal and multimodal functions in evaluating location and fitness changes to determine the location and fitness variations. In addition to the search history, the plot also displays the trajectory, average fitness, and balance curves (refer to Fig. 7). The search history represents the location and distribution of the population during the iteration. When seen as a trajectory, the characteristics of population location shift in the first half of the first dimension can be seen clearly. As illustrated by average fitness, the average fitness deviation pattern changes over time due to the iterative method. Based on the search history plot, the population in various test functions produced a search trajectory similar to the optimal value, successfully exploring reliable search areas and demonstrating excellent accuracy. Nonetheless, the population is generally found in many locations with local optimum conditions, illustrating the population's ability to balance many local optimal conditions. As illustrated in Fig. 6, the trajectory curve exhibits significant variability throughout the initial iterative operation, with up to 50% of the exploration region covered by the location curve. If the function is uniform, the intensity of the population location progressively falls in the latter iteration stage; if the value of the function changes drastically, the magnitude of the population position similarly fluctuates significantly. When considering the average fitness trajectory during the iterative stage, it is possible to identify the fitness level's dynamic characteristics. It is possible to achieve rapid convergence despite an oscillating average fitness curve because average fitness values tend to drop over time, and the rate of oscillations reduces inversely proportional to the number of iterations.

Additionally, examining the exploration and exploitation stages can be used to improve the effectiveness of the proposed CCNMGBO over the basic GBO by identifying areas for improvement. All 10 benchmark functions are employed to study strong important features (exploration and exploitation) in evaluating the competency of the CCNMGBO over GBO. The variation in individual dimensions indicates whether the population is diverging or gathering in a small region. Populations are dispersed around the search region when the algorithm is diverging, which is referred to as diversification or exploration. On the other hand, when the population converges, the disparity is reduced, and the populations meet in a small space, which is referred to as intensification or exploitation. In order to more accurately depict the population's center, dimension-wise diversity assessment is used in this work, as presented in Eq. (54).

$$Div_j = \frac{1}{n}\sum_{i=1}^{n} \text{median}\left(x^j\right) - x_i^j \tag{54}$$

$$Div = \frac{1}{D}\sum_{j=1}^{D} Div_j \tag{55}$$

where n denotes the population size, median $\left(x^j\right)$ denotes the median of the problem dimension j in the total population, x_i^j denotes the dimension j of the individual i. Calculate the average Div_j for all the individuals after calculating the dimension-wise distance of each individual i from the mean dimension. Finally, Div computes the diversity average across all dimensions. It is possible to calculate the proportion of exploitation and exploration for each iteration using Eqs. (56)–(57) after the population diversity has been recorded for every iteration. The balance

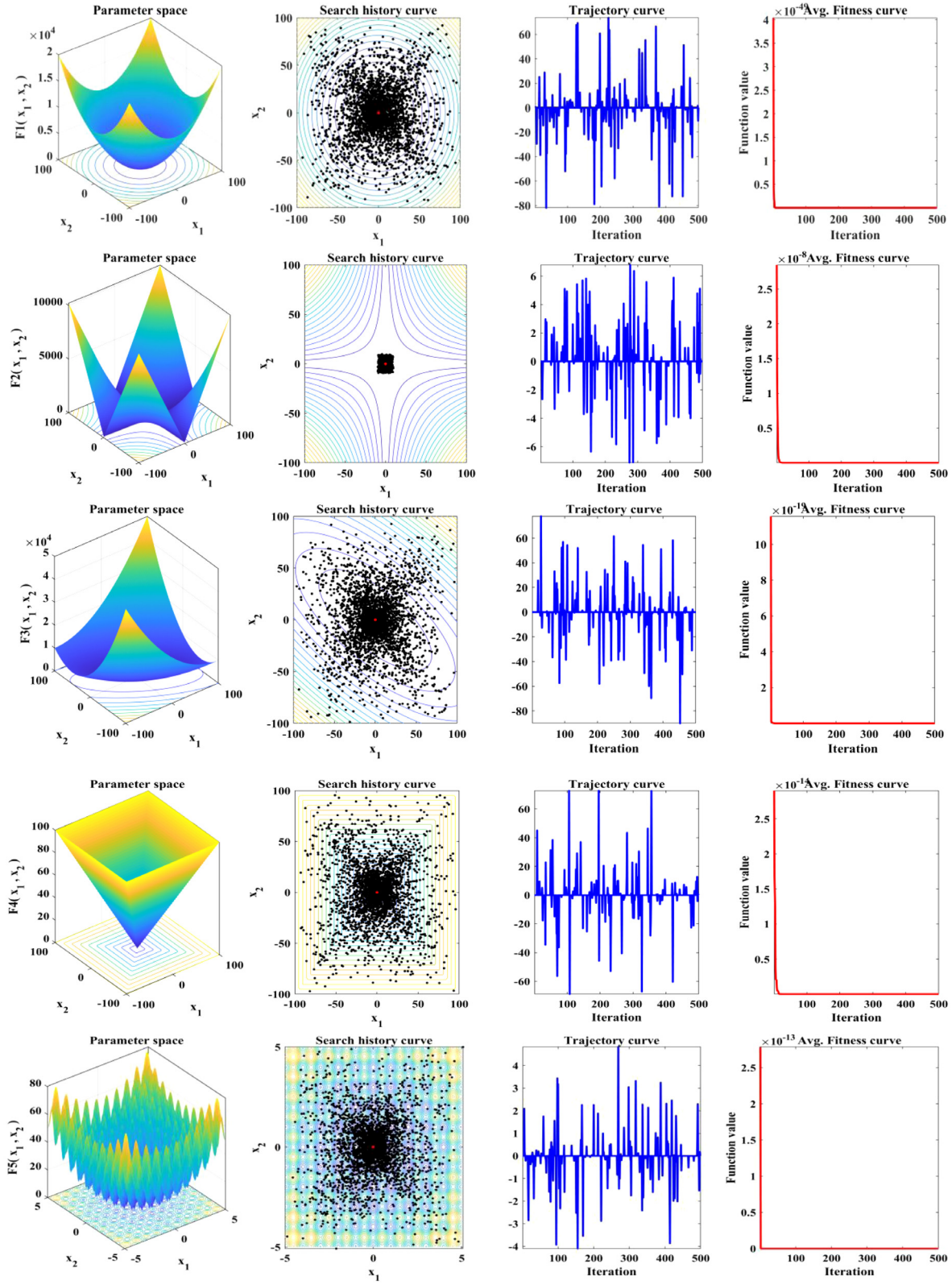

Fig. 6. Various characteristics of the CCNMGBO algorithm on selected 10 benchmark functions.

between exploration and exploitation is calculated using Eq. (58).

$$X_{pl}\,(\%) = \frac{Div}{Div_{max}} \times 100 \tag{56}$$

$$X_{pt}\,(\%) = \frac{|Div - Div_{max}|}{Div_{max}} \times 100 \tag{57}$$

$$X_{bl}\,(\%) = \frac{X_{pl} \times 100 + X_{pt} \times 100}{2} \tag{58}$$

where $X_{pl}\,(\%)$ denotes the exploration in %, $X_{pt}\,(\%)$ denotes the exploitation, $X_{bl}\,(\%)$ denotes the balance between exploration and exploitation, and Div_{max} denotes the maximum diversity in all

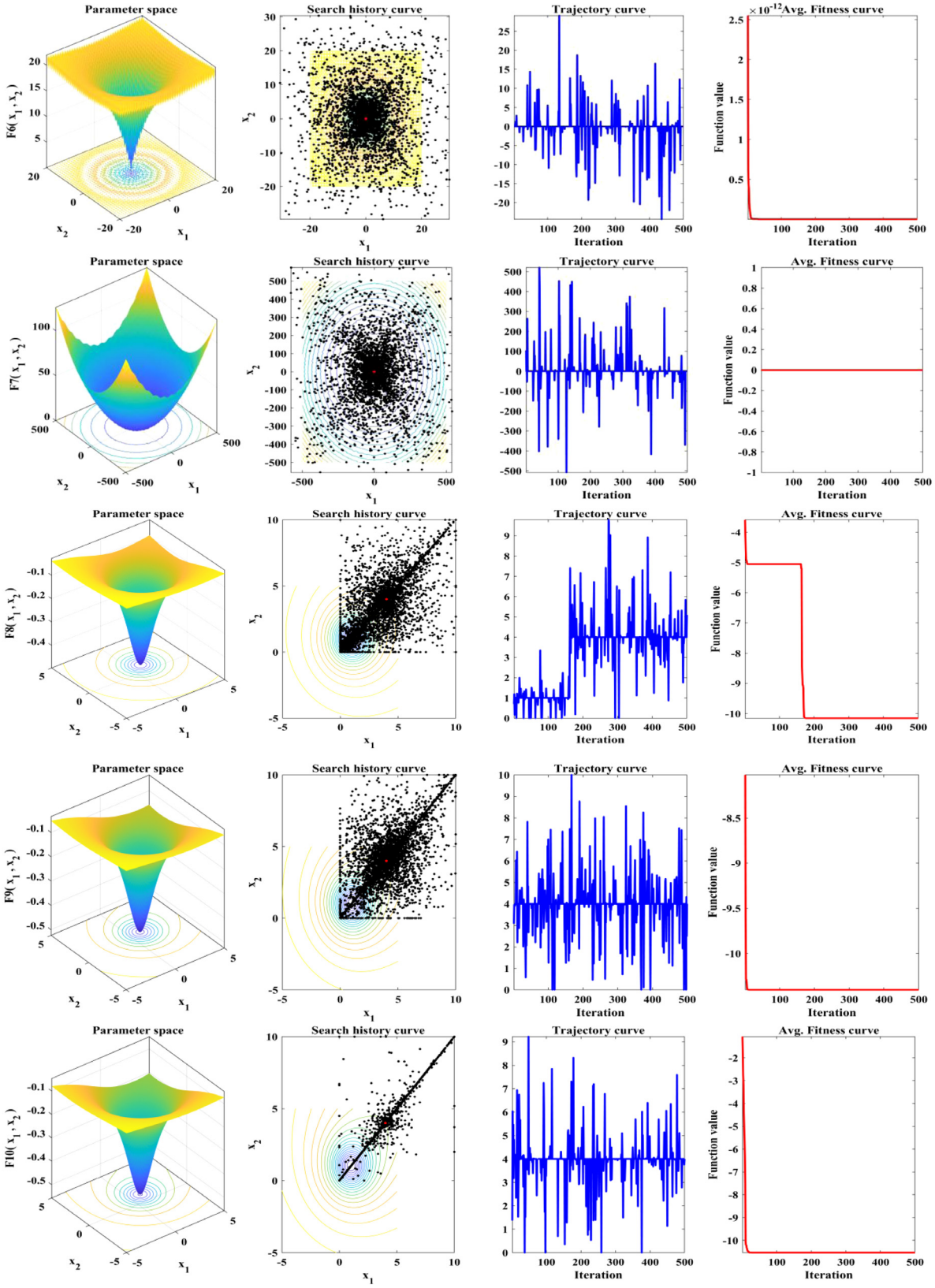

Fig. 6. (*continued*).

Table 3
Mean and STD values found by all algorithms for 10 benchmark test functions.

		CCNMGBO	GBO	EO	GWO	HHO	SCA	WOA	OBLWOA
F1	Mean	**3.761E−286**	1.789E−124	2.624E−42	9.332E−28	1.155E−105	4.866E+00	3.750E−79	1.365E−18
	STD	0.000E+00	1.126E−113	9.586E−42	7.828E−28	2.163E−100	8.502E+00	2.466E−77	1.872E−17
F2	Mean	**2.422E−147**	5.378E−62	2.511E−24	4.103E−17	4.232E−55	2.365E−02	1.466E−54	1.548E−09
	STD	3.026E−141	7.049E−61	4.482E−24	2.911E−17	1.263E−53	3.809E−02	2.828E−51	2.160E−09
F3	Mean	**1.334E−178**	3.269E−101	3.578E−11	8.406E−08	1.074E−83	9.092E+03	4.387E+04	8.824E−20
	STD	0.000E+00	5.425E−99	4.435E−09	4.999E−06	1.036E−72	4.958E+03	1.567E+04	5.899E−16
F4	Mean	**8.801E−110**	4.336E−56	5.635E−11	5.839E−07	1.017E−50	3.789E+01	5.008E+01	1.590E−10
	STD	6.428E−108	1.787E−54	8.491E−10	2.586E−07	1.193E−50	3.992E+00	2.304E+01	1.667E−09
F5	Mean	**0.000E+00**	**0.000E+00**	**0.000E+00**	1.194E−12	**0.000E+00**	2.198E+01	**0.000E+00**	**0.000E+00**
	STD	0.000E+00	0.000E+00	0.000E+00	4.925E+00	0.000E+00	2.081E+01	0.000E+00	0.000E+00
F6	Mean	**8.882E−16**	**8.882E−16**	7.994E−15	1.004E−13	**8.882E−16**	2.024E+01	4.441E−15	1.696E−12
	STD	0.000E+00	0.000E+00	0.000E+00	8.917E−15	0.000E+00	8.827E+00	2.972E−15	2.098E−09
F7	Mean	**0.000E+00**	**0.000E+00**	**0.000E+00**	**0.000E+00**	**0.000E+00**	1.228E+00	**0.000E+00**	**0.000E+00**
	STD	0.000E+00	0.000E+00	0.000E+00	0.000E+00	0.000E+00	5.912E−01	0.000E+00	0.000E+00
F8	Mean	**−10.1532**	**−10.1532**	**−10.1532**	−10.1528	−5.0546	−5.5452	−10.1528	−10.1159
	STD	2.2799	2.7923	3.3643	0.0012	0.0006	2.0864	2.8372	0.0241
F9	Mean	**−10.4029**	−5.0877	**−10.4029**	−10.4020	−5.0871	−9.4351	−10.4005	−10.3664
	STD	0.0000	2.9113	2.9113	0.0013	0.0061	3.4010	2.5994	0.0580
F10	Mean	**−10.5364**	**−10.5364**	**−10.5364**	−10.5354	−5.1285	−3.9913	−10.4669	−10.5204
	STD	0.0005	3.5161	2.9968	2.4185	0.0128	1.4140	2.5939	0.0306

Table 4
FRT values obtained by all algorithms for 10 benchmarks.

	CCNMGBO	GBO	EO	GWO	HHO	SCA	OBLWOA	WOA
F1	1	2	5	6	3	8	4	7
F2	1	2	5	6	3.4	8	3.6	7
F3	1	2	5	6	3	7	8	4
F4	1	2.2	4.2	6	2.8	7.2	7.8	4.8
F5	3.5	3.5	3.5	7	3.5	8	3.5	3.5
F6	2.2	2.2	5	6.4	2.2	8	4.1	5.9
F7	4	4	4	4	4	8	4	4
F8	4	3.4	2.6	2.6	6.8	7.8	5	3.8
F9	2	3.4	2.7	5.1	7.2	6.6	5.8	3.2
F10	2.4	3.9	4.6	2.4	6.4	7.6	5.8	3.4
Average FRT	**2.21**	2.86	4.16	5.15	4.23	7.62	5.16	4.66
Rank	**1**	2	3	6	4	8	7	5

iterations. Therefore, as an extra benefit, Fig. 7 depicts a visual demonstration of a balance between the exploration and exploitation phases, in which the quantities of exploration and exploitation in the search space are displayed. Based on the curves provided in Fig. 7, it can be concluded that CCNMGBO can properly balance the exploitation and exploration proportions for most of the search period.

The STD and mean values of all test functions were utilized to analyze the results to prove the overall quality of the results obtained by CCNMGBO. Table 3 lists all of the statistical findings on 10 typical benchmark functions, as well as a summary of the results. The findings are comparable, and it was discovered that the proposed CCNMGBO obtained a greater proportion of best values (10/10) than the other algorithms, including GBO. As a result, the CCNMGBO algorithm is ranked best among other algorithms, with the GBO and EO algorithms being second and third, respectively. According to Table 3, however, the CCNMGBO provided favorable results for most functions, indicating that the algorithm strikes a reasonable balance between the exploration and exploitation stages.

In addition, as indicated in Table 4, the effectiveness of the CCNMGBO is analyzed using a statistical Friedman's rank test (FRT) to determine its overall effectiveness. For each benchmark function, the FRT results are shown in Table 4. Afterward, as indicated in Table 4, the total sum of all ranks for all 10 benchmark functions was calculated. Such results suggested that the proposed CCNMGBO outperformed the basic GBO and all other selected algorithms compared to their performance in the test.

In addition, the runtime (RT) of the CCNMGBO is compared to that of other methods in Table 5. The basic GBO has the shortest RT, with a total RT of 0.852 s. This is followed by the CCNMGBO, which has a total RT of 0.904 s and is the second-shortest RT. On the other hand, the OBLWOA has the longest RT, clocking in at 30.209 s. Each algorithm has assigned a rank based on the total RT values. Based on RT values, the basic GBO was ranked best, followed by the CCNMGBO, GWO, SCA, EO, HHO, WOA, and OBLWOA.

The CCNMGBO converges significantly quicker than the other methods, as illustrated in Fig. 8. During the iteration phase, the convergence graph indicates the fitness value that is most appropriate for the test functions. The convergence curve depicts how the mean fitness of the optimum fitness value desired by the population varies over time, as measured by the population's fitness. By observing the downward trend of the graph, we can determine the rate of convergence and the point at which it transitions from the exploration to the exploratory phase. Because of CCNM mechanisms, the convergence curve exhibits stable behavior in the last iterations, indicating that the convergence guarantee has been met. The global optimum is discovered for unimodal functions through how the CCNMGBO is formed. When employed for complicated multimodal functions, however, the genuine effectiveness of each process is apparent and helpful due to how the CCNMGBO is developed.

On the other hand, the boxplot is being used to measure the reliability of all of the algorithms that have been selected. As

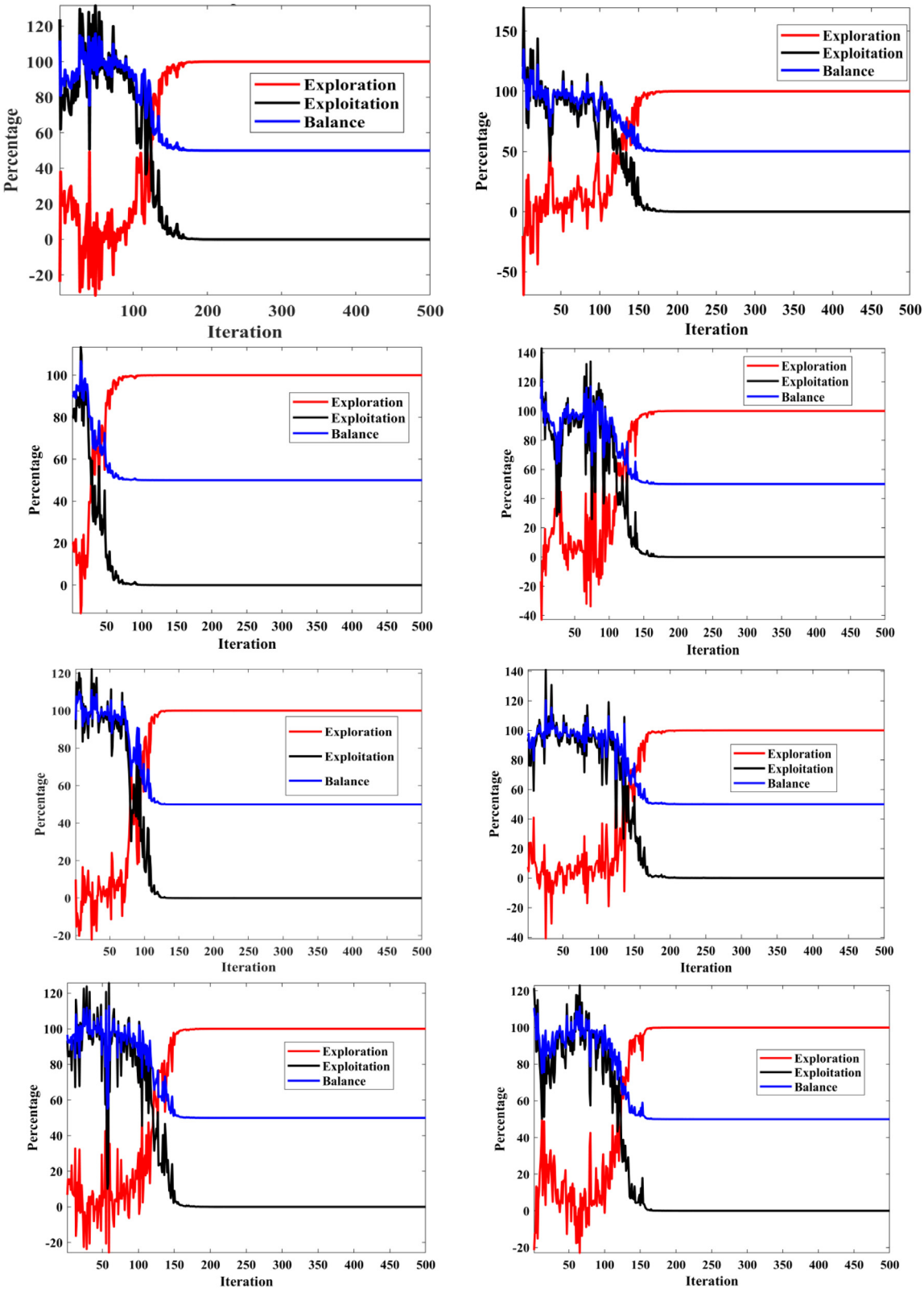

Fig. 7. Exploration and exploitation analysis of CCNMGBO algorithm on selected 10 benchmark functions.

illustrated in Fig. 9, the boxplot assessment of all specified techniques on a set of 10 benchmark test functions was performed. In order to show that the suggested CCNMGBO is more trustworthy than any other method studied, graphical representations are presented.

4.2. Results on solar PV parameter estimation problems

As discussed earlier, the CCNMGBO algorithm is mainly applied to three different PV models: SDM, DDM, and PV modules, to solve unknown parameters. Two data sets are being used in the

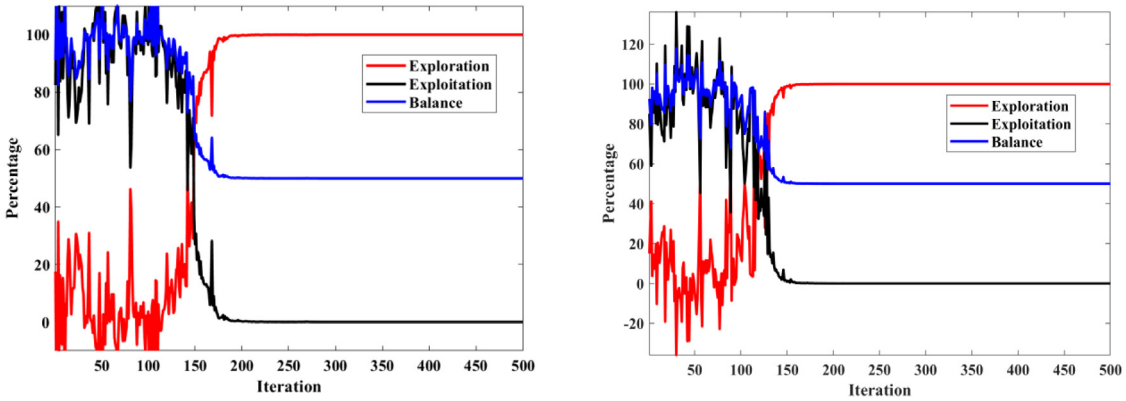

Fig. 7. (*continued*).

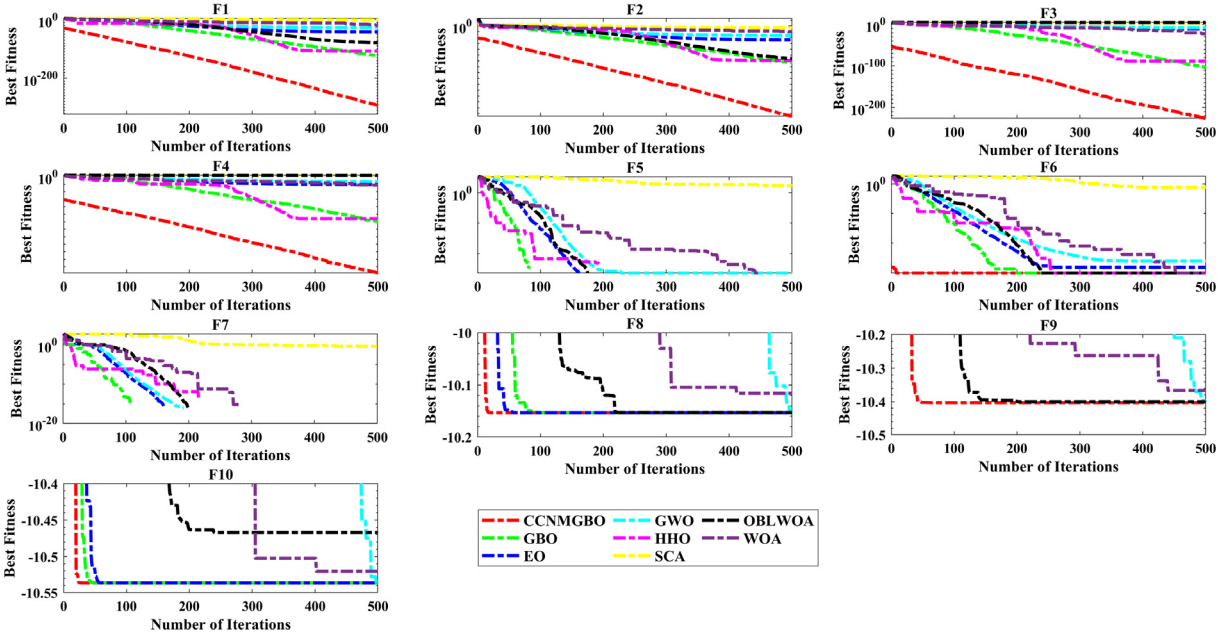

Fig. 8. Convergence plots of all benchmark test functions.

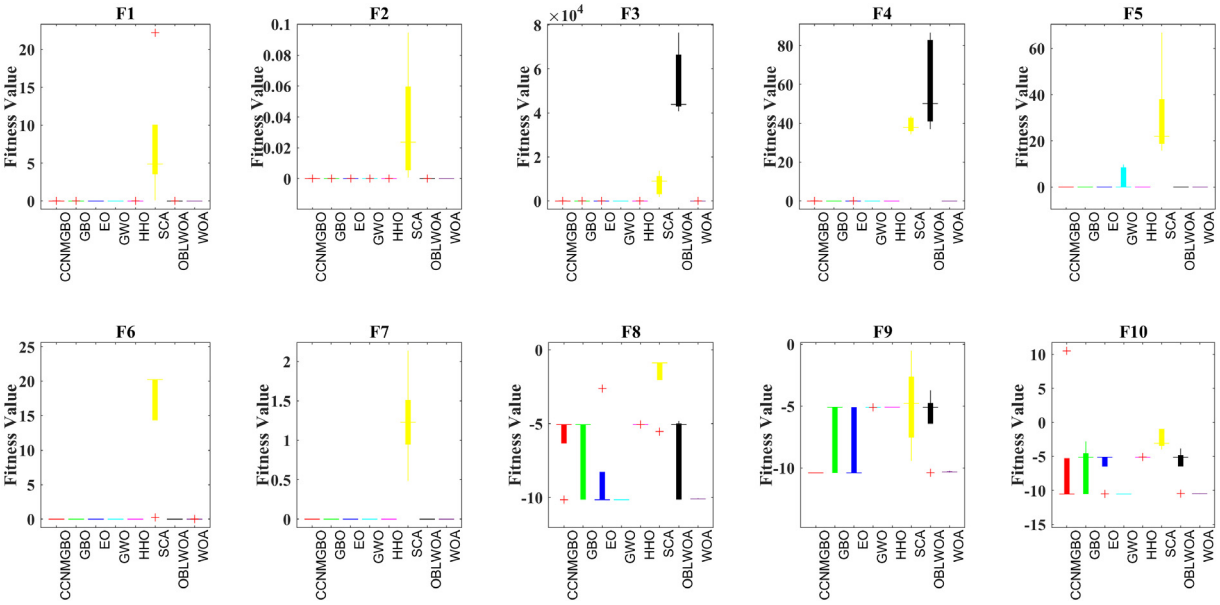

Fig. 9. Boxplot analysis of all benchmark test functions.

Table 5
RT values in seconds obtained by all algorithms for 10 benchmarks.

	CCNMGBO	GBO	EO	GWO	HHO	SCA	OBLWOA	WOA
F1	0.141	0.144	0.609	0.178	0.872	0.138	3.181	0.928
F2	0.063	0.063	0.381	0.081	0.556	0.056	2.775	0.713
F3	0.153	0.156	0.706	0.172	0.719	0.306	2.906	1.347
F4	0.069	0.059	0.397	0.072	0.528	0.072	2.775	0.694
F5	0.106	0.122	0.691	0.156	0.797	0.203	3.628	0.781
F6	0.063	0.081	0.438	0.1	0.506	0.1	2.884	0.709
F7	0.066	0.084	0.438	0.097	0.491	0.125	2.919	0.819
F8	0.056	0.034	0.431	0.047	0.481	0.113	2.919	0.769
F9	0.103	0.059	0.556	0.053	0.609	0.147	3.381	0.916
F10	0.084	0.05	0.463	0.059	0.509	0.144	2.841	0.816
Sum of RT values in seconds	0.904	**0.852**	5.11	1.015	6.068	1.404	30.209	8.492
Rank	2	**1**	5	3	6	4	8	7

Table 6
Parameter bounds for all selected PV models.

Parameters	RTC Cell		PhotoWatt-PWM201		KC200GT		ST40		SM55	
	UB	LB	UB	LB	UB	LB	UB	LB	UB	LB
I_{ph} (A)	1	0	8	0	16.8	0	5.4	0	6.9	0
a (SDM)	2	1	50	1	4	1	4	1	4	1
a_1, a_2 and a_3 (DDM and TDM)	2	1	50	1	4	1	4	1	4	1
I_{sd} (μA) (SDM)	1	0	50	0	100	0	100	0	100	0
I_{sd1}, $I_{sd2,}$ and I_{sd3} (μA) (DDM and TDM)	1	0	50	0	100	0	100	0	100	0
R_{se} (Ω)	0.5	0	0.4	0	2	0	2	0	2	0
R_{sh} (Ω)	100	0	1500	0	5000	0	5000	0	5000	0

Table 7
Estimated parameters by all algorithms for SDM of RTC Si cell.

Algorithm	I_p (A)	I_{sd} (A)	R_{se} (Ω)	R_{sh} (Ω)	a	*RMSE*	*sig*
CCNMGBO	**0.760776**	**3.23E−07**	**0.036377**	**53.71854**	**1.481184**	**0.000986**	
OBLWOA	**0.760775**	**3.23E−07**	**0.036376**	**53.72833**	**1.48122**	**0.000986**	=
GWO	0.758126	8.5E−08	0.041655	58.38624	1.357381	0.003414	+
HHO	0.762128	6.67E−07	0.033834	55.91702	1.558336	0.00242	+
SCA	0.767236	0.000001	0	10.79	1.619492	0.04214	+
WOA	0.760177	3.63E−07	0.036016	70.14889	1.492681	0.001144	+
GBO	0.760775	3.23E−07	0.036377	53.72801	1.481198	0.000987	+
EO	0.760442	4.98E−07	0.034563	71.33316	1.526048	0.001297	+
SMA (Qais et al., 2019b)	0.656057	1.00E−06	0	100	1.61398	0.0098879	+
IJAYA (Wang et al., 2022)	0.760748	3.23E−07	0.036377	54.1794	1.48157	0.000987	+
OLGBO (Ye et al., 2009)	0.760776	3.23E−07	0.0363771	53.7185	1.48118	**0.000986**	=
RBGBO (Ma et al., 2013)	0.7608	3.23E−07	0.036401	53.7185	1.4811	**0.000986**	=
CGBO (Montoya et al., 2020)	0.7608	3.23E−07	0.0364	53.7185	1.4812	**0.000986**	=
MPA (Montoya et al., 2020)	0.7607	9.49E−07	0.0317	99.9999	1.5983	0.002341	+

experiment, one of which includes 26 pairs of voltage and current samples measured from an RTC France Si cell at an irradiance of 1000 W/m^2 and a temperature of 33 °C, and the second of which comprises samples measured from a PhotoWatt-PWP201 PV module consisting of at an irradiance of 1000 W/m^2 and a temperature of 45 °C. Consequently, the SDM and DDM identification experiments for both the RTC France Si cell and the PhotoWatt-PWP201 PV module were carried out in this paper. The upper and lower bounds of all unknown parameters of various PV models are listed in Table 6.

The performance of all algorithms is compared based on the obtained RMSE values, the performance indicators, such as the relative error (RE) and absolute error (IAE), the statistical values of Min, Max, Mean, Median, STD, RT, statistical tests, such as WSRT and FRT, convergence graph, and boxplots. As discussed earlier, each algorithm is run 30 times to observe the reliability of all algorithms. In accordance with the previous statement, the difference between estimated and experimental value is easy to realize that the RMSE can conceptually describe. The lesser the RMSE value, the near the estimated parameter is to the experimental data, indicating that the selected method is more effective in defining unidentified parameters in the PV cell or PV module. In other phrases, the models described by the algorithm represent the real cell and module characteristics. It is also essential to decrease the error value as small as possible.

4.2.1. Case 1: Results of SDM/DDM/TDM of RTC France Si cell

This section discusses the results obtained by all algorithms, including the proposed CCNMGBO algorithm. The reliability and efficiency of the proposed CCNMGBO are increased compared to the basic version of the GBO algorithm. Tables 7–9 list the parameters obtained by all algorithms after 30 individual runs of each algorithm for both SDM, DDM, and TDM PV models, respectively. It can be seen from Table 7 that the RMSE obtained by the opposition-based learning WOA (OBLWOA) and the CCNMGBO is similar, i.e., 9.8602E–04; however, the value is better than all other selected algorithms. It can be seen from Table 8 that the RMSE value of the DDM obtained by the proposed CCNMGBO is very much better than all other algorithms, i.e., 9.8252E–04. Similarly, it can be seen from Table 9 that the RMSE value of the TDM obtained by the proposed CCNMGBO is very much better than all other algorithms, i.e., 9.823E–04. Even though OBLWOA results are equal to the CCNMGBO (in the SDM case), the reliability and convergence speed of the proposed CCNMGBO is higher than the OBLWOA for SDM, DDM, and TDM. The performance of the proposed CCNMGBO was similar to other variants of GBO called OLGBO, RBGBO, and CGBO. However, the convergence speed and runtime of the CCNMGBO are quicker than the other variants. Therefore, the proposed CCNMGBO is a robust tool for solving the parameter estimation problem. To prove the same,

Table 8
Estimated parameters by all algorithms for DDM of RTC Si cell.

Algorithm	I_p (A)	I_{sd1} (A)	R_{se} (Ω)	R_{sh} (Ω)	a_1	I_{sd2} (A)	a_2	*RSME*	*sig*
CCNMGBO	**0.760778**	**2.56E−07**	**0.036609**	**54.91694**	**1.461336**	**5.07E−07**	**1.999971**	**0.000982**	
OBLWOA	0.760698	5.18E−07	0.036685	55.46256	1.999999	2.51E−07	1.459528	0.000984	+
GWO	0.760143	3.36E−07	0.036153	74.72409	1.511655	5.34E−08	1.449055	0.001245	+
HHO	0.758546	2.23E−07	0.040953	64.62528	1.783422	7.91E−08	1.3562	0.002909	+
SCA	0.747457	3.88E−07	0	11.30977	1.975745	5.18E−07	1.546508	0.044195	+
WOA	0.761388	4.35E−07	0.033973	60.58667	1.5165	5.47E−07	1.975304	0.001603	+
GBO	0.760776	2.49E−07	0.036377	53.71822	1.482367	7.4E−08	1.477372	0.000986	+
EO	0.760493	7.96E−08	0.035941	63.29432	1.999562	3.58E−07	1.491978	0.001046	+
SMA (Qais et al., 2019b)	0.68657	8.22E−07	0.0322533	75.5207	1.59994	6.86E−07	1.913999	0.0116001	+
IJAYA (Wang et al., 2022)	0.76097	1.01E−07	0.036588	52.1202	1.70699	2.64E−07	1.46602	0.0009928	+
OLGBO (Ye et al., 2009)	0.760781	7.43E−07	0.036737	55.4710	2.00000	2.27E−07	1.45125	**0.000982**	=
RBGBO (Ma et al., 2013)	0.760781	6.56E−07	0.036689	55.2646	2.00000	2.37E−07	1.45504	0.000983	+
CGBO (Montoya et al., 2020)	0.7608	2.23E−07	0.03681	55.5658	1.4488	8.03E−07	2	0.000983	+
MPA (Montoya et al., 2020)	0.7602	4.52E−08	0.0387	60.6960	1.3342	6.67E−07	1.7063	0.001277	+

Table 9
Estimated parameters by all algorithms for TDM of RTC Si cell.

Algorithm	I_p (A)	I_{sd1} (A)	R_{se} (Ω)	R_{sh} (Ω)	a_1	I_{sd2} (A)	a_2	I_{sd3} (A)	a_3	*RSME*	*sig*
CCNMGBO	0.7608	1.98E−07	0.0365	54.2389	1.9855	2.95E−07	1.4734	5.80E−11	2.0757	**9.823E−04**	
OBLWOA	0.7607	1.31E−10	0.0355	61.1985	1.1712	4.23E−07	1.5110	0.00E+00	3.5007	1.089E−03	+
GWO	0.7625	7.79E−08	0.0312	44.4798	1.7042	7.27E−07	1.5725	4.17E−07	4.9705	3.043E−03	+
HHO	0.7611	9.86E−07	0.0277	51.3586	1.6076	2.46E−07	1.9027	5.30E−07	3.4340	5.466E−03	+
SCA	0.7509	6.85E−07	0.0000	15.9483	1.7307	9.18E−07	1.6443	0.00E+00	3.9203	3.764E−02	+
WOA	0.7608	7.13E−07	0.0316	75.8400	1.5695	2.08E−07	1.8583	5.99E−07	3.8111	2.537E−03	+
GBO	0.7608	6.24E−07	0.0367	55.0811	1.9996	2.40E−07	1.4559	4.61E−07	4.1731	9.845E−04	+
EO	0.7600	4.09E−18	0.0343	99.9854	1.6622	5.65E−07	1.5394	0.00E+00	4.8556	1.542E−03	+
SMA (Qais et al., 2019b)	0.78865	0	0.03674	50.2650	1.9616	1.00E−06	1.8863	0	1.4555	1.176E−03	+
IJAYA (Wang et al., 2022)	0.76084	2.32E−08	0.03645	52.5310	1.47535	2.87E−07	1.4779	3.01E−08	1.9001	9.873E−04	+
OLGBO (Ye et al., 2009)	0.76077	5.10E−10	0.03674	55.4908	1.5843	7.51E−07	2.0000	2.25E−07	1.45076	9.824E−04	+
RBGBO (Ma et al., 2013)	0.76073	8.19E−11	0.03665	56.7349	1.99997	2.27E−07	1.4549	7.84E−07	1.99584	9.841E−04	+

the convergence curve and box plot is illustrated in Figs. 10 and 11, respectively. From Fig. 10, it is observed that the convergence speed of the CCNMGBO is very much higher than all selected algorithms. From Fig. 11, it can be seen that the reliability (very less standard deviation (STD)) of the CCNMGBO is higher than other selected algorithms. In Tables 7 and 8, the symbol '+' indicates that the CCNMGBO is better than the other algorithm, '−' indicates that the CCNMGBO is poor than other algorithms, and '=' indicates that the performance of CCNMGBO is equal to the other algorithm. It is also noted from Tables 7–8 and Figs. 10–11 that the performance of SCA is worse than the CCNMGBO, followed by HHO, GWO, WOA, EO, GBO, MPA, OBLWOA, and other variants of GBO on average. The other statistical analysis of all algorithms in estimating the solar cell parameters is discussed in detail in the later section of this paper. The statistical test analysis is also discussed in the later section to prove the superiority of the CCNMGBO over other algorithms. The boldface in all tables indicates the best results.

In addition to the above-discussed results, the I–V characteristic of the RTC Si cell estimated by the proposed CCNMGBO algorithm for SDM, DDM, and TDM is illustrated in Fig. 12. It can be seen from Fig. 12 that the estimated data points and experimental data points are matching, which proves the efficiency of the CCNMGBO over other algorithms.

Further, to prove the superiority of the proposed CCNMGBO algorithm, the performance indicators, such as IAE and RE, are calculated using the following formulas for all data samples (Muhsen et al., 2016; Nunes et al., 2019).

$$IAE_i = \left|I_{exp} - I_{sim}\right| \tag{59}$$

$$RE = \frac{I_{exp} - I_{sim}}{I_{exp}} \tag{60}$$

$$IAE_P = \left|P_{exp} - P_{sim}\right| \tag{61}$$

where IAE_i denotes the absolute error with respect to the current, I_{exp} denotes the experimental current sample, I_{sim} demotes the estimated/simulated current of the respective PV model, IAE_P denotes the absolute error with respect to the power, P_{exp} denotes the experimental power, i.e., $P_{exp} = V_{exp} \times I_{exp}$, P_{sim} denotes the estimated power, i.e., $P_{exp} = V_{exp} \times I_{sim}$, and V_{exp} denotes the experimental voltage sample. Tables 10–12 list the IAE and RE values for all data samples obtained by the proposed CCNMGBO algorithms. It can be seen from Table 10 that the values of IAE_i are less than 1.300E−03, IAE_P is less than 1.458E−03, and *RE* is less than 8.033E−03. It can be seen from Table 11 that the values of IAE_i are less than 2.500E−03, IAE_P is less than 1.504E−03, and *RE* is less than 7.619E−03. Similarly, it can be seen from Table 12 that the values of IAE_i are less than 1.557E−04, IAE_P is less than 1.407E−04, and *RE* is less than 1.161E−02. The average values of IAE_i, IAE_P, and *RE* are equal to 8.269E−04, 3.344E−04, and 4.674E−03, respectively, for SDM, 4.308E−03, 8.077E−04, and 3.460E−04, respectively for DDM, and 2.053E−03, 8.431E−04, and 1.122E−02, respectively for TDM which shows that the proposed CCNMGBO can able to extract the actual characteristics of SDM, DDM, and TDM.

4.2.2. Case 2: Results of SDM/DDM/TDM of Photowatt- PWP201 PV module

Similar to the PV cell, the reliability and efficiency of the proposed CCNMGBO are increased compared to the basic version of the GBO algorithm for the PV module. Tables 13–15 list the parameters obtained by all algorithms after 30 individual runs of each algorithm for both the SDM, DDM, and TDM PV modules, respectively. It can be seen from Table 13 that the RMSE obtained by the OBLWOA and the CCNMGBO is similar, i.e., 2.425E−03; however, the value is better than all other selected algorithms. Similarly, the RMSE values of the DDM and TDM obtained by the proposed CCNMGBO are very much better than all other algorithms, i.e., 2.425E−03. Even though OBLWOA results are equal to the CCNMGBO (in the SDM case), the reliability and convergence speed of the CCNMGBO is higher than the OBLWOA for SDM, DDM, and TDM. The performance of the proposed CCNMGBO was

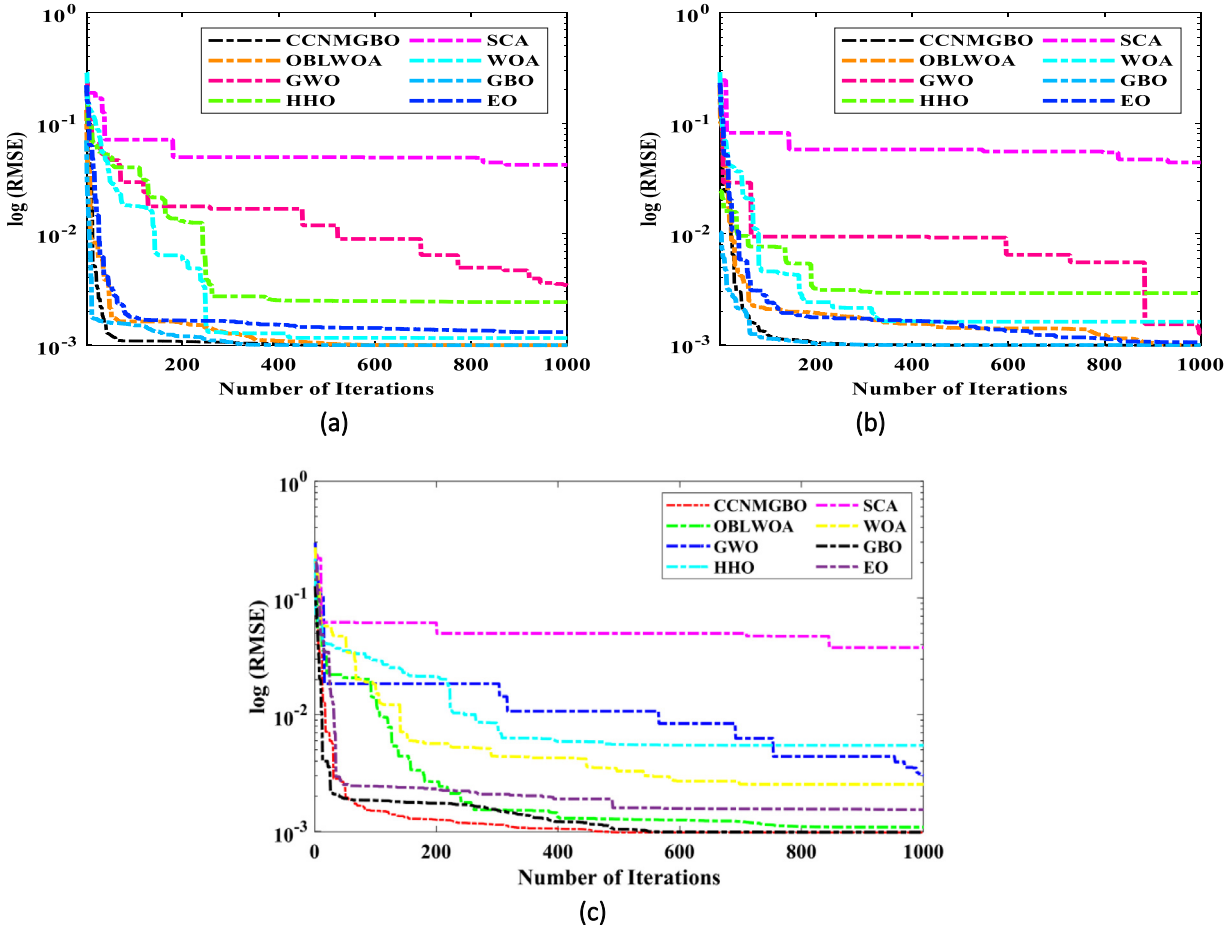

Fig. 10. Convergence curves obtained for case 1; (a) SDM, (b) DDM, (c) TDM.

Table 10
Performance metrics of the CCNMGBO on SDM of the RTC France Si cell.

Data points	V_{exp} (V)	I_{exp} (A)	I_{est} (A)	P_{exp} (W)	P_{est} (W)	IAE_i (A)	IAE_P (W)	RE_i (A)
1	−0.2057	0.764	0.7641	−0.1571548	−1.572E−01	1.000E−04	2.057E−05	1.309E−04
2	−0.1291	0.762	0.7627	−0.0983742	−9.846E−02	7.000E−04	9.037E−05	9.186E−04
3	−0.0588	0.7605	0.7614	−0.0447174	−4.477E−02	9.000E−04	5.292E−05	1.183E−03
4	0.0057	0.7605	0.7602	0.0043349	4.333E−03	3.000E−04	1.760E−06	3.945E−04
5	0.0646	0.76	0.7591	0.049096	4.904E−02	9.000E−04	5.814E−05	1.184E−03
6	0.1185	0.759	0.758	0.0899415	8.982E−02	1.000E−03	1.185E−04	1.318E−03
7	0.1678	0.757	0.7571	0.1270246	1.270E−01	1.000E−04	1.678E−05	1.321E−04
8	0.2132	0.757	0.7561	0.1613924	1.612E−01	9.000E−04	1.919E−04	1.189E−03
9	0.2545	0.7555	0.7551	0.1922748	1.922E−01	4.000E−04	1.018E−04	5.295E−04
10	0.2924	0.754	0.7537	0.2204696	2.204E−01	3.000E−04	8.772E−05	3.979E−04
11	0.3269	0.7505	0.7514	0.2453385	2.456E−01	9.000E−04	2.942E−04	1.199E−03
12	0.3585	0.7465	0.7474	0.2676203	2.679E−01	9.000E−04	3.226E−04	1.206E−03
13	0.3873	0.7385	0.7401	0.2860211	2.866E−01	1.600E−03	6.196E−04	2.167E−03
14	0.4137	0.728	0.7274	0.3011736	3.009E−01	6.000E−04	2.482E−04	8.242E−04
15	0.4373	0.7065	0.707	0.3089525	3.092E−01	5.000E−04	2.186E−04	7.077E−04
16	0.459	0.6755	0.6753	0.3100545	3.100E−01	2.000E−04	9.180E−05	2.961E−04
17	0.4784	0.632	0.6308	0.3023488	3.018E−01	1.200E−03	5.741E−04	1.899E−03
18	0.496	0.573	0.5719	0.284208	2.837E−01	1.100E−03	5.456E−04	1.920E−03
19	0.5119	0.499	0.4996	0.2554381	2.557E−01	6.000E−04	3.071E−04	1.202E−03
20	0.5265	0.413	0.4136	0.2174445	2.178E−01	6.000E−04	3.159E−04	1.453E−03
21	0.5398	0.3165	0.3175	0.1708467	1.714E−01	1.000E−03	5.398E−04	3.160E−03
22	0.5521	0.212	0.2122	0.1170452	1.172E−01	2.000E−04	1.104E−04	9.434E−04
23	0.5633	0.1035	0.1023	0.0583016	5.763E−02	1.200E−03	6.760E−04	7.159E−03
24	0.5736	−0.01	−0.0087	−0.005736	4.990E−03	1.300E−03	7.457E−04	1.300E−03
25	0.5833	−0.123	−0.1255	−0.0717459	7.320E−02	2.500E−03	1.458E−03	8.033E−03
26	0.59	−0.21	−0.2085	−0.1239	1.230E−01	1.500E−03	8.850E−04	7.143E−03
Average			–			8.269E−04	3.344E−04	4.674E−03

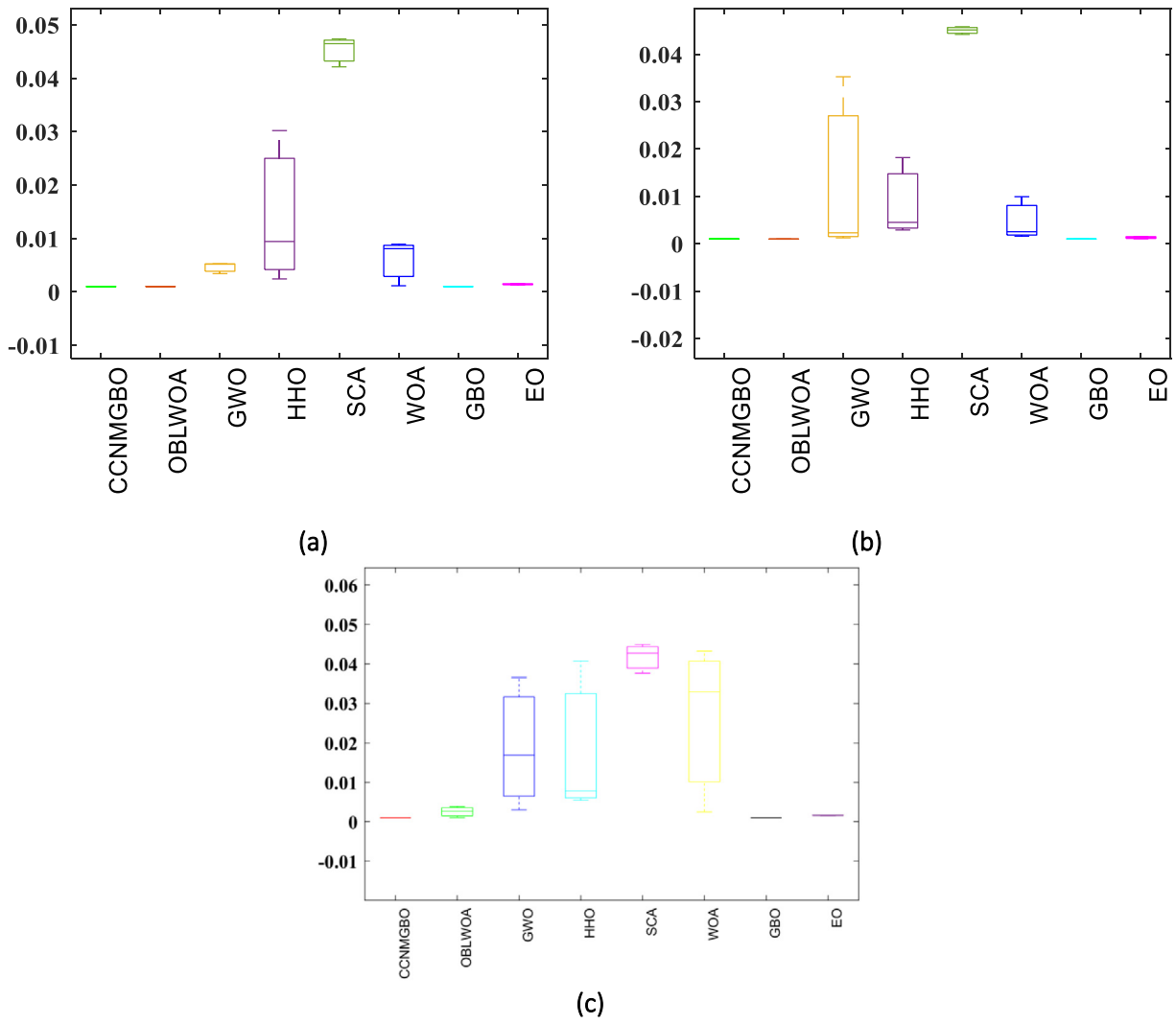

Fig. 11. Box plots obtained for case 1; (a) SDM, (b) DDM, (c) TDM.

also better than other variants of GBO called OLGBO, RBGBO, and CGBO. Therefore, the proposed CCNMGBO is a robust tool for solving the parameter estimation problem. The convergence curve and box plot are illustrated in Figs. 13 and 14, respectively. From Fig. 13, it is observed that the convergence speed of the CCNMGBO is higher than all selected algorithms. From Fig. 14, it can be seen that the reliability of the CCNMGBO is higher than other selected algorithms. It is also noted in Tables 13–15 and Figs. 13–14 that the performance of SCA is worse than the CCNMGBO, followed by WOA, HHO, GWO, EO, GBO, MPA, OBLWOA, and other variants of GBO on average.

In addition to the above-discussed results, the I–V characteristic of the PhotoWatt-PWP-201 PV module estimated by the proposed CCNMGBO algorithm for SDM, DDM, and TDM is illustrated in Fig. 15. It can be seen from Fig. 15 that the estimated data points and experimental data points are matching, which proves the efficiency of the CCNMGBO over other algorithms.

Further, to prove the superiority of the proposed CCNMGBO algorithm, the performance indicators, such as IAE and RE, are calculated. Tables 16–18 list the IAE and RE values for all data samples obtained by the proposed CCNMGBO algorithms. It can be seen from Table 16 that the values of IAE_i are less than 4.800E–03, IAE_P is less than 7.931E–02, and RE is less than 6.931E–03. It can be seen from Table 17 that the values of IAE_i are less than 7.261E–03, IAE_P is less than 8.097E–02, and RE is less than 4.900E–03. Similarly, It can be seen from Table 18 that the values of IAE_i are less than 4.627E–04, IAE_P is less than 7.646E–03, and RE is less than 4.581E–03. The average values of IAE_i, IAE_P, and RE are equal to 4.890E–02, 2.061E–02, and 2.154E–03, respectively, for SDM, 2.188E–03, 2.073E–02, and 1.968E–03, respectively for DDM, 4.743E–03, 4.971E–02, and 7.090E–04, respectively for TDM, which shows that the proposed CCNMGBO can able to extract the actual characteristics of SDM, DDM, and TDM.

4.2.3. Average runtime analysis

The performance of all algorithms is assessed using the computation cost, which is one of the essential performance metrics. The total runtime of all algorithms over 30 runs on two different cases are listed in Table 19. The same has been graphically illustrated in Fig. 16, and it can be seen from Fig. 16 that each algorithm takes different runtimes while solving the various PV models. Out of all algorithms, the EO takes the highest time, i.e., 2.36E+03, and the basic version of GBO takes the lowest time, i.e., 5.98E+02. However, the proposed CCNMGBO takes more time than the basic version but less time than other selected algorithms. The CPU time is high for EO, followed by SCA, HHO, WOA, OBLWOA, GWO, CCNMGBO, and GBO.

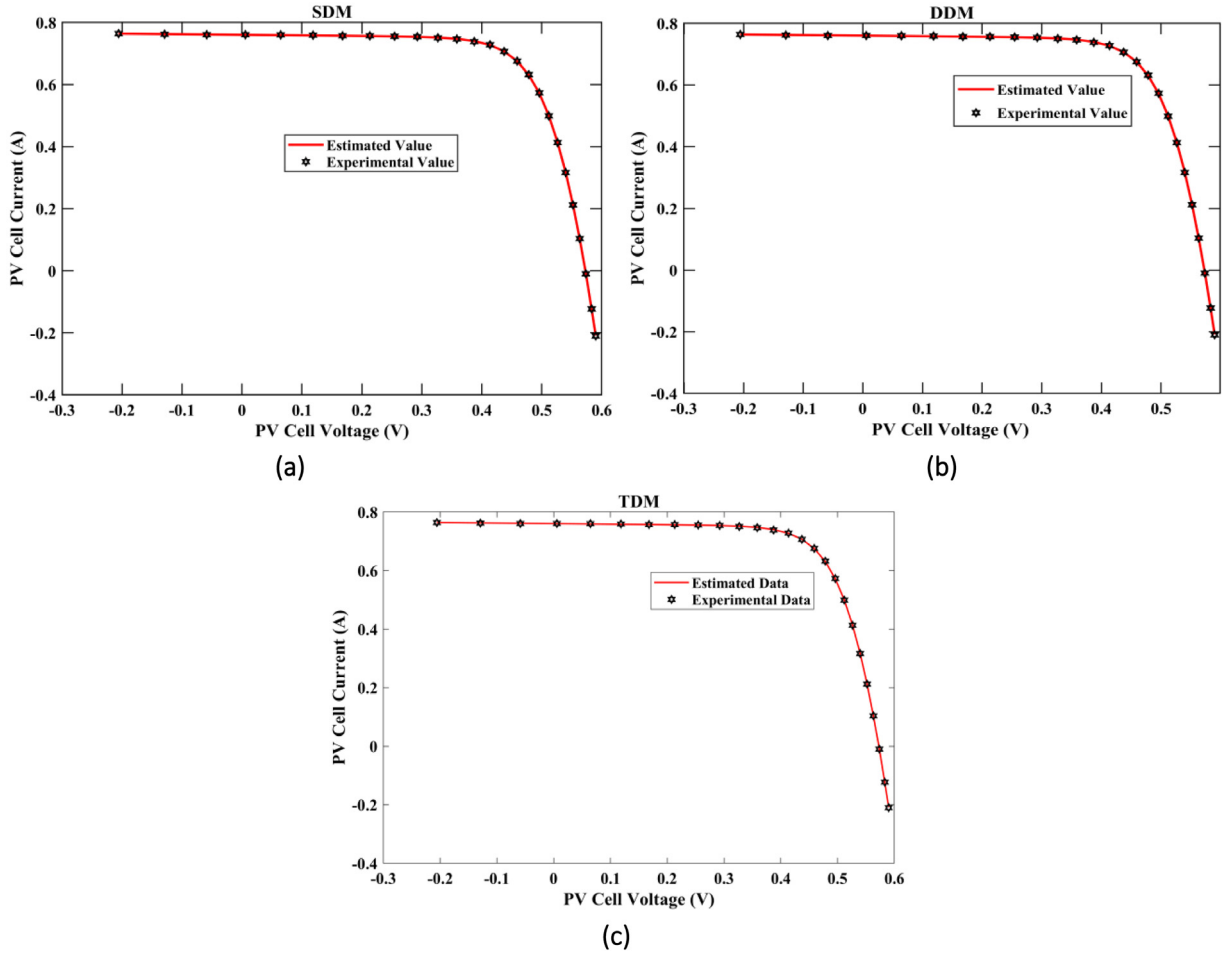

Fig. 12. I–V characteristics of the RTC Si cell by CCNMGBO; (a) SDM, (b) DDM, (c) TDM.

Table 11
Performance metrics of the CCNMGBO on DDM of the RTC France Si cell.

Data points	V_{exp} (V)	I_{exp} (A)	I_{est} (A)	P_{exp} (W)	P_{est} (W)	IAE_i (A)	IAE_P (W)	RE_i (A)
1	−0.2057	0.764	0.764	−0.1572	−1.572E−01	0.000E+00	4.520E−05	0.000E+00
2	−0.1291	0.762	0.7626	−0.0984	−9.845E−02	6.000E−04	5.166E−05	7.874E−04
3	−0.0588	0.7605	0.7613	−0.0447	−4.476E−02	8.000E−04	6.444E−05	1.052E−03
4	0.0057	0.7605	0.7602	0.0043	4.333E−03	3.000E−04	3.314E−05	3.945E−04
5	0.0646	0.76	0.7591	0.0491	4.904E−02	9.000E−04	6.214E−05	1.184E−03
6	0.1185	0.759	0.7581	0.0899	8.983E−02	9.000E−04	6.515E−05	1.186E−03
7	0.1678	0.757	0.7571	0.127	1.270E−01	1.000E−04	4.138E−05	1.321E−04
8	0.2132	0.757	0.7562	0.1614	1.612E−01	8.000E−04	1.782E−04	1.057E−03
9	0.2545	0.7555	0.7551	0.1923	1.922E−01	4.000E−04	1.270E−04	5.295E−04
10	0.2924	0.754	0.7537	0.2205	2.204E−01	3.000E−04	1.181E−04	3.979E−04
11	0.3269	0.7505	0.7514	0.2453	2.456E−01	9.000E−04	3.327E−04	1.199E−03
12	0.3585	0.7465	0.7473	0.2676	2.679E−01	8.000E−04	3.070E−04	1.072E−03
13	0.3873	0.7385	0.74	0.286	2.866E−01	1.500E−03	6.020E−04	2.031E−03
14	0.4137	0.728	0.7273	0.3012	3.009E−01	7.000E−04	3.160E−04	9.615E−04
15	0.4373	0.7065	0.7069	0.309	3.091E−01	4.000E−04	1.274E−04	5.662E−04
16	0.459	0.6755	0.6752	0.3101	3.099E−01	3.000E−04	1.832E−04	4.441E−04
17	0.4784	0.632	0.6308	0.3023	3.018E−01	1.200E−03	5.253E−04	1.899E−03
18	0.496	0.573	0.572	0.2842	2.837E−01	1.000E−03	4.880E−04	1.745E−03
19	0.5119	0.499	0.4997	0.2554	2.558E−01	7.000E−04	3.964E−04	1.403E−03
20	0.5265	0.413	0.4137	0.2174	2.178E−01	7.000E−04	4.130E−04	1.695E−03
21	0.5398	0.3165	0.3175	0.1708	1.714E−01	1.000E−03	5.865E−04	3.160E−03
22	0.5521	0.212	0.2121	0.117	1.171E−01	1.000E−04	1.004E−04	4.717E−04
23	0.5633	0.1035	0.1022	0.0583	5.757E−02	1.300E−03	7.307E−04	1.256E−03
24	0.5736	−0.01	−0.0088	−0.0057	−5.048E−03	1.200E−03	6.523E−04	1.200E−03
25	0.5833	−0.123	−0.1255	−0.0717	−7.320E−02	2.500E−03	1.504E−03	2.033E−03
26	0.59	−0.21	−0.2084	−0.1239	−1.230E−01	1.600E−03	9.440E−04	7.619E−03
Average			–			8.077E−04	3.460E−04	4.308E−03

Table 12
Performance metrics of the CCNMGBO on TDM of the RTC France Si cell.

Data points	V_{exp} (V)	I_{exp} (A)	I_{est} (A)	P_{exp} (W)	P_{est} (W)	IAE_i (A)	IAE_P (W)	RE_i (A)
1	−0.2057	0.764	0.7640	−0.1572	−0.1572	2.582E−07	5.311E−08	3.380E−07
2	−0.1291	0.762	0.7621	−0.0984	−0.0984	5.977E−05	7.716E−06	−7.844E−05
3	−0.0588	0.7605	0.7606	−0.0447	−0.0447	8.211E−05	4.828E−06	−1.080E−04
4	0.0057	0.7605	0.7605	0.0043	0.0043	3.170E−05	1.807E−07	4.168E−05
5	0.0646	0.76	0.7599	0.0491	0.0491	8.725E−05	5.636E−06	1.148E−04
6	0.1185	0.759	0.7589	0.0899	0.0899	8.630E−05	1.023E−05	1.137E−04
7	0.1678	0.757	0.7570	0.1270	0.1270	1.733E−05	2.908E−06	−2.289E−05
8	0.2132	0.757	0.7569	0.1614	0.1614	7.503E−05	1.600E−05	9.912E−05
9	0.2545	0.7555	0.7555	0.1923	0.1923	3.289E−05	8.369E−06	4.353E−05
10	0.2924	0.754	0.7540	0.2205	0.2205	2.833E−05	8.283E−06	3.757E−05
11	0.3269	0.7505	0.7506	0.2454	0.2453	8.685E−05	2.839E−05	−1.157E−04
12	0.3585	0.7465	0.7466	0.2676	0.2676	7.819E−05	2.803E−05	−1.047E−04
13	0.3873	0.7385	0.7386	0.2861	0.2860	1.483E−04	5.744E−05	−2.008E−04
14	0.4137	0.728	0.7279	0.3011	0.3012	7.124E−05	2.947E−05	9.786E−05
15	0.4373	0.7065	0.7065	0.3090	0.3090	3.661E−05	1.601E−05	−5.182E−05
16	0.459	0.6755	0.6755	0.3100	0.3101	2.586E−05	1.187E−05	3.828E−05
17	0.4784	0.632	0.6319	0.3023	0.3023	1.189E−04	5.689E−05	1.881E−04
18	0.496	0.573	0.5729	0.2842	0.2842	9.714E−05	4.818E−05	1.695E−04
19	0.5119	0.499	0.4991	0.2555	0.2554	6.775E−05	3.468E−05	−1.358E−04
20	0.5265	0.413	0.4131	0.2175	0.2174	6.973E−05	3.672E−05	−1.688E−04
21	0.5398	0.3165	0.3166	0.1709	0.1708	9.969E−05	5.381E−05	−3.150E−04
22	0.5521	0.212	0.2120	0.1171	0.1170	1.119E−05	6.177E−06	−5.277E−05
23	0.5633	0.1035	0.1034	0.0582	0.0583	1.280E−04	7.210E−05	1.237E−03
24	0.5736	−0.01	−0.0099	−0.0057	−0.0057	1.161E−04	6.660E−05	1.161E−02
25	0.5833	−0.123	−0.1232	−0.0719	−0.0717	2.412E−04	1.407E−04	−1.961E−03
26	0.59	−0.21	−0.2098	−0.1238	−0.1239	1.557E−04	9.184E−05	7.412E−04
Average						2.053E−03	8.431E−04	1.122E−02

Table 13
Estimated parameters by all algorithms for SDM of PhotoWatt-PWP201.

Algorithm	I_p (A)	I_{sd} (A)	R_{se} (Ω)	R_{sh} (Ω)	a	*RMSE*	*sig*
CCNMGBO	1.030514	3.48E−06	1.201271	981.9819	48.64283	**0.002425074**	
OBLWOA	1.030514	3.48E−06	1.201271	981.9845	48.64284	**0.002425074**	+
GWO	1.034158	4.88E−06	1.153241	766.7075	49.99694	0.003134605	+
HHO	1.028988	4.85E−06	1.049601	768.0139	50	0.010930692	+
SCA	1.440214	0	0	14.52205	19.9714	0.274263463	+
WOA	1.024355	1.46E−06	1.311483	1619.362	45.49246	0.004911533	+
GBO	1.030514	3.48E−06	1.201271	981.9824	48.64283	0.002436141	+
EO	1.028914	4.23E−06	1.181828	1348.228	49.39859	0.002489235	+
OLGBO (Ye et al., 2009)	1.03051	3.48E−06	1.20127	981.983	48.6428	0.002425076	+
RBGBO (Ma et al., 2013)	1.03051	3.48E−06	1.20132	981.983	48.6428	0.002425076	+
CGBO (Montoya et al., 2020)	1.0305	3.48E−06	1.2013	981.982	48.6428	0.002425101	+
MPA (Montoya et al., 2020)	1.0273	4.51E−06	1.1781	1977.6535	49.6486	0.00259141	+

Table 14
Estimated parameters by all algorithms for DDM of PhotoWatt-PWP201.

Algorithm	I_p (A)	I_{sd1} (A)	R_{se} (Ω)	R_{sh} (Ω)	a_1	I_{sd2} (A)	a_2	*RSME*	*sig*
CCNMGBO	1.030514	2.67E−06	1.20127	981.9987	49.30122	3.48E−06	48.64286	**0.002425**	
OBLWOA	1.030514	2.17E−06	1.201271	981.9832	49.98174	3.48E−06	48.64283	0.002427	+
GWO	1.027885	3.17E−06	1.193884	1446.965	21.53034	3.92E−06	49.09356	0.002542	+
HHO	1.029211	2.07E−06	1.242809	1970.148	49.29649	2.07E−06	49.29649	0.006302	+
SCA	1.441171	2.22E−07	1.8986	14.5432	3.62445	0	14.2455	0.27426	+
WOA	1.043373	3.82E−07	1.70134	1681.54	43.69429	5.18E−07	43.94296	0.04202	+
GBO	1.030537	3.65E−09	1.20173	979.1228	49.99977	3.47E−06	48.62751	0.002431	+
EO	1.029252	2.23E−08	1.190952	1199.289	1.189237	3.87E−06	49.04441	0.00245	+
PSO (Jordehi, 2016)	1.0314	3.14E−06	1.1944	694.6947	48.6684	2.61E−07	47.6085	0.0032066	+
SMA (Qais et al., 2019b)	1.0286	4.91E−06	1.2658	1584.412	50	0	50	0.0026081	+
CGBO (Montoya et al., 2020)	1.0305	3.48E−06	1.2013	981.8874	48.6428	3.89E−12	34.7828	0.002451	+
MPA (Montoya et al., 2020)	1.0276	9.71E−13	1.1676	1965.5137	48.1139	4.89E−06	49.9760	0.0026227	+

Table 15
Estimated parameters by all algorithms for TDM of PhotoWatt-PWP201.

Algorithm	I_p (A)	I_{sd1} (A)	R_{se} (Ω)	R_{sh} (Ω)	a_1	I_{sd2} (A)	a_2	I_{sd3} (A)	a_3	*RSME*	*sig*
CCNMGBO	1.0305	3.48E−06	1.2013	982.0998	48.6433	3.27E−12	47.9312	5.94E−08	49.9992	**2.425E−03**	
OBLWOA	1.0316	0.00E+00	1.1599	1000.0000	25.4792	4.83E−06	49.9424	0.00E+00	19.4348	2.750E−03	+
GWO	1.0303	9.94E−07	1.2448	854.8552	48.2595	1.46E−06	47.4705	8.91E−08	43.5191	2.720E−03	+
HHO	1.0339	3.48E−08	1.6238	811.9111	40.1225	3.48E−08	40.1224	1.74E−07	40.1224	2.209E−02	+
SCA	1.0895	0.00E+00	0.0000	63.7053	1.4707	0.00E+00	11.0315	3.83E−06	50.0000	7.643E−02	+
WOA	1.0316	0.00E+00	1.1579	999.9977	49.9999	0.00E+00	49.9999	4.90E−06	49.9999	2.778E−03	+
GBO	1.0305	3.71E−10	1.2012	982.1077	48.4845	3.48E−06	48.6435	2.02E−13	49.9864	2.425E−03	=
EO	1.0306	3.70E−06	1.1937	1000.0000	48.8831	0.00E+00	47.7765	0.00E+00	49.8457	2.435E−03	+

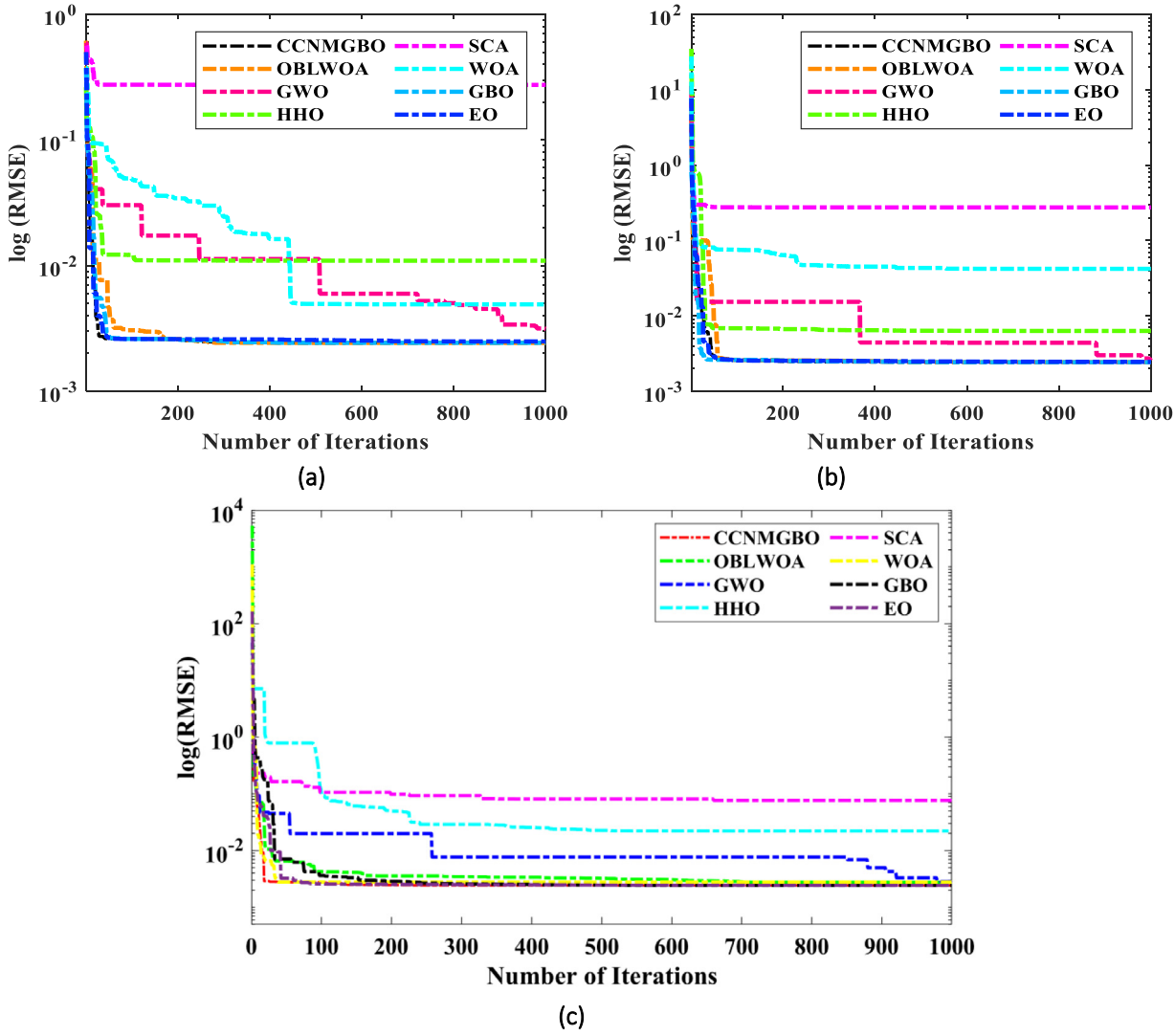

Fig. 13. Convergence curves obtained for case 2; (a) SDM, (b) DDM, (c) TDM.

4.3. Results on commercial PV modules

The proposed CCNMGBO algorithm is also investigated for solving the parameter estimation problem of the commercial PV modules, such as KC200GT, ST40, and SM55 for SDM, DDM, and TDM models. The experimental values of all commercial modules under various temperature and irradiance conditions are collected to validate the performance of the algorithm. The KC200GT is a multi-crystalline module, the ST40 is a thin-film module made up of copper selenide, and the SM55 is a monocrystalline module comprised of 36-series connected cells. The bounds of all PV modules are listed in Table 6. The short-circuit current (SCC) under any operating condition can be calculated using Eq. (62).

$$I_{sc}\,(T, G) = I_{sc-STC} \times \frac{G}{G_{STC}} + \alpha\,(T - T_{STC}) \tag{62}$$

where α represents the temperature coefficient of SCC available in the datasheet, $I_{sc(STC)}$ denotes the SCC under STC, T and G denote the real temperature, and irradiance T_{STC} and G_{STC} represent the temperature and irradiation at STC.

4.3.1. Case 3 – Various irradiation conditions

As discussed earlier, the CCNMGBO is validated on three commercial modules under variable irradiation conditions with a constant temperature. Both SDM and DDM are considered to estimate the parameters using the CCNMGBO algorithm. Various data points from the I–V characteristics of KC200GT, ST40, and SM55 under different irradiation conditions, such as 200 W/m^2, 400 W/m^2, 600 W/m^2, 800 W/m^2, and 1000 W/m^2 with 25 °C constant temperature are collected to calculate the error between the experimental value and the estimated value. The estimated parameters of all PV modules for SDM, DDM, and TDM are listed in Tables 20–28. Tables 20–22 lists the parameters of the KC200GT module, Tables 23–25 lists the parameters of the ST40 module, and Tables 26–28 lists the parameters of the SM55 module. The I–V characteristics of all the selected PV modules for SDM, DDM, and TDM are illustrated in Figs. 17–19. Figs. 17–19 proves the accurate curve fitting of the estimated and experimental data points under various irradiance conditions. The above discussions conclude that the proposed CCNMGBO can solve the multimodal problems accurately.

4.3.2. Case 4 – Various temperature conditions

Various data points from the I–V characteristics of KC200GT, ST40, and SM55 under different temperature conditions, such as 25 °C, 50 °C, and 75 °C, 25 °C, 40 °C, 55 °C, and 70 °C, and 25 °C, 40 °C, and 60 °C with 1000 W/m^2 constant irradiance are collected to calculate the error between the experimental value and the estimated value. The estimated parameters of all

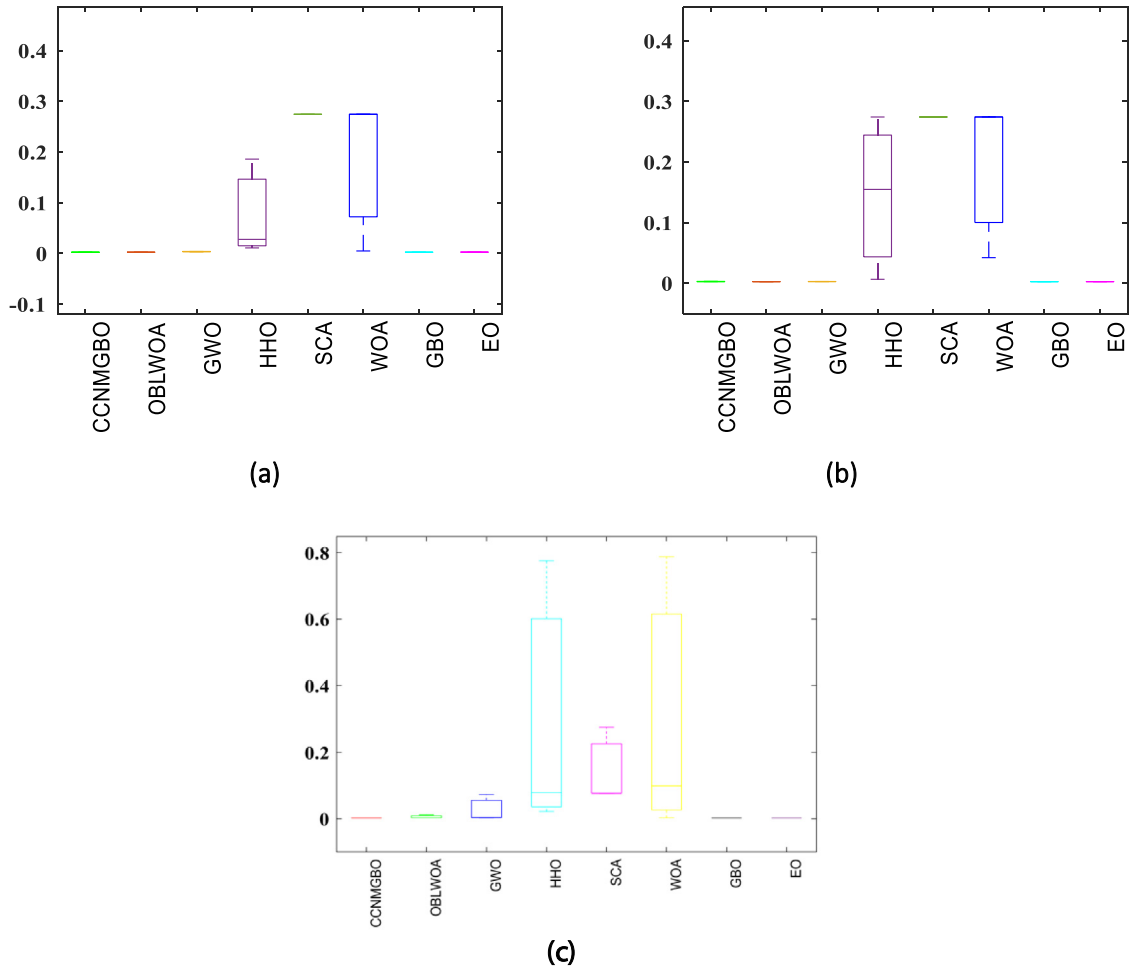

Fig. 14. Box plots obtained for case 2; (a) SDM, (b) DDM, (c) TDM.

Table 16
Performance metrics of the CCNMGBO on SDM of the PhotoWatt-PWP201 module.

Data points	V_{exp} (V)	I_{exp} (A)	I_{est} (A)	P_{exp} (W)	P_{est} (W)	IAE_i (A)	IAE_P (W)	RE_i (A)
1	0.1248	1.0315	1.0291	0.12873	1.284E−01	2.400E−03	2.983E−04	2.327E−03
2	1.8093	1.03	1.0274	1.86358	1.859E+00	2.600E−03	4.705E−03	2.524E−03
3	3.3511	1.026	1.0257	3.43823	3.437E+00	3.000E−04	1.007E−03	2.924E−04
4	4.7622	1.022	1.0241	4.86697	4.877E+00	2.100E−03	9.999E−03	2.055E−03
5	6.0538	1.018	1.0223	6.16277	6.189E+00	4.300E−03	2.603E−02	4.224E−03
6	7.2364	1.0155	1.0199	7.34856	7.380E+00	4.400E−03	3.184E−02	4.333E−03
7	8.3189	1.014	1.0164	8.43536	8.455E+00	2.400E−03	1.997E−02	2.367E−03
8	9.3097	1.01	1.0105	9.4028	9.407E+00	5.000E−04	4.652E−03	4.950E−04
9	10.2163	1.0035	1.0006	10.25206	1.022E+01	2.900E−03	2.963E−02	2.890E−03
10	11.0449	0.988	0.9845	10.91236	1.087E+01	3.500E−03	3.866E−02	3.543E−03
11	11.8018	0.963	0.9595	11.36513	1.132E+01	3.500E−03	4.130E−02	3.634E−03
12	12.4929	0.9255	0.9228	11.56218	1.153E+01	2.700E−03	3.373E−02	2.917E−03
13	13.1231	0.8725	0.8726	11.4499	1.145E+01	1.000E−04	1.317E−03	1.146E−04
14	13.6983	0.8075	0.8073	11.06138	1.106E+01	2.000E−04	2.742E−03	2.477E−04
15	14.2221	0.7265	0.7283	10.33236	1.036E+01	1.800E−03	2.560E−02	2.478E−03
16	14.6995	0.6345	0.6371	9.32683	9.365E+00	2.600E−03	3.822E−02	4.098E−03
17	15.1346	0.5345	0.5362	8.08944	8.115E+00	1.700E−03	2.573E−02	3.181E−03
18	15.5311	0.4275	0.4295	6.63955	6.671E+00	2.000E−03	3.106E−02	4.678E−03
19	15.8929	0.3185	0.3188	5.06189	5.067E+00	3.000E−04	4.767E−03	9.419E−04
20	16.2229	0.2085	0.2074	3.38247	3.365E+00	1.100E−03	1.784E−02	5.276E−03
21	16.5241	0.101	0.0962	1.66893	1.590E+00	4.800E−03	7.931E−02	4.752E−02
22	16.7987	−0.008	−0.0083	−0.13439	−1.394E−01	3.000E−04	5.039E−03	3.750E−03
23	17.0499	−0.111	−0.1109	−1.89254	−1.891E+00	1.000E−04	1.706E−03	9.009E−04
24	17.2793	−0.209	−0.2092	−3.61137	−3.615E+00	2.000E−04	3.460E−03	9.569E−04
25	17.4885	−0.303	−0.3009	−5.29902	−5.262E+00	2.100E−03	3.673E−02	6.931E−03
Average			–			4.890E−02	2.061E−02	2.154E−03

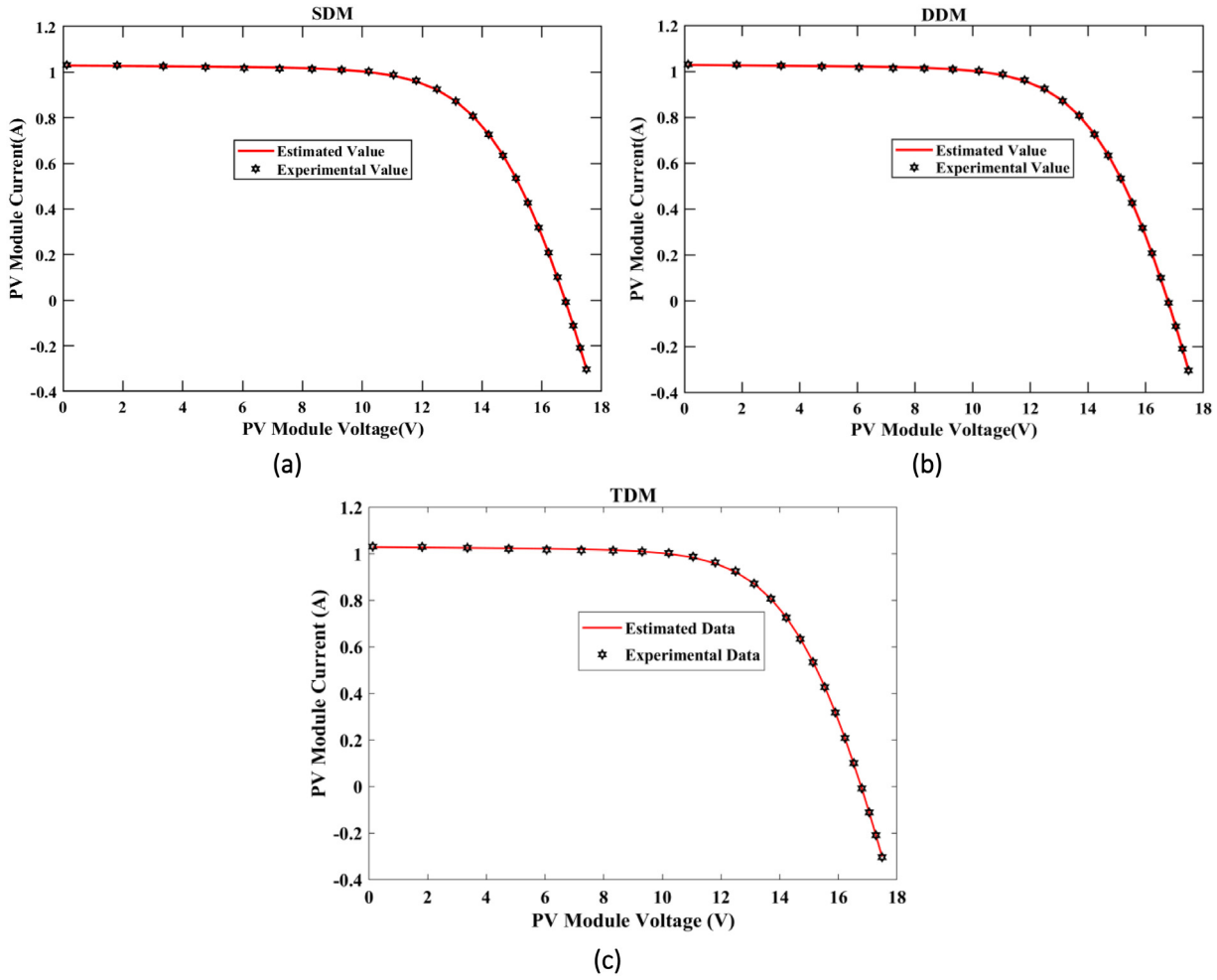

Fig. 15. I–V characteristics of the PhotoWatt-PWP201 by CCNMGBO; (a) SDM, (b) DDM, (c) TDM.

Table 17
Performance metrics of the CCNMGBO on DDM of the PhotoWatt-PWP201 module.

Data points	V_{exp} (V)	I_{exp} (A)	I_{est} (A)	P_{exp} (W)	P_{est} (W)	IAE_i (A)	IAE_P (W)	RE_i (A)
1	0.1248	1.0315	1.029	0.1287312	1.284E−01	2.424E−03	3.120E−04	2.500E−03
2	1.8093	1.03	1.0273	1.863579	1.859E+00	2.621E−03	4.885E−03	2.700E−03
3	3.3511	1.026	1.0257	3.4382286	3.437E+00	2.924E−04	1.005E−03	3.000E−04
4	4.7622	1.022	1.0241	4.8669684	4.877E+00	2.055E−03	1.000E−02	2.100E−03
5	6.0538	1.018	1.0223	6.1627684	6.189E+00	4.224E−03	2.603E−02	4.300E−03
6	7.2364	1.0155	1.0199	7.3485642	7.380E+00	4.333E−03	3.184E−02	4.400E−03
7	8.3189	1.014	1.0164	8.4353646	8.455E+00	2.367E−03	1.997E−02	2.400E−03
8	9.3097	1.01	1.0105	9.402797	9.407E+00	4.950E−04	4.655E−03	5.000E−04
9	10.2163	1.0035	1.0006	10.252057	1.022E+01	2.890E−03	2.963E−02	2.900E−03
10	11.0449	0.988	0.9846	10.912361	1.087E+01	3.441E−03	3.755E−02	3.400E−03
11	11.8018	0.963	0.9596	11.365133	1.133E+01	3.531E−03	4.013E−02	3.400E−03
12	12.4929	0.9255	0.9229	11.562179	1.153E+01	2.809E−03	3.248E−02	2.600E−03
13	13.1231	0.8725	0.8726	11.449905	1.145E+01	1.146E−04	1.312E−03	1.000E−04
14	13.6983	0.8075	0.8073	11.061377	1.106E+01	2.477E−04	2.739E−03	2.000E−04
15	14.2221	0.7265	0.7284	10.332356	1.036E+01	2.615E−03	2.702E−02	1.900E−03
16	14.6995	0.6345	0.6372	9.3268328	9.367E+00	4.255E−03	3.969E−02	2.700E−03
17	15.1346	0.5345	0.5362	8.0894437	8.115E+00	3.181E−03	2.573E−02	1.700E−03
18	15.5311	0.4275	0.4295	6.6395453	6.671E+00	4.678E−03	3.106E−02	2.000E−03
19	15.8929	0.3185	0.3188	5.0618887	5.067E+00	9.419E−04	4.768E−03	3.000E−04
20	16.2229	0.2085	0.2074	3.3824747	3.365E+00	5.276E−03	1.785E−02	1.100E−03
21	16.5241	0.101	0.0961	1.6689341	1.588E+00	4.851E−03	8.097E−02	4.900E−03
22	16.7987	−0.008	−0.0083	−0.1343896	−1.394E−01	3.750E−03	5.040E−03	3.000E−04
23	17.0499	−0.111	−0.1109	−1.8925389	−1.891E+00	9.009E−04	1.705E−03	1.000E−04
24	17.2793	−0.209	−0.2092	−3.6113737	−3.615E+00	9.569E−04	3.456E−03	2.000E−04
25	17.4885	−0.303	−0.3008	−5.2990155	−5.261E+00	7.261E−03	3.847E−02	2.200E−03
Average			–			2.188E−03	2.073E−02	1.968E−03

Table 18
Performance metrics of the CCNMGBO on TDM of the PhotoWatt-PWP201 module.

Data points	V_{exp} (V)	I_{exp} (A)	I_{est} (A)	P_{exp} (W)	P_{est} (W)	IAE_i (A)	IAE_P (W)	RE_i (A)
1	0.1248	1.0315	1.0313	0.1287	0.1287	2.425E−04	3.026E−05	2.351E−04
2	1.8093	1.03	1.0297	1.8631	1.8636	2.627E−04	4.752E−04	2.550E−04
3	3.3511	1.026	1.0260	3.4381	3.4382	3.006E−05	1.007E−04	2.930E−05
4	4.7622	1.022	1.0222	4.8679	4.8670	2.027E−04	9.655E−04	−1.984E−04
5	6.0538	1.018	1.0184	6.1653	6.1628	4.177E−04	2.529E−03	−4.103E−04
6	7.2364	1.0155	1.0159	7.3517	7.3486	4.331E−04	3.134E−03	−4.265E−04
7	8.3189	1.014	1.0142	8.4373	8.4354	2.334E−04	1.942E−03	−2.302E−04
8	9.3097	1.01	1.0101	9.4033	9.4028	5.287E−05	4.922E−04	−5.234E−05
9	10.2163	1.0035	1.0032	10.2493	10.2521	2.741E−04	2.800E−03	2.732E−04
10	11.0449	0.988	0.9877	10.9087	10.9124	3.303E−04	3.648E−03	3.343E−04
11	11.8018	0.963	0.9627	11.3612	11.3651	3.330E−04	3.930E−03	3.458E−04
12	12.4929	0.9255	0.9252	11.5590	11.5622	2.542E−04	3.175E−03	2.746E−04
13	13.1231	0.8725	0.8725	11.4501	11.4499	1.280E−05	1.679E−04	−1.467E−05
14	13.6983	0.8075	0.8075	11.0611	11.0614	2.033E−05	2.785E−04	2.517E−05
15	14.2221	0.7265	0.7267	10.3349	10.3324	1.776E−04	2.525E−03	−2.444E−04
16	14.6995	0.6345	0.6348	9.3306	9.3268	2.531E−04	3.721E−03	−3.989E−04
17	15.1346	0.5345	0.5347	8.0919	8.0894	1.624E−04	2.457E−03	−3.037E−04
18	15.5311	0.4275	0.4277	6.6425	6.6395	1.899E−04	2.950E−03	−4.443E−04
19	15.8929	0.3185	0.3185	5.0623	5.0619	2.292E−05	3.642E−04	−7.196E−05
20	16.2229	0.2085	0.2084	3.3807	3.3825	1.091E−04	1.770E−03	5.234E−04
21	16.5241	0.101	0.1005	1.6613	1.6689	4.627E−04	7.646E−03	4.581E−03
22	16.7987	−0.008	−0.0080	−0.1349	−0.1344	3.204E−05	5.383E−04	4.005E−03
23	17.0499	−0.111	−0.1110	−1.8924	−1.8925	6.356E−06	1.084E−04	5.726E−05
24	17.2793	−0.209	−0.2090	−3.6117	−3.6114	2.135E−05	3.689E−04	−1.022E−04
25	17.4885	−0.303	−0.3028	−5.2954	−5.2990	2.055E−04	3.593E−03	6.781E−04
Average						4.743E−03	4.971E−02	7.090E−04

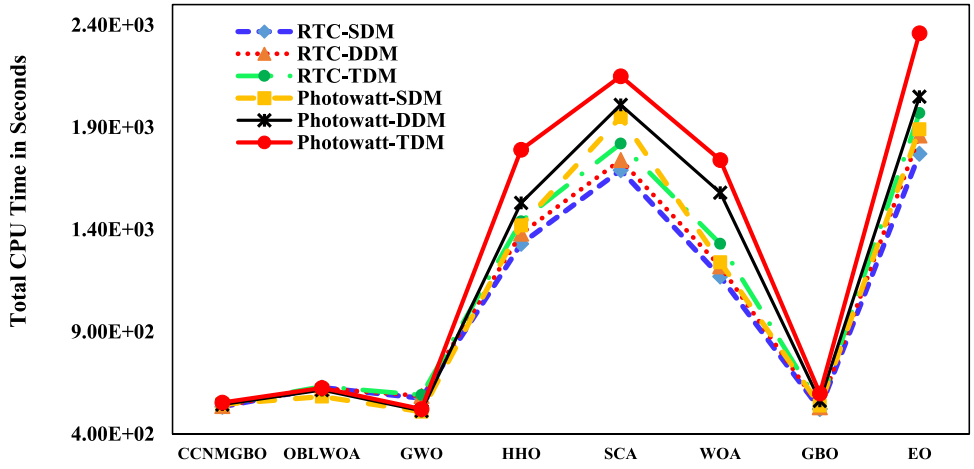

Fig. 16. Total RT of all algorithms.

Table 19
Total RT in seconds over 30 runs of all algorithms for different PV models.

Algorithm	Case 1			Case 2		
	SDM	DDM	TDM	SDM	DDM	TDM
CCNMGBO	5.33E+02	5.37E+02	5.44E+02	5.45E+02	5.44E+02	5.54E+02
OBLWOA	6.27E+02	6.23E+02	6.32E+02	5.83E+02	6.15E+02	6.25E+02
GWO	5.75E+02	5.86E+02	5.91E+02	5.09E+02	5.13E+02	5.22E+02
HHO	1.33E+03	1.38E+03	1.44E+03	1.42E+03	1.53E+03	1.79E+03
SCA	1.69E+03	1.74E+03	1.82E+03	1.95E+03	2.01E+03	2.15E+03
WOA	1.17E+03	1.22E+03	1.33E+03	1.24E+03	1.58E+03	1.74E+03
GBO	**5.22E+02**	**5.31E+02**	**5.41E+02**	**5.39E+02**	**5.62E+02**	**5.98E+02**
EO	1.77E+03	1.86E+03	1.97E+03	1.89E+03	2.05E+03	2.36E+03

Table 20
Estimated parameters of KC200GT module at 25 °C temperature — SDM.

G	I_p (A)	I_{sd} (A)	a	R_{sh} (Ω)	R_{se} (Ω)	$RMSE$
1000 W/m^2	8.2170	2.2436e−09	1.0764	761.7084	0.3438	0.0015
800 W/m^2	6.5694	1.2323e−09	1.0471	845.6946	0.3529	0.0022
600 W/m^2	4.9335	4.0093e−09	1.1060	777.1346	0.3366	0.0013
400 W/m^2	3.2741	5.6793e−09	1.1242	5.0000e+03	0.3060	0.0066
200 W/m^2	1.6453	1.0473e−09	1.0357	733.9223	0.3148	0.0016

Table 21
Estimated parameters of KC200GT module at 25 °C temperature — DDM.

G	I_p (A)	I_{sd1} (A)	a_1	I_{sd2} (A)	R_{sh} (Ω)	R_{se} (Ω)	a_2	*RMSE*
1000 W/m^2	8.2139	3.7958e−07	1.6402	3.7932e−10	1.0326e+03	0.3542	1.0000	0.0028
800 W/m^2	6.5712	4.8990e−07	2.5139	9.4603e−10	756.7999	0.3572	1.0350	0.0016
600 W/m^2	4.9368	3.5559e−09	1.0997	5.1132e−14	656.9794	0.3388	4.0000	0.0017
400 W/m^2	3.2839	1.2993e−11	1.0000	1.9694e−09	941.1714	0.3445	1.0702	0.0022
200 W/m^2	1.6462	4.8477e−10	1.0000	3.0828e−12	686.4898	0.3872	1.2619	0.0014

Table 22
Estimated parameters of KC200GT module at 25 °C temperature — TDM.

G	I_p (A)	I_{sd1} (A)	R_{se} (Ω)	R_{sh} (Ω)	a_1	I_{sd2} (A)	a_2	I_{sd3} (A)	a_3	*RMSE*
1000 W/m^2	8.2020	6.18E−05	0.3319	4980.9703	3.9787	4.66E−05	3.6688	3.68E−09	1.1009	7.633E−03
800 W/m^2	6.5567	6.68E−09	0.3483	4999.9754	3.6626	1.76E−09	1.0640	1.37E−05	3.5454	6.456E−03
600 W/m^2	4.9225	5.01E−09	0.3309	4999.7226	1.1180	3.13E−05	3.9981	7.82E−05	3.9999	5.224E−03
400 W/m^2	3.2767	9.82E−07	0.3314	2552.2145	2.7666	2.51E−09	1.0812	5.58E−05	3.7874	4.758E−03
200 W/m^2	1.6428	1.38E−05	0.2363	869.9931	3.9997	2.21E−09	1.0728	4.71E−07	1.2371	2.355E−03

Table 23
Estimated parameters of ST40 module at 25 °C temperature — SDM.

G	I_p (A)	I_{sd} (A)	a	R_{sh} (Ω)	R_{se} (Ω)	*RMSE*
1000 W/m^2	2.6773	1.5946e−06	1.7554	342.8661	1.1080	9.8848e−04
800 W/m^2	2.1268	2.7185e−06	1.8253	584.1387	1.0625	0.0038
600 W/m^2	1.6048	1.4421e−06	1.7451	347.7406	1.1126	6.7404e−04
400 W/m^2	1.0675	1.8514e−06	1.7787	362.5737	1.0803	6.3073e−04
200 W/m^2	0.5331	1.4349e−06	1.7476	345.0599	1.1839	4.7721e−04

Table 24
Estimated parameters of ST40 module at 25 °C temperature — DDM.

G	I_p (A)	I_{sd1} (A)	a_1	I_{sd2} (A)	R_{sh} (Ω)	R_{se} (Ω)	a_2	*RMSE*
1000 W/m^2	2.6742	1.9496e−06	1.7800	2.5104e−08	386.3744	1.0946	3.9972	0.0012
800 W/m^2	2.1367	1.2705e−06	1.7297	1.6755e−07	350.7341	1.1173	2.6033	9.0981e−04
600 W/m^2	1.6046	2.3810e−05	4.0000	1.2961e−06	355.4385	1.1185	1.7326	6.8569e−04
400 W/m^2	1.0669	8.7618e−06	2.2023	7.9166e−08	395.7687	1.1889	1.4776	9.4555e−04
200 W/m^2	0.5303	7.8566e−18	3.9987	9.0314e−06	382.1779	1.1981	2.0331	0.0012

Table 25
Estimated parameters of ST40 module at 25 °C temperature — TDM.

G	I_p (A)	I_{sd1} (A)	R_{se} (Ω)	R_{sh} (Ω)	a_1	I_{sd2} (A)	a_2	I_{sd3} (A)	a_3	*RMSE*
1000 W/m^2	2.6738	3.93E−07	1.1024	394.0940	1.7670	1.46E−06	1.7760	6.19E−14	1.0371	1.123E−03
800 W/m^2	2.1200	1.72E−07	0.9921	1819.3043	3.9371	5.02E−06	1.9132	1.00E−04	3.9999	6.567E−03
600 W/m^2	1.6019	3.16E−12	0.9997	398.6377	3.8552	1.53E−06	3.9485	3.04E−06	1.8422	1.733E−03
400 W/m^2	1.0675	6.20E−06	1.0932	367.1611	2.9622	2.29E−11	3.9998	1.54E−06	1.7561	6.546E−04
200 W/m^2	0.5331	3.09E−07	1.5668	374.2474	1.5673	9.44E−05	4.0000	3.46E−05	3.9996	4.708E−04

Table 26
Estimated parameters of SM55 module at 25 °C temperature — SDM.

G	I_p (A)	I_{sd} (A)	a	R_{sh} (Ω)	R_{se} (Ω)	*RMSE*
1000 W/m^2	3.4501	1.7115e−07	1.3958	483.9004	0.3291	0.0011
800 W/m^2	2.7603	1.4759e−07	1.3832	463.1399	0.3362	6.7220e−04
600 W/m^2	2.0709	1.5500e−07	1.3873	449.8587	0.3307	8.2399e−04
400 W/m^2	1.3828	1.0050e−07	1.3521	427.0898	0.3966	7.0761e−04
200 W/m^2	0.6911	3.3873e−07	1.4577	458.8255	1.3374e−08	7.8064e−04

PV modules for SDM, DDM, and TDM are listed in Tables 29–37. Tables 29–31 lists the parameters of the KC200GT module, Tables 32–34 lists the parameters of the ST40 module, and Tables 35–37 lists the parameters of the SM55 module. The I–V characteristics of all the selected PV modules for both SDM and DDM are illustrated in Figs. 20–22. Figs. 20–22 proves the accurate curve fitting of the estimated and experimental data points under various temperature conditions.

The above-all discussions show that the experimental and estimated data points under different operating conditions are matched well for all selected PV modules. Besides, the RMSE value obtained by the proposed CCNMGBO algorithm is less on collected data samples. The I–V characteristics of the respective model prove the accuracy and efficiency of the proposed CCNMGBO algorithm. It is summarized that the proposed CCNMGBO is an accurate and efficient tool for obtaining the unknown parameters of various PV models.

4.4. Statistical analysis

The performance of the proposed CCNMGBO is proved through detailed comparisons, statistical data analysis, and statistical tests, such as WSRT and FRT. The comparison is made between the proposed algorithm and a few other state-of-the-art algorithms, such as GWO, HHO, EO, WOA, SCA, OBLWOA, and GBO. The performance metrics, such as Min, Max, Mean, Median, STD, and RT, are listed in Table 38 for case 1. Based on the Min

Table 27
Estimated parameters of SM55 module at 25 °C temperature — DDM.

G	I_p (A)	I_{sd1} (A)	a_1	I_{sd2} (A)	R_{sh} (Ω)	R_{se} (Ω)	a_2	*RMSE*
1000 W/m^2	3.4489	2.4274e−08	1.2646	2.0257e−06	561.1451	0.3455	1.8503	0.0018
800 W/m^2	2.7456	2.1870e−07	3.9799	6.4981e−07	4.9555e+03	0.2603	1.5150	0.0065
600 W/m^2	2.0700	1.4128e−07	1.3798	3.5469e−05	484.7809	0.3331	3.9929	8.9725e−04
400 W/m^2	1.3827	9.5778e−08	1.3481	7.5709e−09	423.1464	0.3989	3.9971	7.5515e−04
200 W/m^2	0.6917	2.9943e−24	3.9967	1.7555e−07	445.2607	0.2264	1.3967	5.4799e−04

Table 28
Estimated parameters of SM55 module at 25 °C temperature — TDM.

G	I_p (A)	I_{sd1} (A)	R_{se} (Ω)	R_{sh} (Ω)	a_1	I_{sd2} (A)	a_2	I_{sd3} (A)	a_3	*RMSE*
1000 W/m^2	3.4510	3.26E−08	0.3301	462.5610	3.9870	1.65E−07	1.3928	1.32E−09	3.3241	1.199E−03
800 W/m^2	2.7594	8.67E−07	0.3063	517.0696	3.9999	2.42E−07	1.4243	4.90E−14	1.9444	1.439E−03
600 W/m^2	2.0683	5.73E−05	0.3363	541.8843	4.0000	4.79E−06	3.9999	1.31E−07	1.3738	1.242E−03
400 W/m^2	1.3820	2.71E−13	0.3327	456.0567	4.0000	1.70E−07	1.3957	1.17E−07	3.9999	9.737E−04
200 W/m^2	0.6911	5.74E−05	0.3201	484.5100	4.0000	1.07E−07	1.3545	1.53E−10	3.9472	6.758E−04

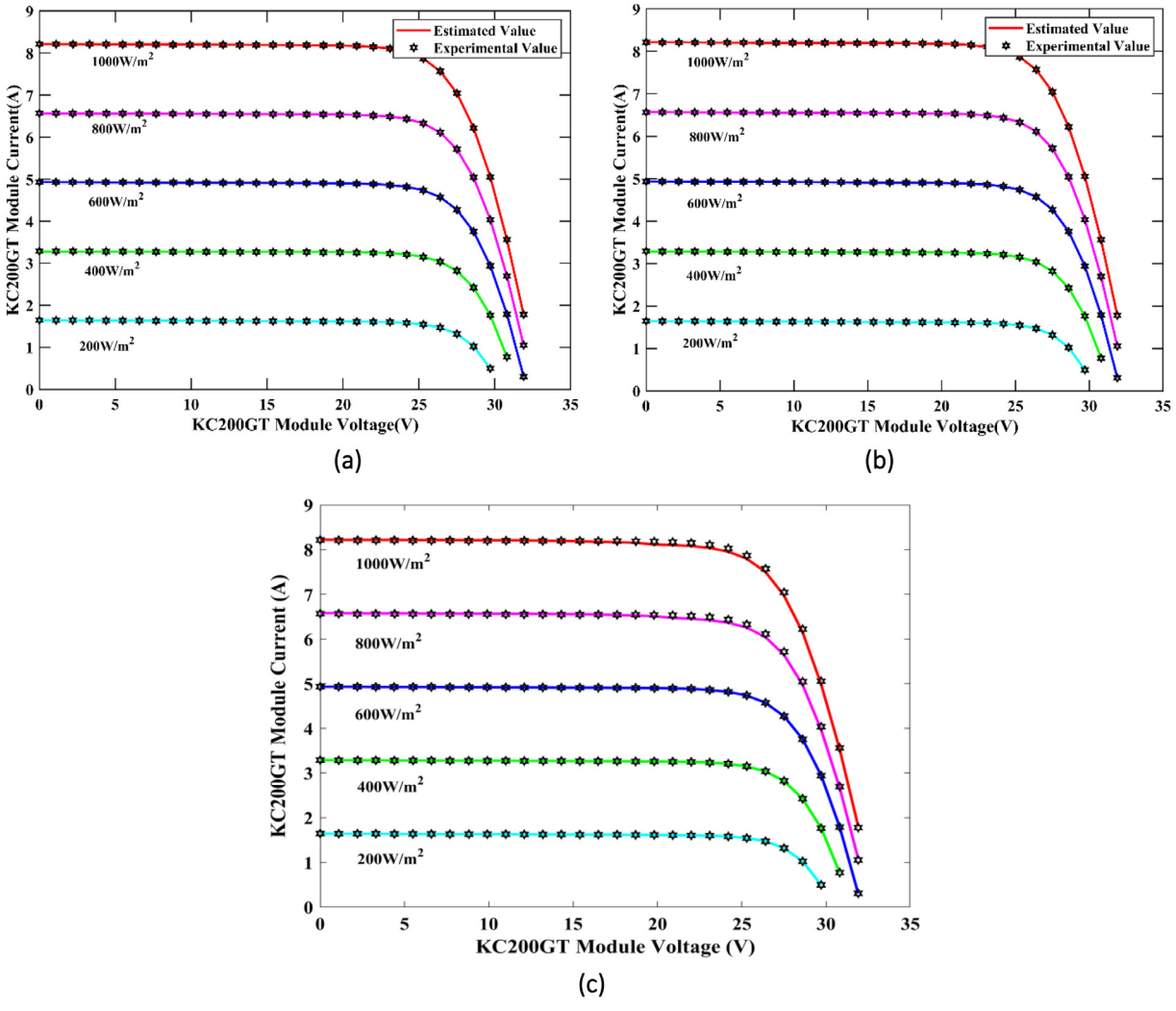

Fig. 17. I–V curves of KC200GT module for Case 3; (a) SDM, (b) DDM, (c) TDM.

Table 29
Estimated parameters of KC200GT module at 1000 W/m^2 irradiation — SDM.

T	I_p (A)	I_{sd} (A)	a	R_{sh} (Ω)	R_{se} (Ω)	*RMSE*
25 °C	8.2167	2.2550e−09	1.0767	771.4306	0.3437	0.0015
50 °C	8.2951	1.2657e−07	1.1176	966.1297	0.3356	0.0027
75 °C	8.3777	1.6308e−06	1.1015	790.5583	0.3425	0.0045

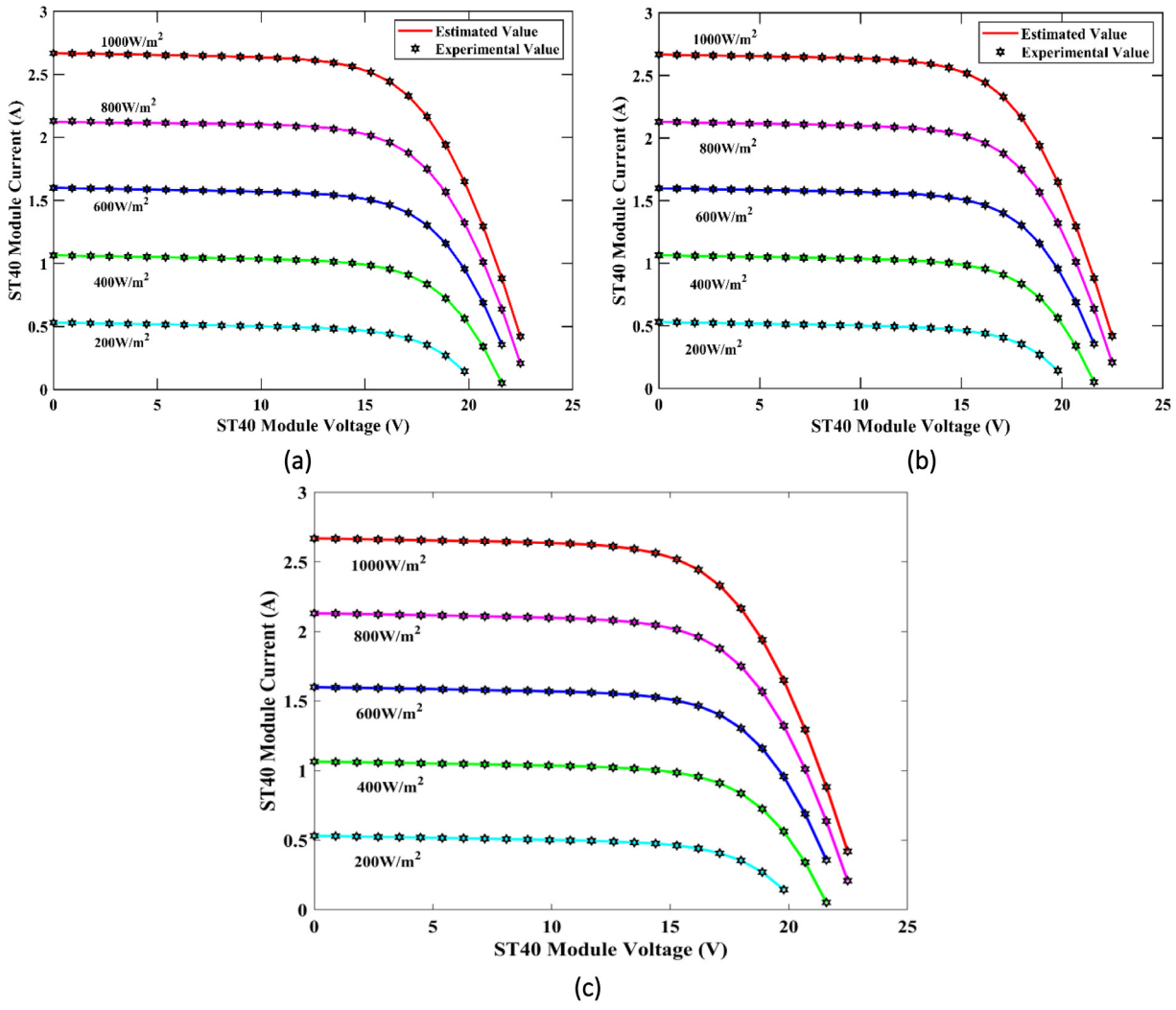

Fig. 18. I–V curves of ST40 module for Case 3; (a) SDM, (b) DDM, (c) TDM.

Table 30
Estimated parameters of KC200GT module at 1000 W/m^2 irradiation — DDM.

T	I_p (A)	I_{sd1} (A)	R_s (Ω)	R_p (Ω)	n_1	I_{sd2} (A)	n_2	*RMSE*
25 °C	8.2057	9.9999e−05	0.3449	4.0326e+03	3.5427	1.8077e−09	1.0663	0.0037
50 °C	8.2943	2.6159e−07	0.3404	1.0896e+03	1.2131	7.5989e−09	1.0000	0.0030
75 °C	8.3771	9.8959e−05	0.3427	863.8974	3.8130	1.5968e−06	1.1000	0.0045

Table 31
Estimated parameters of KC200GT module at 1000 W/m^2 irradiation — TDM.

G	I_p (A)	I_{sd1} (A)	R_{se} (Ω)	R_{sh} (Ω)	a_1	I_{sd2} (A)	a_2	I_{sd3} (A)	a_3	*RMSE*
25 °C	8.2047	3.18E−09	0.3376	4879.1064	1.0936	6.05E−05	3.9665	3.69E−05	3.9860	5.173E−03
50 °C	8.2876	3.46E−05	0.3341	3673.4378	3.8427	1.31E−07	1.1201	4.94E−05	3.1034	3.809E−03
75 °C	8.3683	1.82E−06	0.3399	4913.3998	1.1093	4.84E−06	3.5428	9.99E−05	2.9585	5.532E−03

Table 32
Estimated parameters of ST40 module at 1000 W/m^2 irradiation — SDM.

T	I_p (A)	I_{sd} (A)	a	R_{sh} (Ω)	R_{se} (Ω)	*RMSE*
25 °C	2.6758	1.5283e−06	1.7503	357.5578	1.1133	7.3410e−04
40 °C	2.6809	5.6639e−06	1.7225	364.3001	1.1293	0.0013
50 °C	2.6920	1.8681e−05	1.7176	295.0222	1.1496	0.0018
70 °C	2.6923	8.7522e−05	1.7273	367.7535	1.1259	7.7772e−04

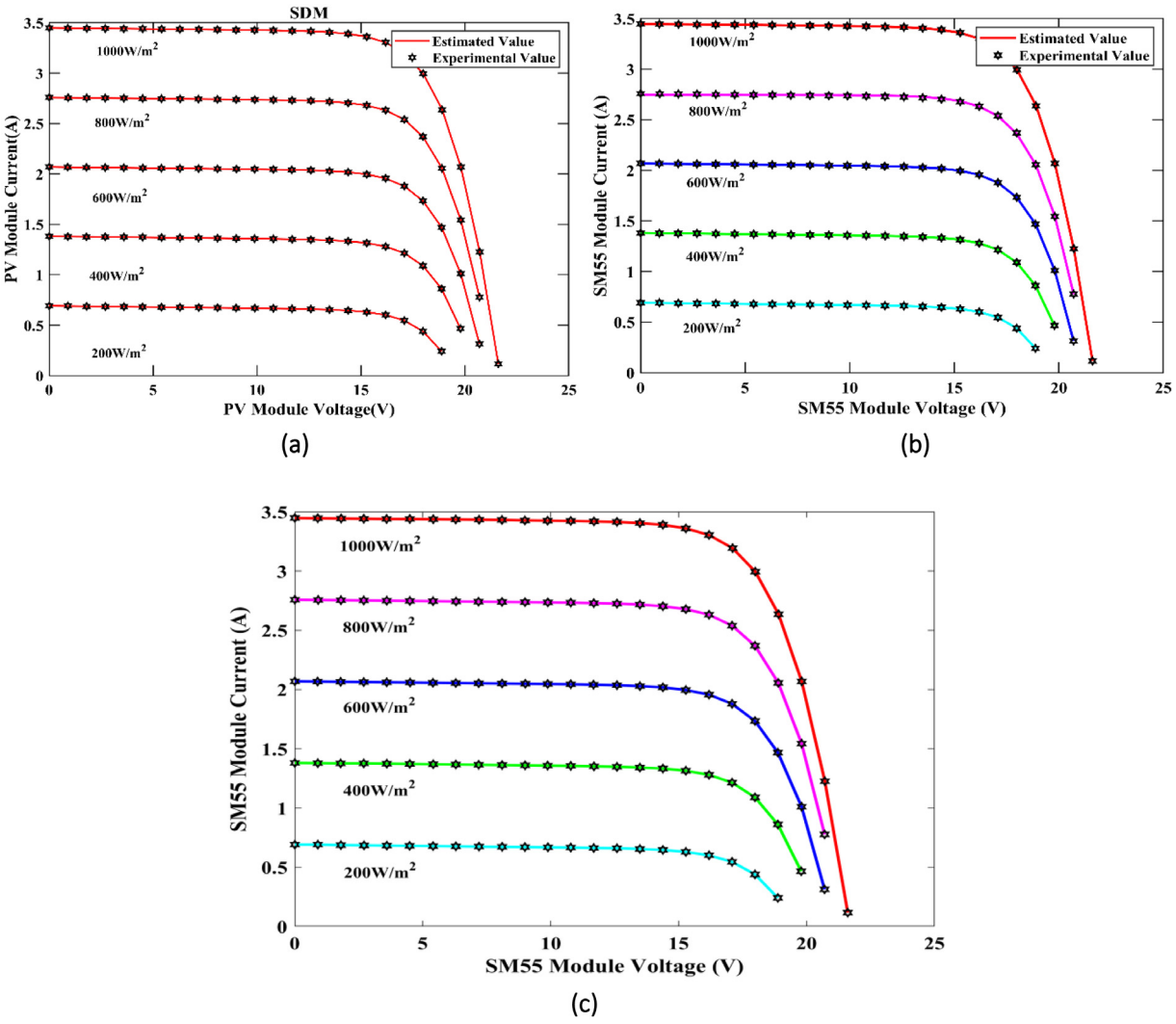

Fig. 19. I–V curves of SM55 module for Case 3; (a) SDM, (b) DDM, (c) TDM.

Table 33
Estimated parameters of ST40 module at 1000 W/m^2 irradiation — DDM.

T	I_p (A)	I_{sd1} (A)	a_1	I_{sd2} (A)	R_{sh} (Ω)	R_{se} (Ω)	a_2	*RMSE*
25 °C	2.6760	5.1684e−09	4	1.5165e−06	355.1516	1.1136	1.7494	7.3618e−04
40 °C	2.6809	5.6692e−06	1.7229	2.1020e−09	364.1438	1.1293	1.5326	0.0013
50 °C	2.6920	1.8674e−05	1.7175	1.9482e−07	295.0527	1.1496	3.4200	0.0018
70 °C	2.6921	8.1521e−06	4.0000	8.6755e−05	370.5408	1.1268	1.7259	7.8388e−04

Table 34
Estimated parameters of ST40 module at 1000 W/m^2 irradiation — TDM.

G	I_p (A)	I_{sd1} (A)	R_{se} (Ω)	R_{sh} (Ω)	a_1	I_{sd2} (A)	a_2	I_{sd3} (A)	a_3	*RMSE*
25 °C	2.6755	5.03E−06	1.1167	365.7610	3.9991	1.40E−06	1.7405	1.52E−05	3.9953	7.532E−04
40 °C	2.6808	1.10E−12	1.1298	365.4562	3.9961	1.61E−16	3.9255	5.64E−06	1.7219	1.323E−03
50 °C	2.6913	2.96E−05	1.1543	314.3532	3.9223	9.88E−05	3.8413	1.65E−05	1.7013	1.781E−03
70 °C	2.6919	4.42E−05	1.1267	384.4513	1.7297	4.12E−05	1.7173	7.91E−05	3.7189	7.934E−04

Table 35
Estimated parameters of SM55 module at 1000 W/m^2 irradiation — SDM.

T	I_p (A)	I_{sd} (A)	a	R_{sh} (Ω)	R_{se} (Ω)	*RMSE*
25 °C	3.4499	1.7284e−07	1.3966	490.5339	0.3290	0.0012
40 °C	3.4691	1.1451e−06	1.4178	533.0525	0.3131	0.0038
60 °C	3.4946	6.9131e−06	1.4052	485.0551	0.3187	0.0038

Table 36
Estimated parameters of SM55 module at 1000 W/m^2 irradiation — DDM.

T	I_p (A)	I_{sd1} (A)	a_1	I_{sd2} (A)	R_{sh} (Ω)	R_{se} (Ω)	a_2	*RMSE*
25 °C	3.4461	2.4176e−05	4.0000	1.8140e−07	613.7870	0.3270	1.4007	0.0018
40 °C	3.4691	8.0089e−06	4.0000	1.1338e−06	537.6240	0.3133	1.4169	0.0038
60 °C	3.4837	4.5383e−05	1.9068	1.9587e−06	4.9192e+03	0.3238	1.3023	0.0054

Table 37
Estimated parameters of SM55 module at 1000 W/m^2 irradiation — TDM.

G	I_p (A)	I_{sd1} (A)	R_{se} (Ω)	R_{sh} (Ω)	a_1	I_{sd2} (A)	a_2	I_{sd3} (A)	a_3	*RMSE*
25 °C	3.4502	3.93E−09	0.3284	483.5813	2.0009	1.74E−07	1.3973	1.35E−07	3.9996	1.155E−03
40 °C	3.4714	1.05E−06	0.3155	459.6443	1.4097	2.69E−08	3.9945	4.28E−11	3.6955	3.901E−03
60 °C	3.4945	8.84E−13	0.3189	490.9974	2.0665	6.85E−06	1.4043	1.92E−05	4.0000	3.786E−03

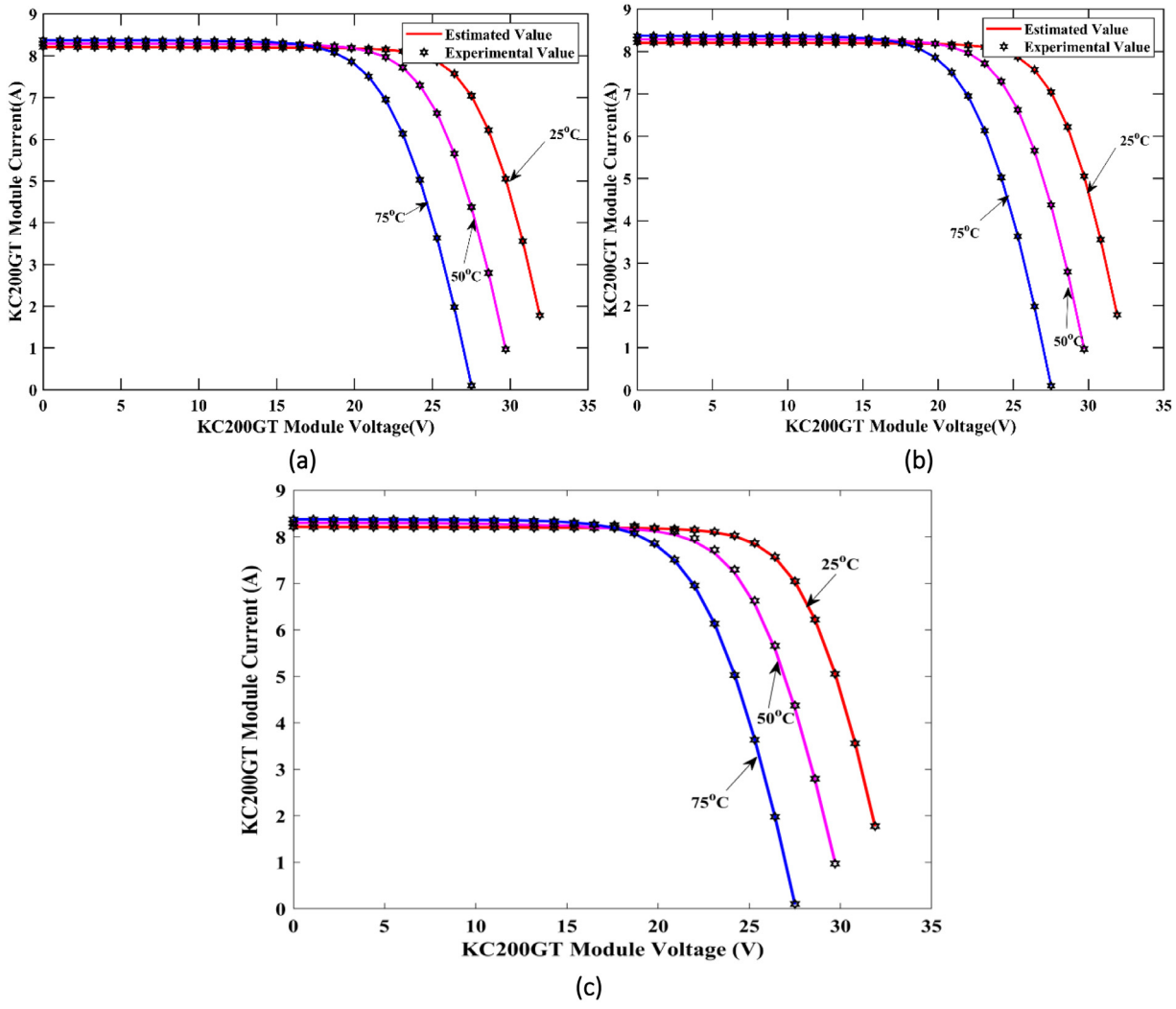

Fig. 20. I–V curves of KC200GT module for Case 4; (a) SDM, (b) DDM, (c) TDM.

value of all algorithms, the ranking is provided using FRT. The proposed CCNMGBO gives a minimum RMSE value compared to all other algorithms, i.e., 9.8602E−04 (SDM), 9.8252E−04 (DDM), and 9.823E−04 (TDM), followed by OBLWOA, GBO, EO, GWO, WOA, HHO, and SCA. The STD value decides the reliability of any algorithm. Therefore, Table 38 shows that the reliability (i.e., lowest STD value) of the CCNMGBO is better than other algorithms for both SDM, DDM, and TDM of the PV cell. The RT of the CCNMGBO is slightly higher than the basic GBO algorithm; however, lesser than other selected algorithms. Based on FRT, the CCNMGBO algorithm stands first, followed by OBLWOA, GBO, EO, WOA, GWO, HHO, and SCA for case 1. In addition, WSRT was also carried out at a significant level of 0.05 to assess the performance of the algorithms. The WSRT is a nonparametric statistical test, and it finds the statistical difference between the two algorithms. The results for SDM, DDM, and TDM are listed in Table 39. The above discussion concludes that the proposed CCNMGBO performs better than the selected algorithms for case 1.

Similar to case 1, the performance metrics, such as Min, Max, Mean, Median, STD, and RT, are listed in Table 40 for case 2.

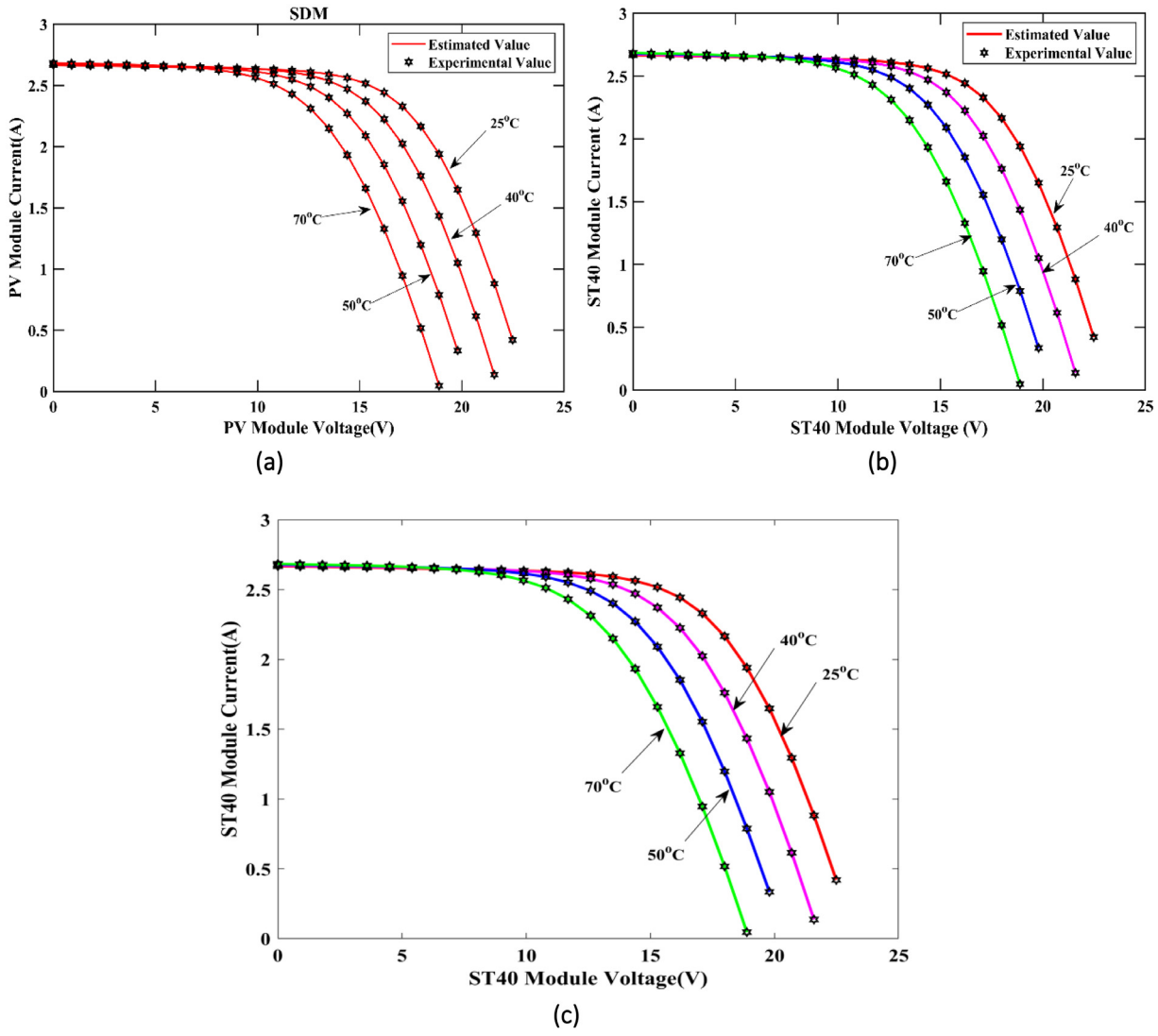

Fig. 21. I–V curves of ST40 module for Case 4; (a) SDM, (b) DDM, (c) TDM.

Based on the Min value of all algorithms, the ranking is provided using FRT. The proposed CCNMGBO gives a minimum RMSE value compared to all other algorithms, i.e., 2.425E–04 (SDM), 2.425E–04 (DDM), and 2.425E–03 (TDM), followed by GBO, OBLWOA, EO, GWO, HHO, WOA, and SCA. Table 40 shows that the reliability (i.e., lowest STD value) of the CCNMGBO is better than other algorithms for SDM, DDM, and TDM of the PV module. The RT of the CCNMGBO is slightly higher than the basic GBO algorithm; however, lesser than other selected algorithms. Based on FRT, the CCNMGBO algorithm stands first, followed by GBO, OBLWOA, EO, GWO, HHO, WOA, and SCA for case 2. In addition, WSRT was also carried out at a significant level of 0.05 to assess the performance of the algorithms. The test results for both SDM and DDM are listed in Table 41. The above discussion concludes that the proposed CCNMGBO performs better than the selected algorithms for case 2.

5. Conclusions

This paper proposes an enhanced version of the GBO algorithm called CCNMGBO comprising the concept of the Criss-Cross algorithm and Nelder–Mead simplex strategy to identify the unknown parameters of various PV models of the cell and module. The CC algorithm operators (vertical and horizontal crossover), the GBO algorithm operators (LEO and GSR), and the NM simplex strategy improve the exploration and exploitation ability of the proposed algorithm. The performance of the CCNMGBO is compared with the other state-of-the-art algorithms, such as GBO, GWO, HHO, SCA, WOA, OBLWOA, and EO and the results demonstrate that the proposed CCNMGBO is superior in handling the PV parameter estimation problems to the other algorithms. This conclusion was made based on the obtained RMSE values, statistical data, namely Min, Max, Mean, Median, RT, convergence curve, and two statistical ranking tests, namely WSRT and FRT, for all test cases, including three commercial modules, namely KC200GT, SM55, and ST40 under various operating conditions. In addition, the superiority of the CCNMGBO algorithm is also verified by plotting I–V curves using both experimental and estimated data points. All I–V curves demonstrate the accurate curve fitting between the experimental and simulated curves. The detailed discussions conclude that the proposed CCNMGBO is a robust tool for estimating or identifying the unknown parameters of the solar PV cells and modules. With Friedman's rank test values of

Table 38
Statistical data, including FRT of all algorithms for case 1.

	Min	Max	Mean	Median	STD	RT in Seconds	FRT
SDM							
CCNMGBO	**0.000986**	**0.000986**	**0.000986**	**0.000986**	**2.25E−08**	18.0625	**1.66667**
OBLWOA	**0.000986**	**0.000986**	**0.000986**	**0.000986**	4.94E−08	20.90625	2
GWO	0.003414	0.005261	0.004619	0.005182	0.001044	19.15625	5.666667
HHO	0.00242	0.030195	0.014016	0.009432	0.014444	44.22396	6.333333
SCA	0.04214	0.047351	0.045324	0.046482	0.002792	56.20313	8
WOA	0.001144	0.008918	0.006051	0.00809	0.004269	39.04167	5.666667
GBO	0.000987	0.000988	0.000987	0.000987	1.95E−07	**17.76563**	2.66667
EO	0.001297	0.001535	0.001422	0.001435	0.00012	58.98438	4
DDM							
CCNMGBO	**0.000982**	**0.000985**	**0.000983**	**0.000983**	**5.62E−07**	18.71354	**1.66667**
OBLWOA	0.000984	0.000986	0.000985	0.000985	7.98E−05	20.76042	2
GWO	0.001245	0.035258	0.012938	0.002311	0.019337	19.54688	5.666667
HHO	0.002909	0.018195	0.008538	0.004512	0.008401	45.91667	6.666667
SCA	0.044195	0.045823	0.045052	0.045138	0.000818	58.04167	8
WOA	0.001603	0.009935	0.004692	0.002538	0.004565	40.72396	5.333333
GBO	0.000986	0.001018	0.001002	0.001002	1.6E−05	**17.90104**	2.333333
EO	0.001046	0.001538	0.001312	0.001353	0.000249	61.9375	4.333333
TDM							
CCNMGBO	0.000982	0.000983	0.000983	0.000983	3.86E−07	19.10154	**1**
OBLWOA	0.001089	0.003878	0.002558	0.002706	0.0014	21.45698	4.333333
GWO	0.003043	0.036557	0.018834	0.016903	0.016841	20.45893	5.666667
HHO	0.005466	0.040702	0.017998	0.007826	0.019698	46.98751	5.666667
SCA	0.037636	0.044911	0.041742	0.042679	0.003727	60.45896	8
WOA	0.002537	0.043285	0.02625	0.032929	0.021179	41.59845	6
GBO	0.000984	0.000986	0.000985	0.000985	9.16E−07	**18.47815**	2
EO	0.001542	0.001743	0.001665	0.001709	0.000107	63.45874	3.333333

Table 39
Statistical WSRT results of all algorithms for case 1.

CCNMGBO vs.	*R+*	*R−*	*p-value*
SDM			
OBLWOA	14	7	0.035
GWO	15	6	0.025
HHO	15	6	0.025
SCA	15	6	0.025
WOA	15	6	0.025
GBO	13	8	0.045
EO	15	6	0.025
DDM			
OBLWOA	14	7	0.035
GWO	15	6	0.025
HHO	15	6	0.025
SCA	15	6	0.025
WOA	15	6	0.025
GBO	12	9	0.045
EO	14	7	0.035
TDM			
OBLWOA	15	6	0.025
GWO	15	6	0.025
HHO	15	6	0.025
SCA	15	6	0.025
WOA	15	6	0.025
GBO	12	9	0.045
EO	15	6	0.025

2.21 for numerical optimization and 1.66 for parameter estimation optimization, the CCNMGBO stood first among all selected algorithms.

Adding CC and NM concepts to the basic version of GBO increases computation time. Therefore, the research will be carried out to reduce the computation burden in the future. In addition, research on the multiobjective version of CCNMGBO will be carried out to solve complex multiobjective real-world problems. As an immediate future work, the proposed algorithm can be applied to the parameter estimation of the PV model by considering multiobjective optimization. It is worth noting that robust optimization by considering measurement errors may be an effective future work of the proposed algorithm. The proposed algorithm can also be applied to other engineering fields, such as feature selection, economic load dispatch, optimal power flow, electric vehicle charge scheduling, unit commitment problems, filter design, parameter estimation of the chaotic operator, image segmentation, wireless sensor networks, etc.

CRediT authorship contribution statement

M. Premkumar: Conceptualization, Data curation, Methodology, Investigation, Visualization, Formal analysis, Software, Validation, Writing - original draft. **Pradeep Jangir:** Conceptualization, Data curation, Methodology, Software, Writing - original draft. **C. Ramakrishnan:** Data curation, Visualization, Writing - review & editing. **C. Kumar:** Data curation, Visualization, Writing - review & editing. **R. Sowmya:** Conceptualization, Validation, Visualization, Writing - original draft. **Sanchari Deb:** Validation, Writing – review & editing. **Nallapaneni Manoj Kumar:** Conceptualization, Validation, Visualization, Writing – review & editing.

Declaration of competing interest

The authors declare that they have no known competing financial interests or personal relationships that could have appeared to influence the work reported in this paper.

Data availability

Data will be made available on request.

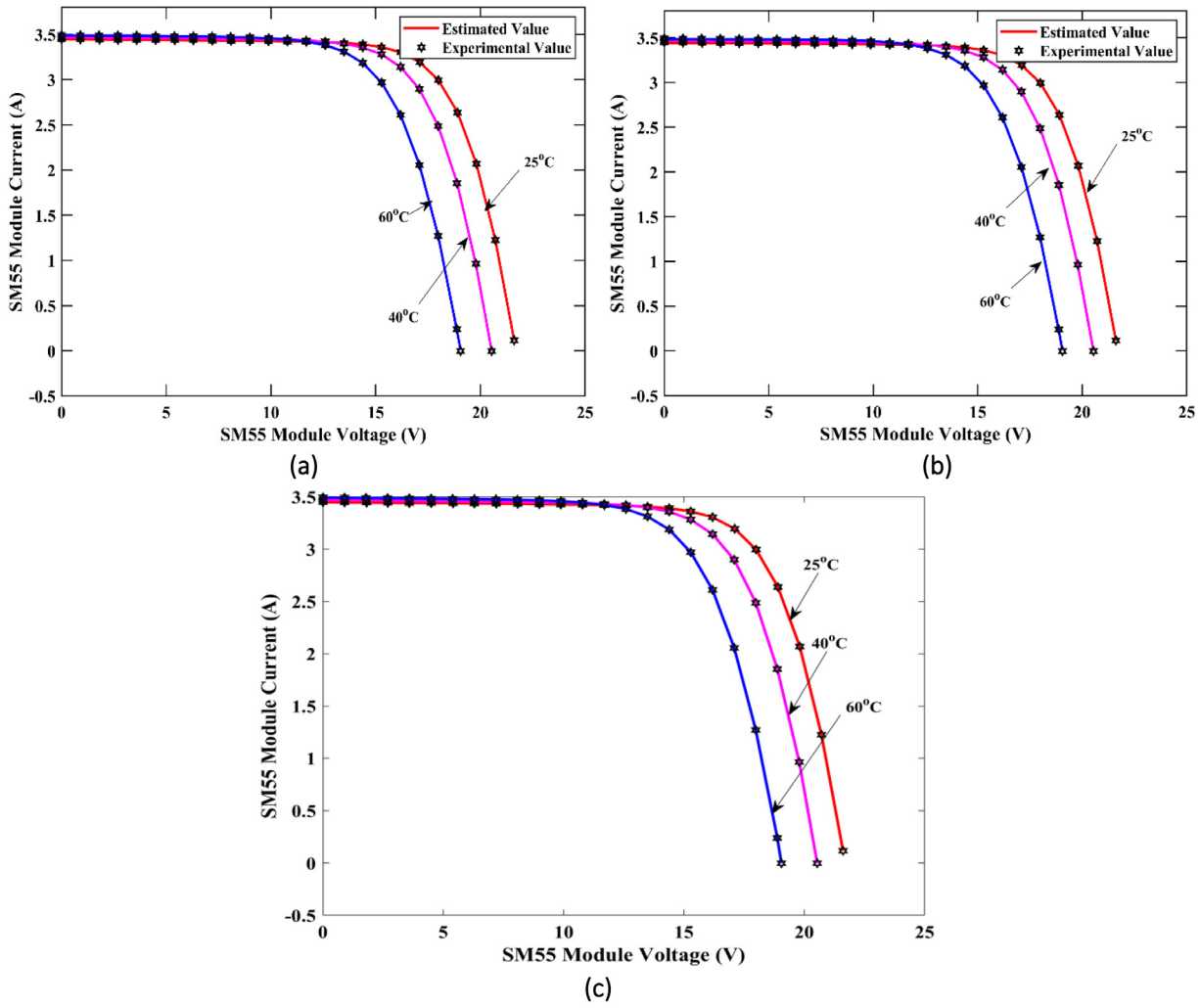

Fig. 22. I–V curves of SM55 module for Case 4; (a) SDM, (b) DDM, (c) TDM.

Table 40
Statistical data, including FRT of all algorithms for case 2.

	Min	Max	Mean	Median	STD	RT in Seconds	FRT
SDM							
CCNMGBO	0.00242507	0.00242507	0.00242507	0.00242507	1.59133E−13	17.10417	1.333333
OBLWOA	0.00242507	0.00242507	0.00242509	0.00242510	2.29828E−09	19.44271	3
GWO	0.00313460	0.00395278	0.00362645	0.00379197	0.00043347	18.12521	5
HHO	0.01093069	0.18593167	0.07486917	0.02774514	0.09654968	43.68229	6.333333
SCA	0.27426346	0.27427849	0.27427188	0.27427370	7.68026E−06	53.89063	7.666667
WOA	0.00491153	0.27454781	0.18457279	0.27425904	0.15559128	37.90625	7
GBO	0.00243614	0.00242507	0.00242507	0.00242507	3.7537E−13	16.66146	1.666667
EO	0.00248923	0.00251005	0.00249959	0.002499485	1.04108E−05	55.32813	4
DDM							
CCNMGBO	0.002425	0.002993	0.002617	0.002433	3.26E−08	18.291666	2
OBLWOA	0.002427	0.002453	0.002443	0.002449	1.53E−05	20.484375	2.666667
GWO	0.002542	0.002661	0.002605	0.002613	5.96E−05	19.640625	4.666667
HHO	0.006302	0.274252	0.145092	0.154723	0.134234	44.401041	6.333333
SCA	0.27426	0.274269	0.274263	0.27426	5.29E−06	55.244791	7.333333
WOA	0.04202	0.274326	0.196882	0.2743	0.134114	41.328125	7
GBO	0.002431	0.002438	0.002429	0.002425	7.1E−06	18.171875	2.3333333
EO	0.00245	0.002526	0.002487	0.002485	3.8E−05	63.046875	4
TDM							
CCNMGBO	0.002425	0.002461	0.002438	0.002428	2.02E−05	19.174585	**1.666667**
OBLWOA	0.00275	0.011786	0.005768	0.002767	0.005212	21.458648	4.666667
GWO	0.00272	0.072911	0.026636	0.004276	0.040083	20.145212	4.666667

(*continued on next page*)

Table 40 (*continued*).

	Min	Max	Mean	Median	STD	RT in Seconds	FRT
HHO	0.022091	0.77576	0.292177	0.07868	0.41975	45.145136	7.333333
SCA	0.076432	0.274348	0.142712	0.077357	0.114001	57.488953	6.666667
WOA	0.002778	0.787598	0.296495	0.099109	0.428027	42.015486	6.666667
GBO	0.002425	0.002502	0.002451	0.002425	4.46E−05	**18.987452**	**1.666667**
EO	0.002435	0.00247	0.002451	0.002448	1.79E−04	65.748963	2.666667

Table 41
Statistical WSRT results of all algorithms for case 2.

CCNMGBO vs.	*R*+	*R*−	*p-value*
SDM			
OBLWOA	14	7	0.035
GWO	15	6	0.025
HHO	15	6	0.025
SCA	15	6	0.025
WOA	15	6	0.025
GBO	15	6	0.025
EO	15	6	0.025
DDM			
OBLWOA	15	6	0.025
GWO	15	6	0.025
HHO	15	6	0.025
SCA	15	6	0.025
WOA	15	6	0.025
GBO	15	6	0.025
EO	15	6	0.025
TDM			
OBLWOA	15	6	0.025
GWO	15	6	0.025
HHO	15	6	0.025
SCA	15	6	0.025
WOA	15	6	0.025
GBO	13	8	0.045
EO	14	7	0.035

Acknowledgments

This project has received funding from the European Union's Horizon 2020 research and innovation programme under the Marie Skłodowska-Curie grant agreement No 945380.

References

Abd Elaziz, M., Oliva, D., 2018. Parameter estimation of solar cells diode models by an improved opposition-based whale optimization algorithm. Energy Convers. Manage. 171, 1843–1859. http://dx.doi.org/10.1016/j.enconman.2018.05.062.

Abd Elminaam, D.S., Ibrahim, S.A., Houssein, E.H., Elsayed, S.M., 2022. An efficient chaotic gradient-based optimizer for feature selection. IEEE Access 10, 9271–9286. http://dx.doi.org/10.1109/ACCESS.2022.3143802.

Abdel-basset, M., Mohamed, R., Mirjalili, S., Chakrabortty, R.K., Ryan, M.J., 2020. Solar photovoltaic parameter estimation using an improved equilibrium optimizer. Sol. Energy 209, 694–708. http://dx.doi.org/10.1016/j.solener.2020.09.032.

Abido, M.A., Khalid, M.S., 2018. Seven-parameter PV model estimation using differential evolution. Electr. Eng. 100, 971–981. http://dx.doi.org/10.1007/s00202-017-0542-2.

Ahmadianfar, I., Bozorg-haddad, O., Chu, X., 2020. Gradient-based optimizer: A new metaheuristic optimization algorithm. Inf. Sci. (N.Y.) 540, 131–159. http://dx.doi.org/10.1016/j.ins.2020.06.037.

Alam, D.F., Yousri, D.A., Eteiba, M.B., 2015. Flower Pollination Algorithm based solar PV parameter estimation. Energy Convers. Manage. 101, 410–422. http://dx.doi.org/10.1016/j.enconman.2015.05.074.

Askari, Q., Younas, I., Saeed, M., 2020. Political optimizer: A novel socio-inspired meta-heuristic for global optimization. Knowl. Based Syst. 195, 105709. http://dx.doi.org/10.1016/j.knosys.2020.105709.

Askarzadeh, A., Rezazadeh, A., 2013. Artificial bee swarm optimization algorithm for parameters identification of solar cell models. Appl. Energy 102, 943–949. http://dx.doi.org/10.1016/J.APENERGY.2012.09.052.

Ayang, A., Wamkeue, R., Ouhrouche, M., Djongyang, N., Essiane Salomé, N., Pombe, J.K., et al., 2019. Maximum likelihood parameters estimation of single-diode model of photovoltaic generator. Renew. Energy 130, http://dx.doi.org/10.1016/j.renene.2018.06.039.

Bana, S., Saini, R.P., 2017. Identification of unknown parameters of a single diode photovoltaic model using particle swarm optimization with binary constraints. Renew. Energy 101, 1299–1310. http://dx.doi.org/10.1016/j.renene.2016.10.010.

Batzelis, E.I., Papathanassiou, S.A., 2016. A method for the analytical extraction of the single-diode PV model parameters. IEEE Trans. Sustain. Energy 7, 504–512. http://dx.doi.org/10.1109/TSTE.2015.2503435.

Beigi, A.M., Maroosi, A., 2018. Parameter identification for solar cells and module using a Hybrid Firefly and Pattern Search Algorithms. Sol. Energy 171, 435–446. http://dx.doi.org/10.1016/j.solener.2018.06.092.

Benayad, A., Berrah, S., 2019. InGaN/GaN tandem solar cell parameter estimation: A comparative study. Turk. J. Electr. Eng. Comput. Sci. 27, 1896–1907. http://dx.doi.org/10.3906/elk-1810-22.

Bendaoud, R., Amiry, H., Benhmida, M., Zohal, B., Yadir, S., Bounouar, S., et al., 2019. New method for extracting physical parameters of PV generators combining an implemented genetic algorithm and the simulated annealing algorithm. Sol. Energy 194, 239–247. http://dx.doi.org/10.1016/j.solener.2019.10.040.

Beşkirli, A., Dağ, İ., 2022. An efficient tree seed inspired algorithm for parameter estimation of photovoltaic models. Energy Rep. 8, 291–298. http://dx.doi.org/10.1016/J.EGYR.2021.11.103.

Ćalasan, M., Abdel Aleem, S.H.E., Zobaa, A.F., 2020. On the root mean square error (RMSE) calculation for parameter estimation of photovoltaic models: A novel exact analytical solution based on lambert w function. Energy Convers. Manage. 210, 112716. http://dx.doi.org/10.1016/j.enconman.2020.112716.

Ćalasan, M., Jovanović, D., Rubežić, V., Mujović, S., Dukanović, S., 2019a. Estimation of single-diode and two-diode solar cell parameters by using a chaotic optimization approach. Energies (Basel) 12, http://dx.doi.org/10.3390/en12214209.

Ćalasan, M., Jovanović, D., Rubežić, V., Mujović, S., Dukanović, S., 2019b. Estimation of single-diode and two-diode solar cell parameters by using a chaotic optimization approach. Energies 12, 4209. http://dx.doi.org/10.3390/EN12214209.

Chen, H., Jiao, S., Heidari, A.A., Wang, M., Chen, X., Zhao, X., 2019a. An opposition-based sine cosine approach with local search for parameter estimation of photovoltaic models. Energy Convers. Manage. 195, 927–942. http://dx.doi.org/10.1016/j.enconman.2019.05.057.

Chen, X., Xu, B., Mei, C., Ding, Y., Li, K., 2018. Teaching–learning–based artificial bee colony for solar photovoltaic parameter estimation. Appl. Energy 212, 1578–1588. http://dx.doi.org/10.1016/j.apenergy.2017.12.115.

Chen, X., Yu, K., 2019. Hybridizing cuckoo search algorithm with biogeography-based optimization for estimating photovoltaic model parameters. Sol. Energy 180, 192–206. http://dx.doi.org/10.1016/j.solener.2019.01.025.

Chen, X., Yue, H., Yu, K., 2019b. Perturbed stochastic fractal search for solar PV parameter estimation. Energy 189, 116247. http://dx.doi.org/10.1016/j.energy.2019.116247.

Chin, V.J., Salam, Z., Ishaque, K., 2015. Cell modelling and model parameters estimation techniques for photovoltaic simulator application: A review. Appl. Energy 154, 500–519. http://dx.doi.org/10.1016/j.apenergy.2015.05.035.

Diab, A.A.Z., Sultan, H.M., Do, T.D., Kamel, O.M., Mossa, M.A., 2020. Coyote optimization algorithm for parameters estimation of various models of solar cells and PV modules. IEEE Access 8, 111102–111140. http://dx.doi.org/10.1109/ACCESS.2020.3000770.

Elazab, O.S., Hasanien, H.M., Alsaidan, I., Abdelaziz, A.Y., Muyeen, S.M., 2020. Parameter estimation of three diode photovoltaic model using grasshopper optimization algorithm. Energies (Basel) 13, http://dx.doi.org/10.3390/en13020497.

Faramarzi, A., Heidarinejad, M., Stephens, B., Mirjalili, S., 2020. Equilibrium optimizer: A novel optimization algorithm. Knowl. Based Syst. 191, http://dx.doi.org/10.1016/j.knosys.2019.105190.

Fathabadi, H., 2013. Novel neural-analytical method for determining silicon/plastic solar cells and modules characteristics. Energy Convers. Manage. 76, 253–259. http://dx.doi.org/10.1016/j.enconman.2013.07.055.

Gao, F., Han, L., 2012. Implementing the Nelder–Mead simplex algorithm with adaptive parameters. Comput. Optim. Appl. 51, 259–277. http://dx.doi.org/10.1007/s10589-010-9329-3.

Jamadi, M., Merrikh-Bayat, F., Bigdeli, M., 2016. Very accurate parameter estimation of single- and double-diode solar cell models using a modified artificial bee colony algorithm. Int. J. Energy Environ. Eng. 7, 13–25. http://dx.doi.org/10.1007/s40095-015-0198-5.

Javier Toledo, F., Blanes, J.M., Galiano, V., 2018. Two-step linear least-squares method for photovoltaic single-diode model parameters extraction. IEEE Trans. Ind. Electron. 65, 6301–6308. http://dx.doi.org/10.1109/TIE.2018.2793216.

Jervase, J.A., Bourdoucen, H., Al-Lawati, A., 2001. Solar cell parameter extraction using genetic algorithms. Meas. Sci. Technol. 12, 1922–1925. http://dx.doi.org/10.1088/0957-0233/12/11/322.

Jian, X., Weng, Z., 2020. A logistic chaotic JAYA algorithm for parameters identification of photovoltaic cell and module models. Optik (Stuttg.) 203, 164041. http://dx.doi.org/10.1016/j.ijleo.2019.164041.

Jordehi, A.R., 2016. Time varying acceleration coefficients particle swarm optimisation (TVACPSO): A new optimisation algorithm for estimating parameters of PV cells and modules. Energy Convers. Manage. 129, 262–274. http://dx.doi.org/10.1016/j.enconman.2016.09.085.

Kang, T., Yao, J., Jin, M., Yang, S., Duong, T., 2018. A novel improved cuckoo search algorithm for parameter estimation of photovoltaic (PV) models. Energies (Basel) 11, 1060. http://dx.doi.org/10.3390/en11051060.

Khanna, V., Das, B.K., Bisht, D., Vandana, Singh, P.K., 2015. A three diode model for industrial solar cells and estimation of solar cell parameters using PSO algorithm. Renew. Energy 78, 105–113. http://dx.doi.org/10.1016/j.renene.2014.12.072.

Kiani, A.T., Faisal Nadeem, M., Ahmed, A., Sajjad, I.A., Raza, A., Khan, I.A., 2020. Chaotic inertia weight particle swarm optimization (CIWPSO): An efficient technique for solar cell parameter estimation. In: 2020 3rd International Conference on Computing, Mathematics and Engineering Technologies: Idea to Innovation for Building the Knowledge Economy, ICoMET 2020. pp. 1–6. http://dx.doi.org/10.1109/iCoMET48670.2020.9074085.

Kumar, C., Mary, D.M., 2021. Parameter estimation of three-diode solar photovoltaic model using an improved-african vultures optimization algorithm with Newton–Raphson method. J. Comput. Electron. 20 (6), 2563–2593. http://dx.doi.org/10.1007/S10825-021-01812-6.

Kumar, C., Raj, T.D., Premkumar, M., Raj, T.D., 2020. A new stochastic slime mould optimization algorithm for the estimation of solar photovoltaic cell parameters. Optik (Stuttg.) 165277. http://dx.doi.org/10.1016/j.ijleo.2020.165277.

Kumari, P.A., Geethanjali, P., 2017. Adaptive genetic algorithm based multi-objective optimization for photovoltaic cell design parameter extraction. Energy Procedia 117, 432–441. http://dx.doi.org/10.1016/j.egypro.2017.05.165.

Laghari, J.A., Mokhlis, H., Bakar, A.H.A., Mohamad, H., 2013. Application of computational intelligence techniques for load shedding in power systems: A review. Energy Convers. Manage. 75, 130–140. http://dx.doi.org/10.1016/j.enconman.2013.06.010.

Li, S., Chen, H., Wang, M., Asghar, A., Mirjalili, S., 2020. Slime mould algorithm : A new method for stochastic optimization. Future Gener. Comput. Syst. 111, 300–323. http://dx.doi.org/10.1016/j.future.2020.03.055.

Li, S., Gong, W., Yan, X., Hu, C., Bai, D., Wang, L., et al., 2019. Parameter extraction of photovoltaic models using an improved teaching-learning-based optimization. Energy Convers. Manage. 186, 293–305. http://dx.doi.org/10.1016/j.enconman.2019.02.048.

Liao, Z., Chen, Z., Li, S., 2020. Parameters extraction of photovoltaic models using triple-phase teaching-learning-based optimization. IEEE Access 8, 69937–69952. http://dx.doi.org/10.1109/ACCESS.2020.2984728.

Liu, Y., Chong, G., Heidari, A.A., Chen, H., Liang, G., Ye, X., et al., 2020. Horizontal and vertical crossover of harris hawk optimizer with Nelder–Mead simplex for parameter estimation of photovoltaic models. Energy Convers. Manage. 223, 113211. http://dx.doi.org/10.1016/j.enconman.2020.113211.

Long, W., Cai, S., Jiao, J., Xu, M., Wu, T., 2020. A new hybrid algorithm based on grey wolf optimizer and cuckoo search for parameter extraction of solar photovoltaic models. Energy Convers. Manage. 203, 112243. http://dx.doi.org/10.1016/j.enconman.2019.112243.

Louzazni, M., Khouya, A., Amechnoue, K., Craciunescu, A., 2017. Parameter estimation of photovoltaic module using bio-inspired firefly algorithm. In: Proceedings of 2016 International Renewable and Sustainable Energy Conference, IRSEC 2016. pp. 591–596. http://dx.doi.org/10.1109/IRSEC.2016.7983895.

Lun, S. xian, Wang, S., Yang, G. hong, Guo, T. ting, 2015. A new explicit double-diode modeling method based on Lambert W-function for photovoltaic arrays. Sol. Energy 116, http://dx.doi.org/10.1016/j.solener.2015.03.043.

Ma, J., Man, K.L., Guan, S.-U., Ting, T.O., Wong, P.W.H., 2016. Parameter estimation of photovoltaic model via parallel particle swarm optimization algorithm. Int. J. Energy Res. 40, 343–352. http://dx.doi.org/10.1002/er.3359.

Ma, J., Ting, T.O., Man, K.L., Zhang, N., Guan, S.U., Wong, P.W.H., 2013. Parameter estimation of photovoltaic models via cuckoo search. J. Appl. Math. 2013, 10–12. http://dx.doi.org/10.1155/2013/362619.

Manoharan, P., Subramaniam, U., Babu, T.S., Padmanaban, S., Holm-Nielsen, J.B., Mitolo, M., et al., 2020. Improved perturb & observation maximum power point tracking technique for solar photovoltaic power generation systems. IEEE Syst. J. 1–13. http://dx.doi.org/10.1109/JSYST.2020.3003255.

Md Sabudin, S.N., Jamil, N.M., 2019. Parameter estimation in mathematical modelling for photovoltaic panel. IOP Conf. Ser. Mater. Sci. Eng. 536, http://dx.doi.org/10.1088/1757-899X/536/1/012001.

Menesy, A.S., Sultan, H.M., Kamel, S., 2020. Extracting model parameters of proton exchange membrane fuel cell using equilibrium optimizer algorithm. In: 2020 International Youth Conference on Radio Electronics, Electrical and Power Engineering. REEPE, pp. 1–7. http://dx.doi.org/10.1109/REEPE49198.2020.9059219.

Meng, A.B., Chen, Y.C., Yin, H., Chen, S.Z., 2014. Crisscross optimization algorithm and its application. Knowl. Based Syst. 67, 218–229. http://dx.doi.org/10.1016/j.knosys.2014.05.004.

Meng, A., Ge, J., Yin, H., Chen, S., 2016. Wind speed forecasting based on wavelet packet decomposition and artificial neural networks trained by crisscross optimization algorithm. Energy Convers. Manage. 114, 75–88. http://dx.doi.org/10.1016/j.enconman.2016.02.013.

Meng, A., Zeng, C., Wang, P., Chen, D., Zhou, T., Zheng, X., et al., 2021. A high-performance crisscross search based grey wolf optimizer for solving optimal power flow problem. Energy 225, 120211. http://dx.doi.org/10.1016/J.ENERGY.2021.120211.

Messaoud, R. Ben, 2020a. Extraction of uncertain parameters of single and double diode model of a photovoltaic panel using Salp Swarm algorithm. Measurement (Lond.) 154, 107446. http://dx.doi.org/10.1016/j.measurement.2019.107446.

Messaoud, R. ben, 2020b. Extraction of uncertain parameters of single and double diode model of a photovoltaic panel using Salp Swarm algorithm. Measurement 154, 107446. http://dx.doi.org/10.1016/j.measurement.2019.107446.

Mirjalili, S., 2016. SCA: A Sine Cosine Algorithm for solving optimization problems. Knowl. Based Syst. 96, 120–133. http://dx.doi.org/10.1016/j.knosys.2015.12.022.

Mirjalili, S., Mirjalili, S.M., Lewis, A., 2014. Grey wolf optimizer. Adv. Eng. Softw. 69, 46–61. http://dx.doi.org/10.1016/j.advengsoft.2013.12.007.

Mohamed, N., Alrahim, A., Yahaya, N.Z., Singh, B., 2013. Single-diode model and two-diode model of PV modules : A comparison. In: 2013 IEEE International Conference on Control System, Computing and Engineering. pp. 210–214.

Mohamed, A.A., Kamel, S., Hassan, M.H., Mosaad, M.I., Aljohani, M., 2022. Optimal power flow analysis based on hybrid gradient-based optimizer with moth–flame optimization algorithm considering optimal placement and sizing of FACTS/Wind power. Mathematics 10, 361. http://dx.doi.org/10.3390/MATH10030361.

Montano, J., Tobón, A.F., Villegas, J.P., Durango, M., 2020. Grasshopper optimization algorithm for parameter estimation of photovoltaic modules based on the single diode model. Int. J. Energy Environ. Eng. 11, 367–375. http://dx.doi.org/10.1007/s40095-020-00342-4.

Montoya, O.D., Gil-González, W., Grisales-Noreña, L.F., 2020. Sine-cosine algorithm for parameters' estimation in solar cells using datasheet information. J. Phys. Conf. Ser. 1671, 012008. http://dx.doi.org/10.1088/1742-6596/1671/1/012008.

Moshksar, E., Ghanbari, T., 2017. Adaptive estimation approach for parameter identification of photovoltaic modules. IEEE J. Photovolt. 7, 614–623. http://dx.doi.org/10.1109/JPHOTOV.2016.2633815.

Muhsen, D.H., Ghazali, A.B., Khatib, T., Abed, I.A., 2016. A comparative study of evolutionary algorithms and adapting control parameters for estimating the parameters of a single-diode photovoltaic module's model. Renew. Energy 96, 377–389. http://dx.doi.org/10.1016/J.RENENE.2016.04.072.

Naeijian, M., Rahimnejad, A., Ebrahimi, S.M., Pourmousa, N., Gadsden, S.A., 2021. Parameter estimation of PV solar cells and modules using Whippy Harris Hawks Optimization Algorithm. Energy Rep. 7, 4047–4063. http://dx.doi.org/10.1016/J.EGYR.2021.06.085.

Naraharisetti, J.N.L., Devarapalli, R., Bathina, V., 2020. Parameter extraction of solar photovoltaic module by using a novel hybrid marine predators–success history based adaptive differential evolution algorithm. Energy Sources A http://dx.doi.org/10.1080/15567036.2020.1806956.

Nayak, B., Mohapatra, A., Mohanty, K.B., 2019. Parameter estimation of single diode PV module based on GWO algorithm. Renew. Energy Focus 30, 1–12. http://dx.doi.org/10.1016/j.ref.2019.04.003.

Ndi, F.E., Perabi, S.N., Ndjakomo, S.E., Ondoua Abessolo, G., Mengounou Mengata, G., 2021. Estimation of single-diode and two diode solar cell parameters by equilibrium optimizer method. Energy Rep. 7, 4761–4768. http://dx.doi.org/10.1016/J.EGYR.2021.07.025.

Nunes, H.G.G., Pombo, J.A.N., Bento, P.M.R., Mariano, S.J.P.S., Calado, M.R.A., 2019. Collaborative swarm intelligence to estimate PV parameters. Energy Convers. Manage. 185, 866–890. http://dx.doi.org/10.1016/j.enconman.2019.02.003.

Nunes, H.G.G., Pombo, J.A.N., Mariano, SJ.P.S., Calado, M.R.A., Felippe de Souza, J.A.M., 2018. A new high performance method for determining the parameters of PV cells and modules based on guaranteed convergence particle swarm optimization. Appl. Energy 211, 774–791. http://dx.doi.org/10.1016/j.apenergy.2017.11.078.

Oliva, D., Abd El Aziz, M., Ella Hassanien, A., 2017. Parameter estimation of photovoltaic cells using an improved chaotic whale optimization algorithm. Appl. Energy 200, 141–154. http://dx.doi.org/10.1016/j.apenergy.2017.05.029.

Oliva, D., Cuevas, E., Pajares, G., 2014. Parameter identification of solar cells using artificial bee colony optimization. Energy 72, 93–102. http://dx.doi.org/10.1016/j.energy.2014.05.011.

Premkuma, M., et al., 2019. Certain study on MPPT algorithms to track the global MPP under partial shading on solar PV module/array. Int. J. Comput. Digit. Syst. 8, 405–416. http://dx.doi.org/10.12785/ijcds/080409.

Premkumar, M., 2021. Classical benchmark test functions. pp. 1–2, https://premkumarmanoharan.wixsite.com/mysite/downloads (accessed June 4, 2021).

Premkumar, M., Jangir, P., Elavarasan, R.M., Sowmya, R., 2021a. Opposition decided gradient-based optimizer with balance analysis and diversity maintenance for parameter identification of solar photovoltaic models. J. Ambient Intell. Humaniz. Comput. 1, 1–23. http://dx.doi.org/10.1007/S12652-021-03564-4/TABLES/16.

Premkumar, M., Jangir, P., Kumar, C., David Thanasingh Sundarsingh Jebaseelan, S., Haes Alhelou, H., Madurai Elavarasan, R., et al., 2022. Constraint estimation in three-diode solar photovoltaic model using Gaussian and Cauchy mutation-based hunger games search optimizer and enhanced Newton–Raphson method. IET Renew. Power Gener. 16, 1733–1772. http://dx.doi.org/10.1049/RPG2.12475.

Premkumar, M., Jangir, P., Ramakrishnan, C., Nalinipriya, G., Alhelou, H.H., Kumar, B.S., 2021b. Identification of solar photovoltaic model parameters using an improved gradient-based optimization algorithm with chaotic drifts. IEEE Access 9, 62347–62379. http://dx.doi.org/10.1109/ACCESS.2021.3073821.

Premkumar, M., Jangir, P., Sowmya, R., 2021c. MOGBO: A new Multiobjective Gradient-Based Optimizer for real-world structural optimization problems. Knowl. Based Syst. 218, 106856. http://dx.doi.org/10.1016/j.knosys.2021.106856.

Premkumar, M., Jangir, P., Sowmya, R., Elavarasan, R.M., 2021d. Many-objective gradient-based optimizer to solve optimal power flow problems: Analysis and validations. Eng. Appl. Artif. Intell. 106, 104479. http://dx.doi.org/10.1016/J.ENGAPPAI.2021.104479.

Premkumar, M., Jangir, P., Sowmya, R., Elavarasan, R.M., Santosh Kumar, B., 2021e. Enhanced chaotic JAYA algorithm for parameter estimation of photovoltaic cell/modules. ISA Trans. 116, 139–166. http://dx.doi.org/10.1016/j.isatra.2021.01.045.

Premkumar, M., Karthick, K., Sowmya, R., 2018. A review on solar PV based grid connected microinverter control schemes and topologies. Int. J. Renew. Energy Dev. 7, 171. http://dx.doi.org/10.14710/ijred.7.2.171-182.

Premkumar, M., Kumar, C., Sowmya, R., 2020a. Mathematical modelling of solar photovoltaic cell/panel/array based on the physical parameters from the manufacturer's datasheet. Int. J. Renew. Energy Dev. 9, 7–22. http://dx.doi.org/10.14710/ijred.9.1.7-22.

Premkumar, M., Sowmya, R., Jangir, P., Sivakumar, J.S.V., 2020b. A new and reliable objective functions for extracting the unknown parameters of solar photovoltaic cell using political optimizer algorithm. In: 2020 International Conference on Data Analytics for Business and Industry: Way Towards a Sustainable Economy (ICDABI), Sakheer, Bahrain. pp. 1–6. http://dx.doi.org/10.1109/ICDABI51230.2020.9325627.

Premkumar, M., Sowmya, R., Umashankar, S., Jangir, P., 2020c. Extraction of uncertain parameters of single-diode photovoltaic module using hybrid particle swarm optimization and grey wolf optimization algorithm. Mater. Today Proc. http://dx.doi.org/10.1016/j.matpr.2020.08.784.

Premkumar, M., Subramaniam, U., Sudhakar Babu, T., Elavarasan, R.M., Mihet-Popa, L., 2020d. Evaluation of mathematical model to characterize the performance of conventional and hybrid PV array topologies under static and dynamic shading patterns. Energies (Basel) 13, http://dx.doi.org/10.3390/en13123216.

Premkumar, M., Sudhakar, T., Umashankar, S., Sowmya, R., 2020e. A new metaphor-less algorithms for the photovoltaic cell parameter estimation. Optik 208, 164559. http://dx.doi.org/10.1016/j.ijleo.2020.164559.

Qais, M.H., Hasanien, H.M., Alghuwainem, S., 2019a. Identification of electrical parameters for three-diode photovoltaic model using analytical and sunflower optimization algorithm. Appl. Energy 250, 109–117. http://dx.doi.org/10.1016/j.apenergy.2019.05.013.

Qais, M.H., Hasanien, H.M., Alghuwainem, S., 2020. Parameters extraction of three-diode photovoltaic model using computation and Harris Hawks optimization. Energy 195, 117040. http://dx.doi.org/10.1016/j.energy.2020.117040.

Qais, M.H., Hasanien, H.M., Alghuwainem, S., Nouh, A.S., 2019b. Coyote optimization algorithm for parameters extraction of three-diode photovoltaic models of photovoltaic modules. Energy 187, 116001. http://dx.doi.org/10.1016/j.energy.2019.116001.

Ramadan, A., Kamel, S., Korashy, A., Yu, J., 2020. Photovoltaic cells parameter estimation using an enhanced teaching–learning-based optimization algorithm. Iran. J. Sci. Technol. - Trans. Electr. Eng. 44, http://dx.doi.org/10.1007/s40998-019-00257-9.

Rana, N., Latiff, M.S.A., Abdulhamid, S.M., Chiroma, H., 2020. Whale Optimization Algorithm: A Systematic Review of Contemporary Applications, Modifications and Developments. Vol. 32. Springer London, http://dx.doi.org/10.1007/s00521-020-04849-z.

Rao, R.V., 2020. Rao algorithms: Three metaphor-less simple algorithms for solving optimization problems. Int. J. Ind. Eng. Comput. 11, 107–130. http://dx.doi.org/10.5267/j.ijiec.2019.6.002.

Rezk, H., Abdelkareem, M.A., 2022. Optimal parameter identification of triple diode model for solar photovoltaic panel and cells. Energy Rep. 8, 1179–1188. http://dx.doi.org/10.1016/J.EGYR.2021.11.179.

Ridha, H.M., 2020. Parameters extraction of single and double diodes photovoltaic models using Marine Predators Algorithm and Lambert W function. Sol. Energy 209, 674–693. http://dx.doi.org/10.1016/j.solener.2020.09.047.

Sandrolini, L., Artioli, M., Reggiani, U., 2010. Numerical method for the extraction of photovoltaic module double-diode model parameters through cluster analysis. Appl. Energy 87, 442–451. http://dx.doi.org/10.1016/j.apenergy.2009.07.022.

Sankaranarayanan, R.S.V., 2022. Optimal vehicle-to-grid and grid-to-vehicle scheduling strategy with uncertainty management using improved marine predator algorithm. Comput. Electr. Eng. 100, 107949. http://dx.doi.org/10.1016/J.COMPELECENG.2022.107949.

Saxena, A., Sharma, A., Shekhawat, S., 2020. Parameter extraction of solar cell using intelligent grey wolf optimizer. Evol. Intell. http://dx.doi.org/10.1007/s12065-020-00499-1.

Shayeghi, H., Mahdavi, M., Bagheri, A., 2010. An improved DPSO with mutation based on similarity algorithm for optimization of transmission lines loading. Energy Convers. Manage. 51, 2715–2723. http://dx.doi.org/10.1016/j.enconman.2010.06.007.

Sheraz, M., Abido, M.A., 2014. An efficient approach for parameter estimation of PV model using de and fuzzy based MPPT controller. In: 2014 IEEE Conference on Evolving and Adaptive Intelligent Systems, EAIS 2014 - Conference Proceedings. pp. 1–5. http://dx.doi.org/10.1109/eais.2014.6867487.

Soliman, M.A., Hasanien, H.M., 2020. Marine predators algorithm for parameters identification of triple-diode photovoltaic models. IEEE Access 8, 155832. http://dx.doi.org/10.1109/ACCESS.2020.3019244.

Wang, D., Sun, X., Kang, H., Shen, Y., Chen, Q., 2022. Heterogeneous differential evolution algorithm for parameter estimation of solar photovoltaic models. Energy Rep. 8, 4724–4746. http://dx.doi.org/10.1016/J.EGYR.2022.03.144.

Wei, T., Yu, F., Huang, G., Xu, C., 2019. A particle-swarm-optimization-based parameter extraction routine for three-diode lumped parameter model of organic solar cells. IEEE Electron Device Lett. 40, 1511–1514. http://dx.doi.org/10.1109/LED.2019.2926315.

Weng, X., Heidari, A.A., Liang, G., Chen, H., Ma, X., 2021. An evolutionary Nelder–Mead slime mould algorithm with random learning for efficient design of photovoltaic models. Energy Rep. 7, 8784–8804. http://dx.doi.org/10.1016/J.EGYR.2021.11.019.

Wolpert, D.H., Macready, W.G., 1997. No free lunch theorems for optimization. IEEE Trans. Evol. Comput. 1, 67–82.

Wu, Z., Yu, D., Kang, X., 2017. Parameter identification of photovoltaic cell model based on improved ant lion optimizer. Energy Convers. Manage. 151, 107–115. http://dx.doi.org/10.1016/j.enconman.2017.08.088.

Xiong, G., Zhang, J., Shi, D., He, Y., 2018a. Parameter extraction of solar photovoltaic models using an improved whale optimization algorithm. Energy Convers. Manage. 174, 388–405. http://dx.doi.org/10.1016/j.enconman.2018.08.053.

Xiong, G., Zhang, J., Yuan, X., Shi, D., He, Y., Yao, G., 2018b. Parameter extraction of solar photovoltaic models by means of a hybrid differential evolution with whale optimization algorithm. Sol. Energy 176, 742–761. http://dx.doi.org/10.1016/j.solener.2018.10.050.

Ye, M., Wang, X., Xu, Y., 2009. Parameter extraction of solar cells using particle swarm optimization. J. Appl. Phys. 105, 0–8. http://dx.doi.org/10.1063/1.3122082.

Yousri, D., Thanikanti, S.B., Allam, D., Ramachandaramurthy, V.K., Eteiba, M.B., 2020. Fractional chaotic ensemble particle swarm optimizer for identifying the single, double, and three diode photovoltaic models' parameters. Energy 195, 116979. http://dx.doi.org/10.1016/j.energy.2020.116979.

Yu, K., Chen, X., Wang, X., Wang, Z., 2017a. Parameters identification of photovoltaic models using self-adaptive teaching-learning-based optimization. Energy Convers. Manage. 145, 233–246. http://dx.doi.org/10.1016/j.enconman.2017.04.054.

Yu, S., Heidari, A.A., Liang, G., Chen, C., Chen, H., Shao, Q., 2022. Solar photovoltaic model parameter estimation based on orthogonally-adapted gradient-based optimization. Optik (Stuttg.) 252, 168513. http://dx.doi.org/10.1016/J.IJLEO.2021.168513.

Yu, K., Liang, J.J., Qu, B.Y., Chen, X., Wang, H., 2017b. Parameters identification of photovoltaic models using an improved JAYA optimization algorithm. Energy Convers. Manage. 150, 742–753. http://dx.doi.org/10.1016/j.enconman.2017.08.063.

Yu, H., Zhang, Y., Cai, P., Yi, J., Li, S., Wang, S., 2021. Stochastic multiple chaotic local search-incorporated gradient-based optimizer. Discrete Dyn. Nat. Soc. 2021, http://dx.doi.org/10.1155/2021/3353926.

Yuan, Z., Wang, W., Wang, H., Razmjooy, N., 2020. A new technique for optimal estimation of the circuit-based PEMFCs using developed Sunflower Optimization Algorithm. Energy Rep. 6, 662–671. http://dx.doi.org/10.1016/j.egyr.2020.03.010.

Zhang, H., Heidari, A.A., Wang, M., Zhang, L., Chen, H., Li, C., 2020. Orthogonal Nelder–Mead moth flame method for parameters identification of photovoltaic modules. Energy Convers. Manage. 211, http://dx.doi.org/10.1016/j.enconman.2020.112764.